Supplementary Information

Concerted Nucleophilic Aromatic Substitutions

Eugene E. Kwan, Yuwen Zeng, Harrison A. Besser, and Eric N. Jacobsen*

Department of Chemistry and Chemical Biology, Harvard University,
12 Oxford Street, Cambridge, Massachusetts 02138, United States

jacobsen@chemistry.harvard.edu

Contents

1. Abbreviations

at = acquisition time, d1 = recycle delay, dB = decibels, dm = decoupling mode, dpwr = decoupler power, F = fractional conversion, FID = free induction decay, KIE = kinetic isotope effect, MQF = multiple quantum filtered, NA = not applicable, ND = not determined, nt = number of scans, ppm = parts per million, rt = room temperature, T1 = spin–lattice relaxation time, tof = transmitter offset.

TBAF = tetra-*n*-butylammonium fluoride, TMAF = tetramethylammonium fluoride, THF = tetrahydrofuran, DMF = dimethylformamide, DMSO = dimethyl sulfoxide

2. Synthesis and Characterization

(a) Compound **7** (S_N2 reaction)

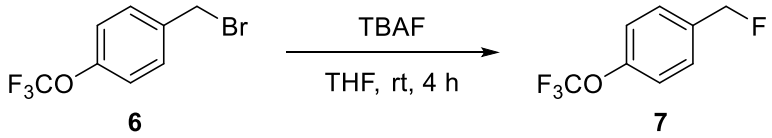

6 **7**

Full conversion:

To a dry 50 mL flask was added *p*-trifluoromethoxybenzyl bromide (765 mg, 3 mmol, 1 equiv) in diethyl ether (10 mL). TBAF (1M in THF, 7.5 mL, 2.5 equiv) was added dropwise and the reaction was stirred at room temperature for 4 hours. The reaction mixture was diluted with Et_2O (150 mL) and washed with water (3x150 mL). The organic phase was dried over $MgSO_4$ and concentrated carefully (due to its low boiling point) to give the crude product. The product was purified by silica gel chromatography (elution with pentane) to yield **7** as a colorless oil (530 mg, 91%).

Note: *p*-trifluoromethoxybenzyl bromide was first purified by passage through a short pad of silica gel and distillation under house vacuum (113 ^oC).

Partial conversion:

To a dry 100 mL flask flask was added *p*-trifluoromethoxybenzyl bromide (10.200 g, 40 mmol, 1 equiv) in Et_2O (10 mL). TBAF (1M in THF, 4 mL, 0.1 equiv) was added dropwise and the reaction was stirred at room temperature for 4 hours. After reaction, a certain amount of *p*-difluorobenzene was added as an internal standard. Conversion (10.3%) was determined by quantitative proton-decoupled ^{19}F spectra (delay = 30 sec with tof set to the midpoint between the fluorine peaks of the internal standard and the product; correction factor: s = 1.08, see below). Pyrrolidine (9 mL, 3 equiv) was added (to react with excess **6**) and stirred overnight. (Control experiments show that pyrrolidine does not react with **7**.) The reaction mixture was diluted with Et_2O (200 mL) and washed with 1 M HCl (2x150 mL) and water (3x150 mL). The organic phase was dried over $MgSO_4$ and concentrated (carefully as before). The product was purified by silica gel chromatography (elution with pentane) to yield **7** as a colorless oil (540 mg, 7.0%).

For KIE measurements using impure materials, the crude product was used directly without purification by column chromatography.

Calibration of internal standard and **7** in quantitative ^{19}F NMR:

p-Difluorobenzene (18.1 mg) and **7** (19.9 mg) were dissolved in $CDCl_3$ (0.6 mL) and a quantitative ^{19}F NMR spectrum was obtained. The integral ratio of internal standard to **7** was 3.355 compared to a theoretical value of [(18.1/114.09)*2]/(19.9/194.13) = 3.095. Therefore a correction factor of s = 3.355/3.095 = 1.084 was applied to determinations of conversion.

Characterization of **7** (new compound):

^{1}H NMR: (500 MHz, $CDCl_3$, 25 °C): δ 7.41 (d, *J* = 8.2 Hz, 2H), 7.24 (d, *J* = 8.6 Hz, 2H), 5.37 (d, *J* = 47.6 Hz, 2H).

^{19}F NMR: (471 MHz, $CDCl_3$, 25 °C): δ -58.31 (s, 3F), -209.99 (t, *J* = 47.6 Hz, 1F).

^{13}C NMR: (125 MHz, $CDCl_3$, 25 °C): δ 144.64, 130.12 (d, *J* = 17.6 Hz), 124.11 (d, *J* = 5.9 Hz), 116.29, 115.66 (q, *J* = 257.0 Hz), 78.79 (d, *J* = 167.3 Hz).

IR (ATR film): 2963, 2903, 1512, 1253, 1216, 1201, 1156, 988, 849, 815.

HRMS (GC-FTMS, EI): calc'd for $C_8H_6F_4O$ [M^+], 194.0355; found 194.0349.

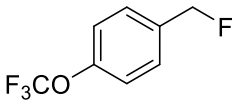

7

^{1}H NMR spectrum of **7**:

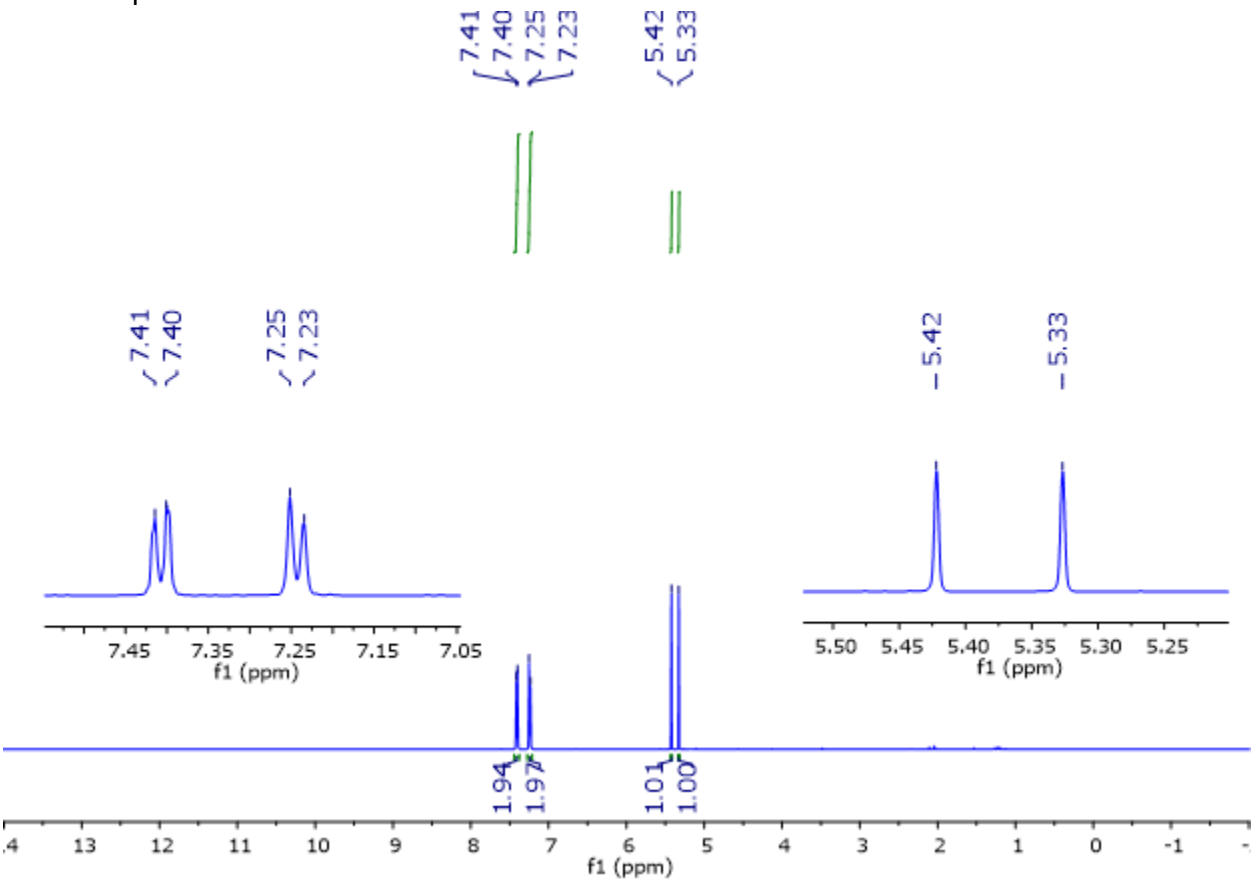

^{19}F NMR spectrum of **7**:

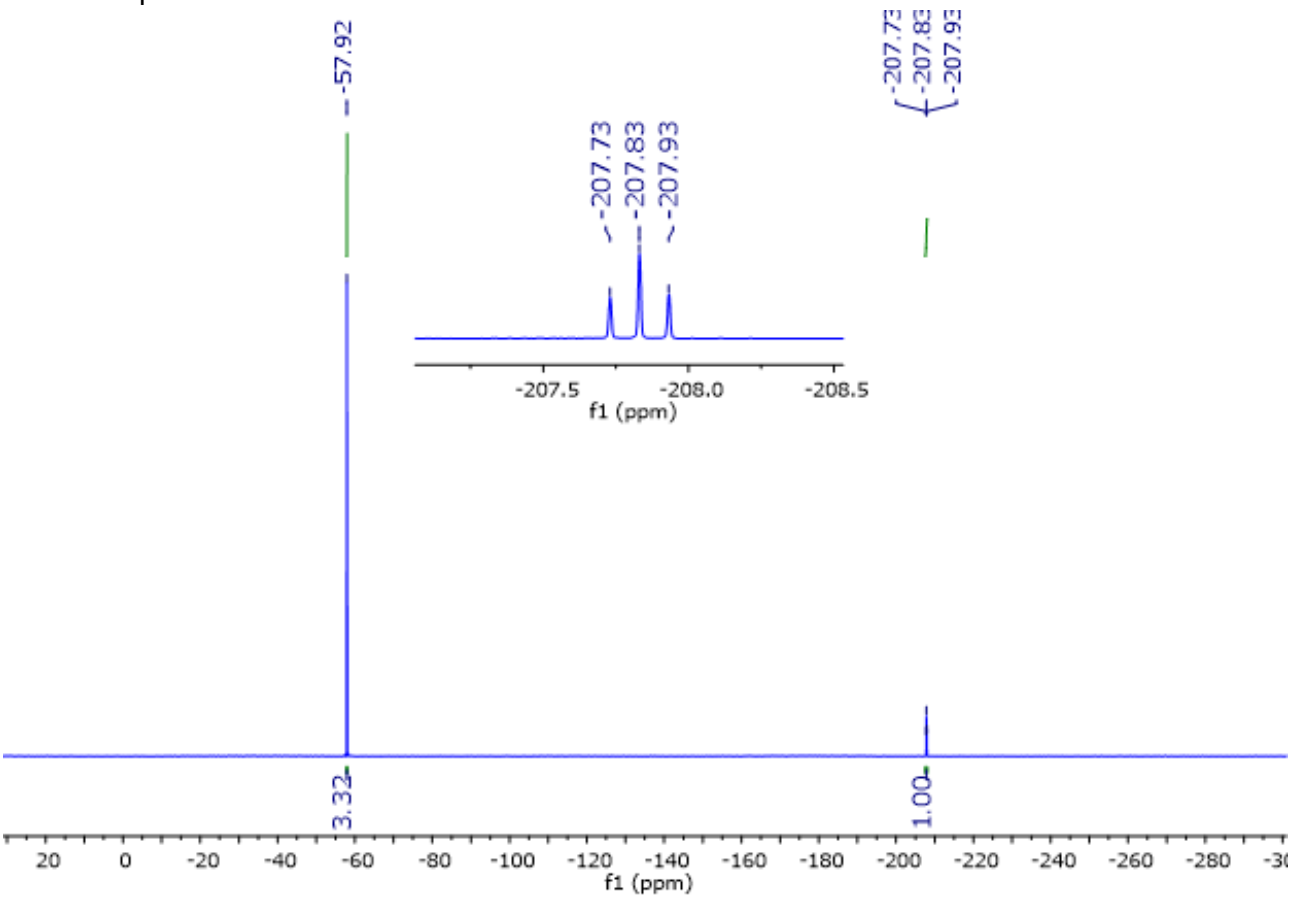

^{13}C NMR spectrum of **7** (H decoupled, F coupled):

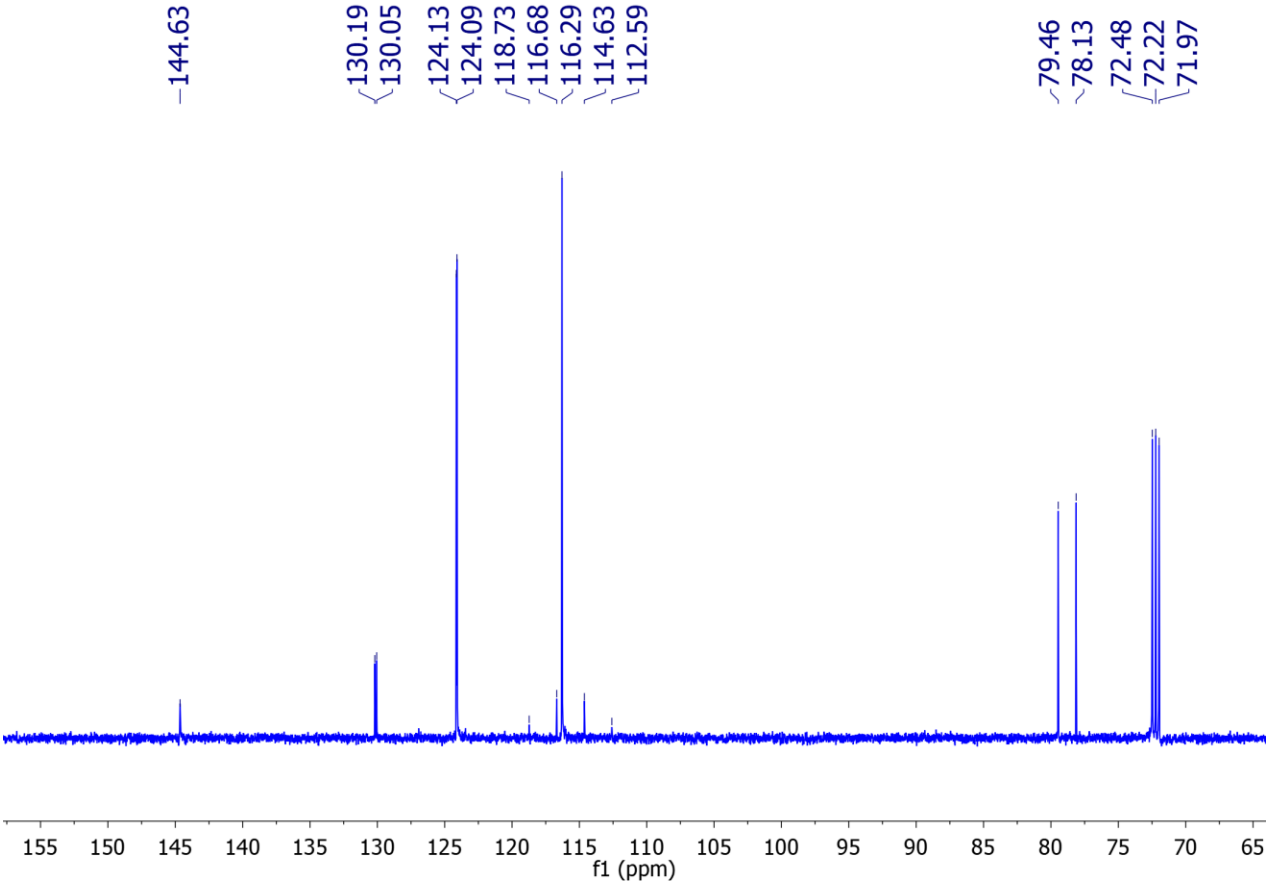

^{13}C NMR spectrum of **7** (H decoupled, F decoupled):

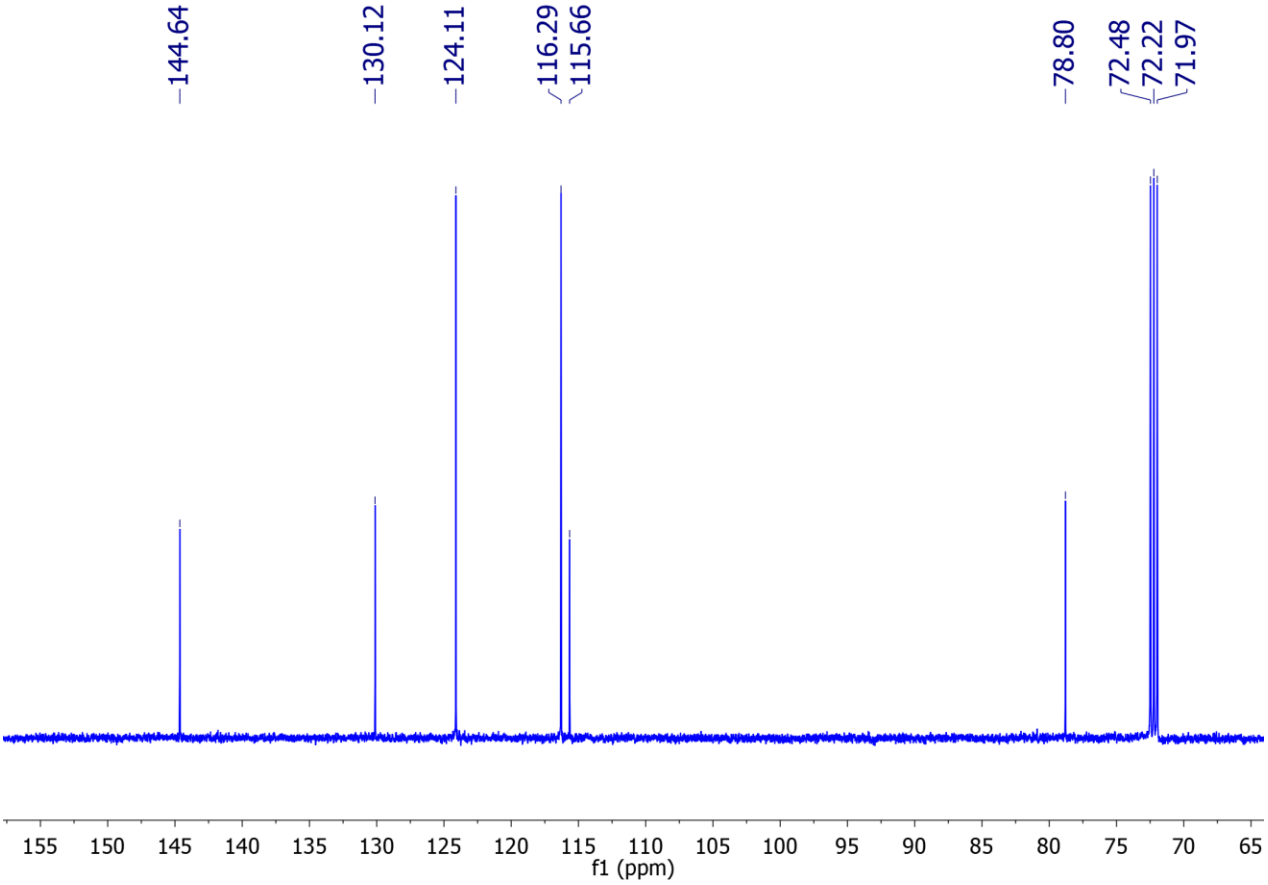

NMR spectra of “impure” sample:

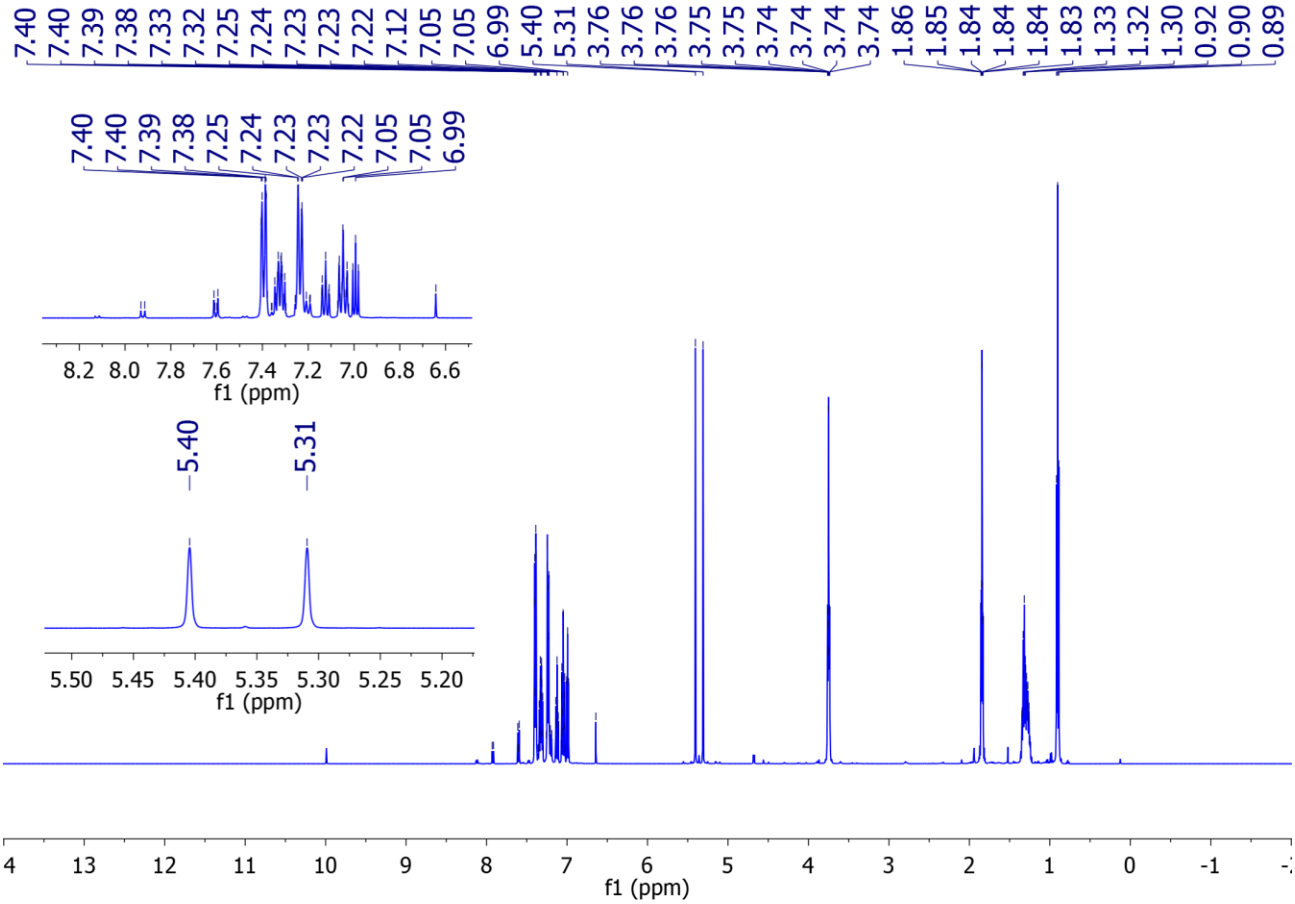

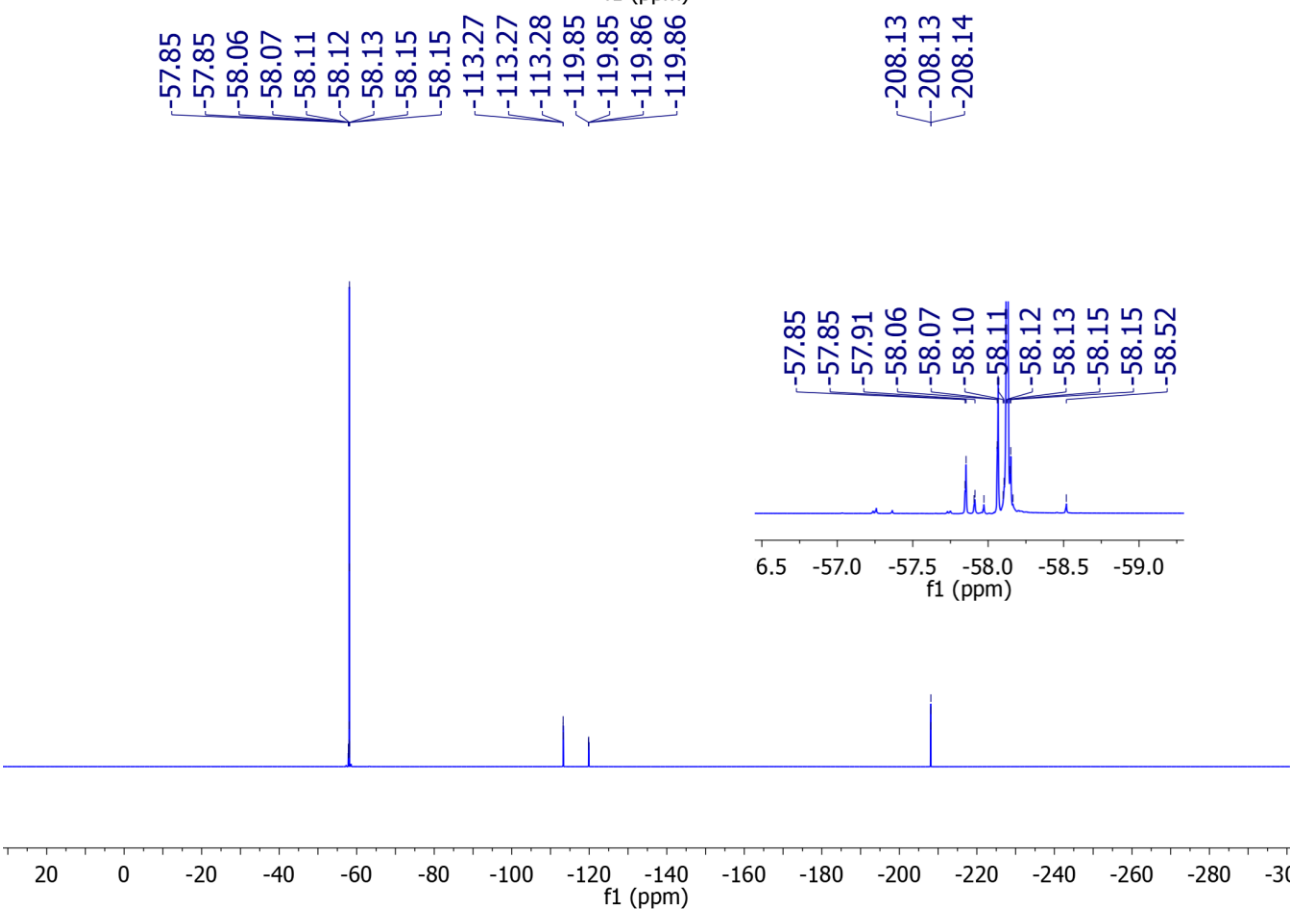

(b) Compound **1**[82, 83] (reaction A)

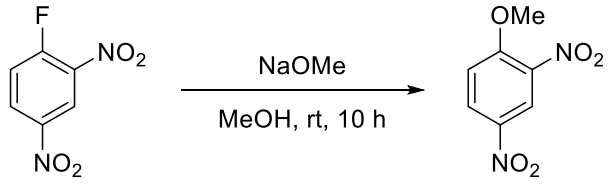

1 **2**

0% conversion:
Pure starting material from Alfa was used as received.

High conversion:

To a dry 100 mL flask was added 2,4-dinitrofluorobenzene (1.489 g, 8 mmol, 1 equiv) and naphthalene (internal standard, 406 mg) in MeOH (16 mL). A small aliquot (0.1 mL) was withdrawn for later HPLC analysis. Sodium methoxide (0.5 M in MeOH, 14.0 mL, 0.875 equiv) was added dropwise (over more than 15 minutes). The reaction was stirred at room temperature for 10 hours. Another small aliquot (0.1 mL) was taken for HPLC analysis. Conversion (86.4%) was determined on crude material by HPLC by comparing the ratio change in starting material and naphthalene (before and after reaction). The reaction mixture was concentrated *in vacuo* and the resulting residue was purified by flash column chromatography (gradient elution from 0 to 25% EtOAc/hexanes). Only unreacted **1** was recovered as a colorless oil (202 mg, 12.7%).

Calibration of naphthalene and dinitrofluorobenzene for HPLC analysis (A: naphthalene; B: 2,4-dinitrofluorobenzene):

7 different samples were prepared. In each sample, the concentration of A was held constant (0.5 mg/mL) but the concentration of B was varied from 0.0625 to 5.625 mg/mL. The integral ratio of B and A plotted against the known concentration of B. A linear correlation (R^2 = 0.9998) was observed, which implies that the response factor of B does not change over this range of concentrations.

	concentration of B	ratio (B/A)
Sample 1	5.625	23.6375
Sample 2	1.875	7.9059
Sample 3	1.25	5.2911
Sample 4	0.625	2.6162
Sample 5	0.375	1.8205
Sample 6	0.1875	0.9029
Sample 7	0.0625	0.2722

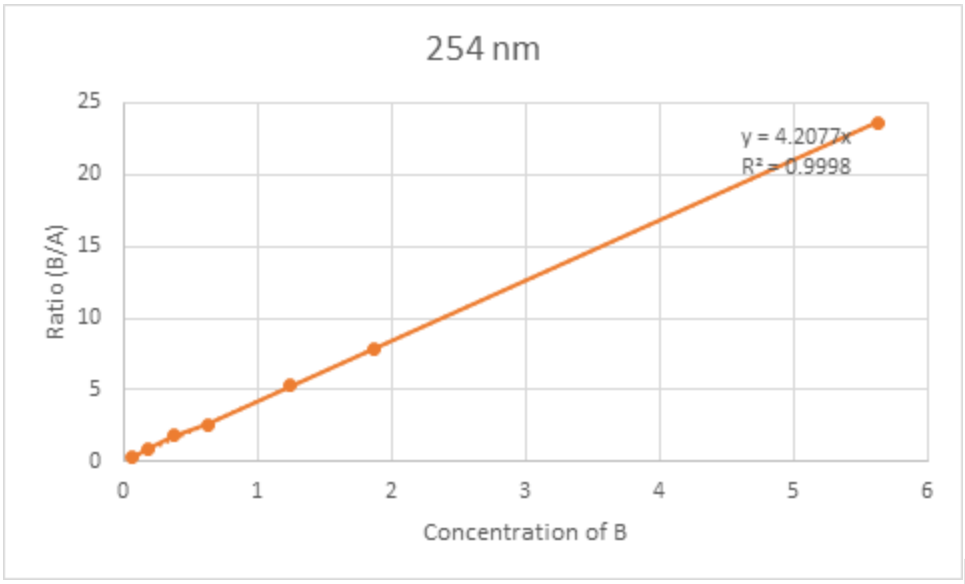

[A] = 0.5 mg/mL

Conditions: AD-H column, 10% isopropanol in hexanes, 1 mL/min, 20 min method, 254 nm
Retention time: T_A = 3.971 min; T_B = 15.391 min

Determination of the conversion of 2,4-dinitrofluorobenzene (**1**):

Two small aliquots (from before and after reaction) were diluted (concentration of A ~ 0.5 mg/mL) and measured by HPLC. Because [A] remains the same over the reaction, conversion can be determined by comparing the change in ratios (B/A):

	ratio (B/A)	
	before	after
	7.9444	1.1647
	7.9754	1.1637
average	7.9599	1.1642

Conversion: $F = 1 - (B/A)_t/(B/A)_0 = 1 - 1.1642/7.9599 = 0.8537$

NMR spectra of recovered starting material **1** (known compound)[82]:

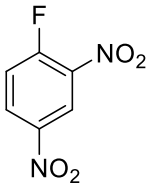

1

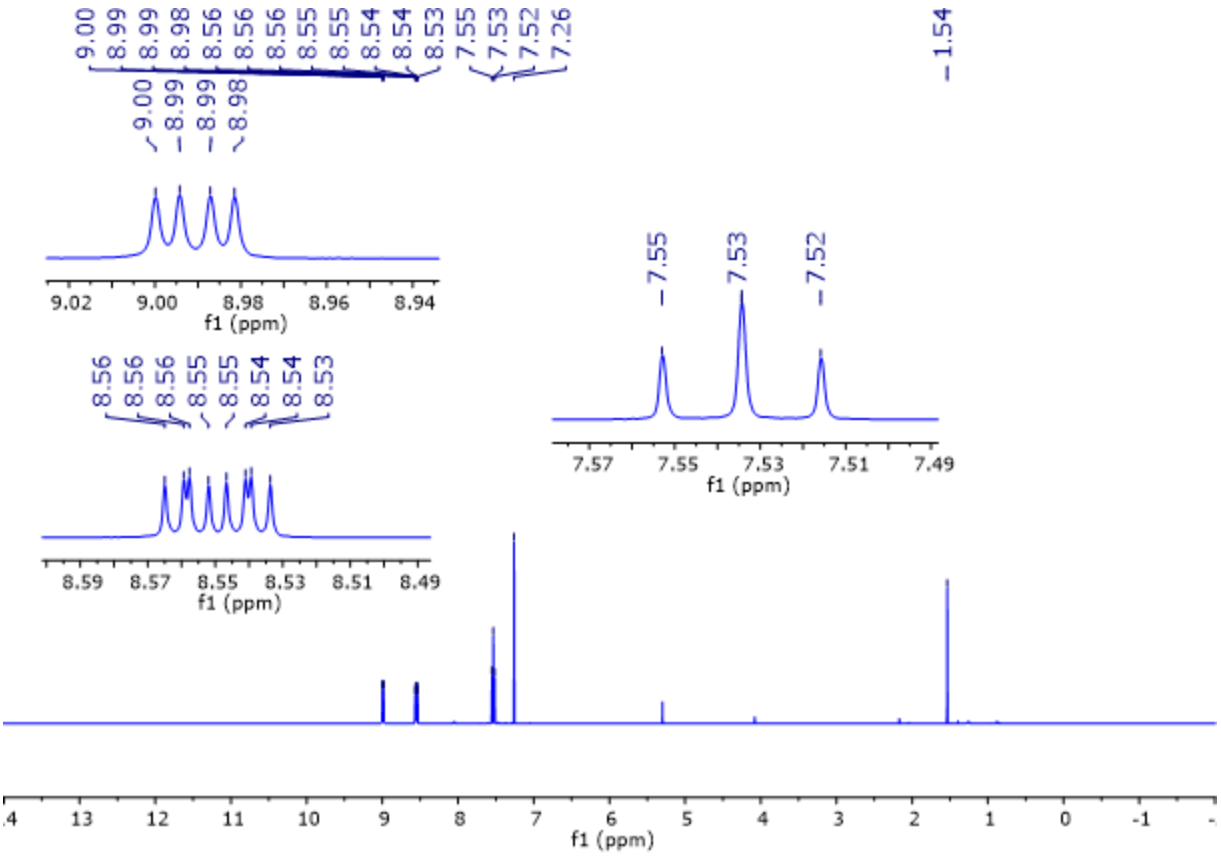
9.00
8.99
8.99
8.98
8.56
8.56
8.56
8.55
8.55
8.54
8.54
8.53
7.55
7.53
7.52
7.26
1.54
9.02
9.00
8.98
8.96
8.94
f1 (ppm)
7.55
7.53
7.52
7.57
7.55
7.53
7.51
7.49
f1 (ppm)
8.59
8.57
8.55
8.53
8.51
8.49
f1 (ppm)
f1 (ppm)

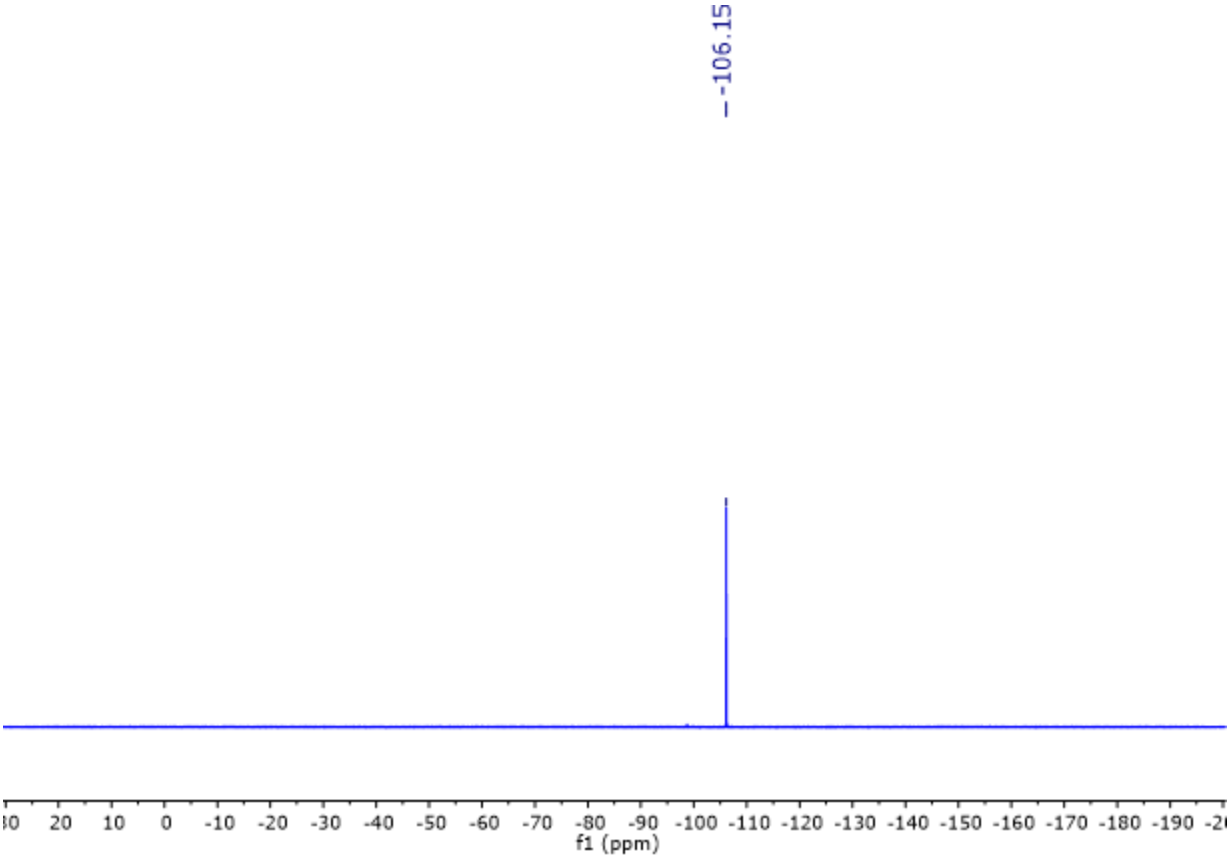
-106.15
f1 (ppm)

NMR spectra of pure starting material **1** (for 0% conversion sample, used as received):

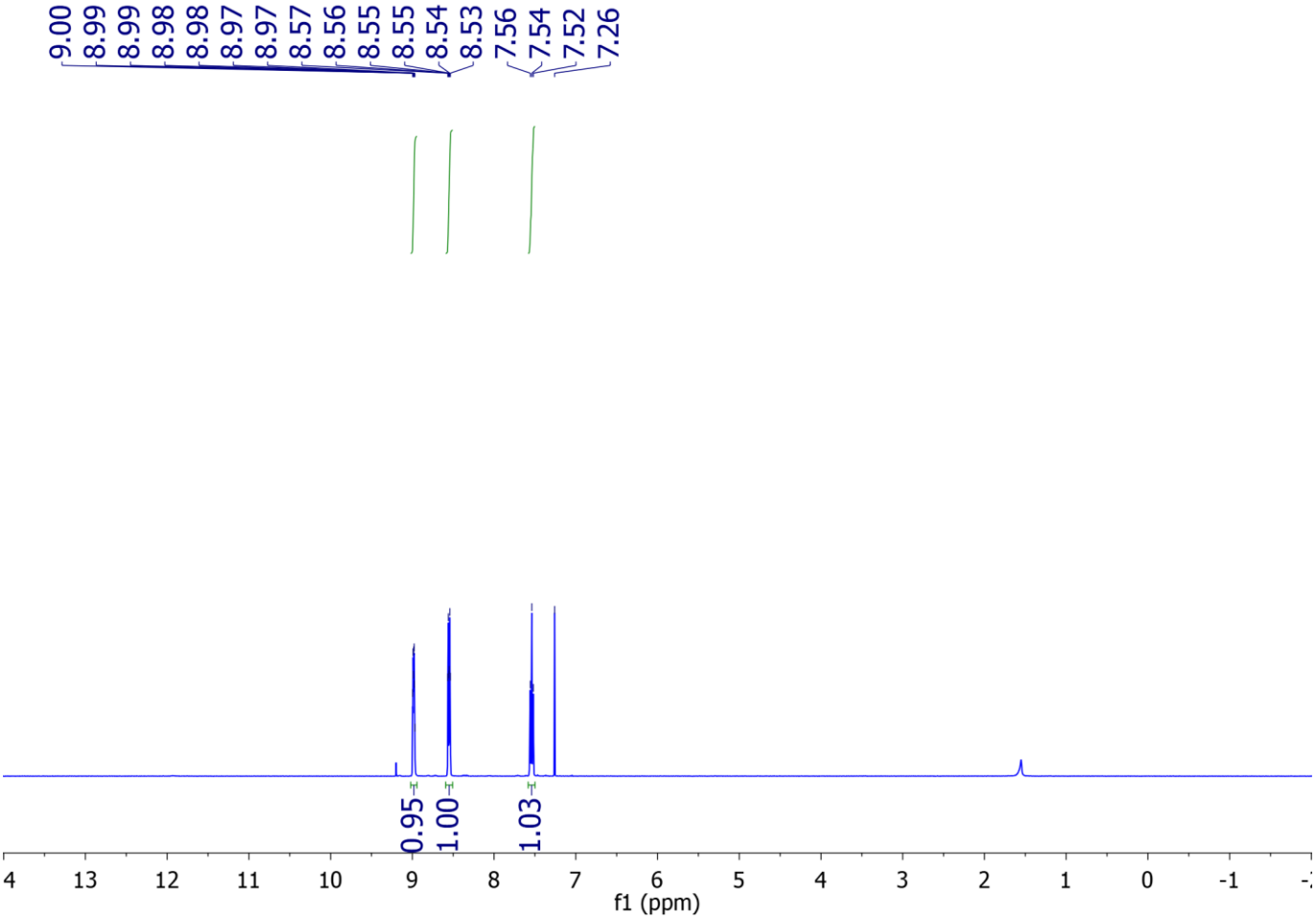

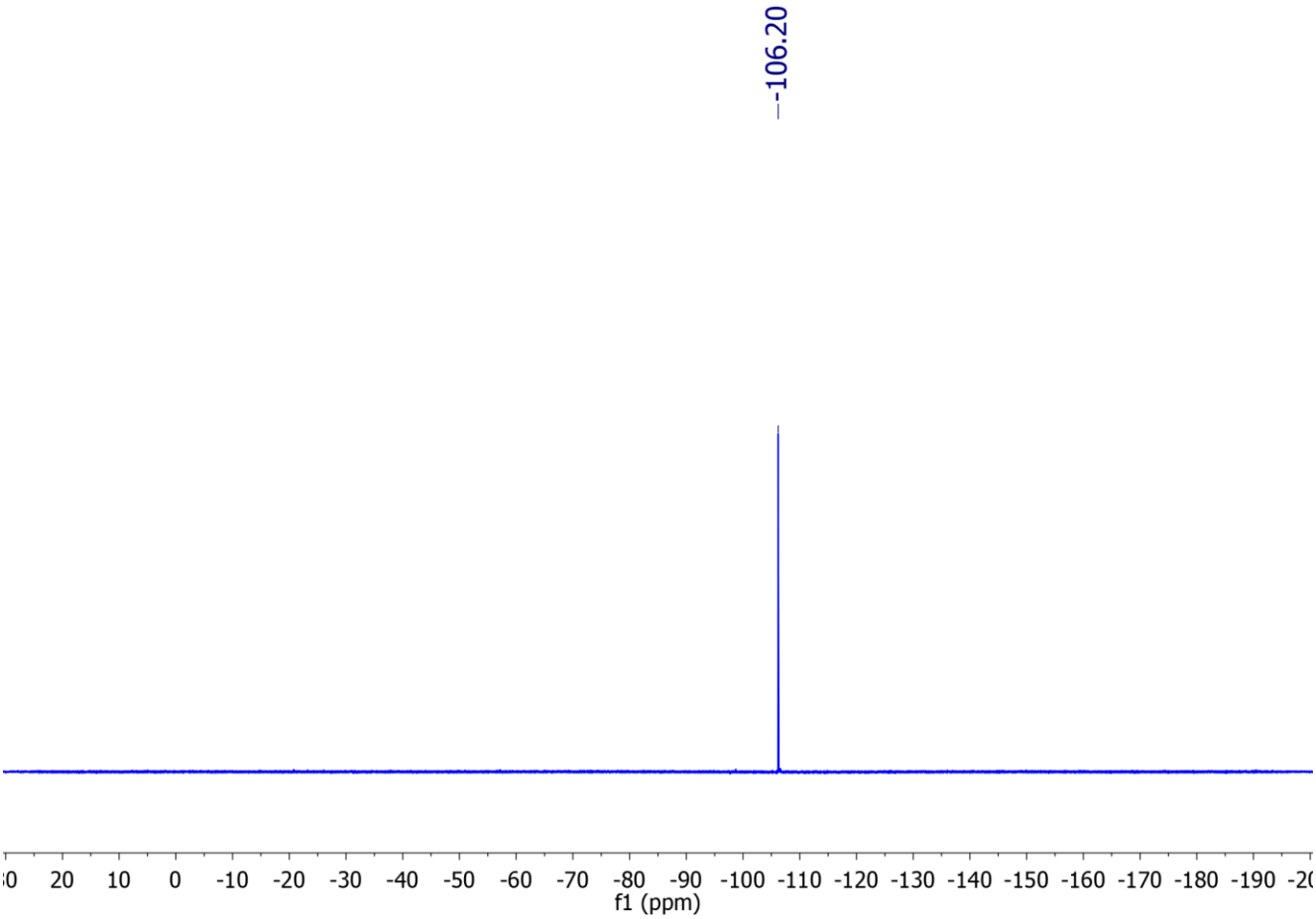
-106.20
30 20 10 0 -10 -20 -30 -40 -50 -60 -70 -80 -90 -100 -110 -120 -130 -140 -150 -160 -170 -180 -190 -20
f1 (ppm)

NMR spectra of **2**[83]:

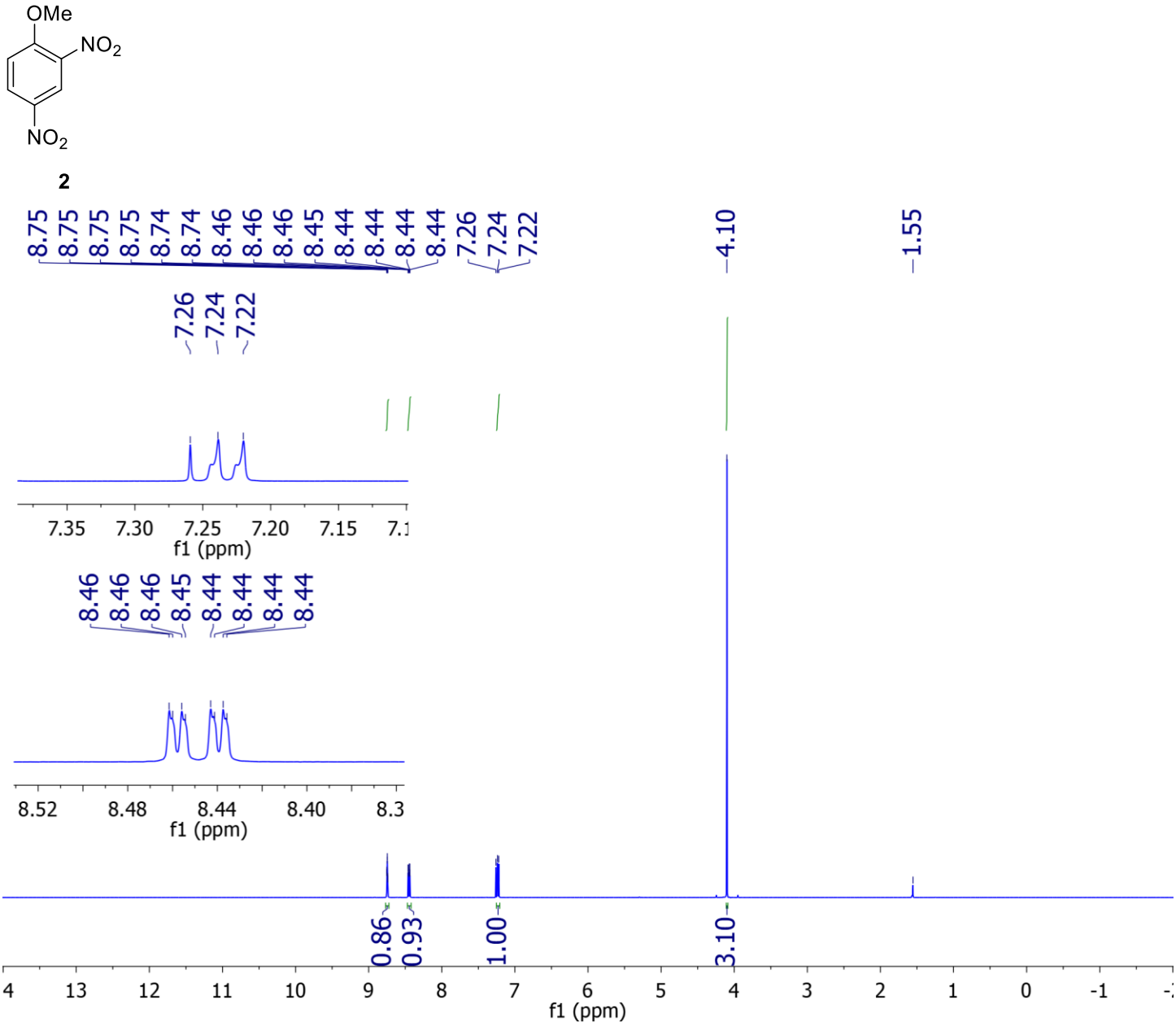

2

(c) Compound **4**[84] (reaction B)

Full conversion:

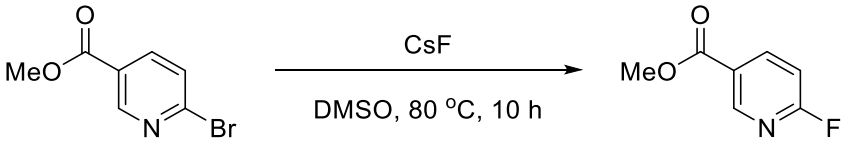

3 **4**

To a dry 50 mL flask was added CsF (1.215 g, 8 mmol, 4 equiv) and methyl 6-bromonicotinate (432 mg, 2 mmol, 1 equiv) in DMSO (10 mL). The mixture was stirred at 80 °C for 10 hours. The reaction mixture was diluted with Et_2O (200 mL) and washed with water (3x300 mL) and brine (150 mL). The organic phase was

dried over $MgSO_4$ and concentrated *in vacuo*. The crude product was further purified by flash column chromatography (gradient elution: 0% to 20% EtOAc/hexanes) to afford methyl 6-fluoronicotinate as a white solid (287 mg, 93%).

Partial conversion:

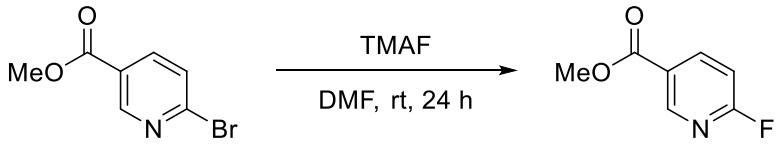

3 **4**

To a dry 50 mL flask was added methyl 6-bromonicotinate (used as received, 864 mg, 8 mmol, 1 equiv) and TMAF (765 mg) in 10 mL of DMF. The mixture was stirred at room temperature for 24 hours. After reaction, a certain amount of *p*-difluorobenzene was added as internal standard and the conversion (25.8%) of starting material was determined by quantitative proton-decoupled ^{19}F spectra (delay = 30 sec with tof set to the midpoint between the fluorine peaks of the internal standard and the product; correction factor: s = 0.93, see below). The reaction mixture was diluted with Et_2O (200 mL) and washed with water (3x300 mL) and brine (150 mL). The organic phase was dried over $MgSO_4$ and concentrated *in vacuo* to yield a mixture of starting material and product. The mixture of starting material and product was subjected to Kugelrohr distillation to afford a product-enriched mixture (white solid, 180 mg, **4**:**3** = 5:3). A new mixture (80 mg of **4** and 100 mg of **3**) was made from this product-enriched mixture (153 mg) and pure **3** (27 mg) and then used directly in KIE measurement. To minimize variations in response factors, unreacted starting material **3** (100 mg) was added to the pure material **4** generated in the full conversion reaction (80 mg) to create a mixture of identical composition for KIE analysis.

Calibration of internal standard and **4** in quantitative ^{19}F NMR:

p-Difluorobenzene (13.9 mg) and **4** (28.9 mg) were dissolved in $CDCl_3$ (0.6 mL) and a quantitative ^{19}F NMR spectrum was obtained. The integral ratio of internal standard and **4** was 1.2143, compared with a theoretical value of [(13.9/114.09)*2]/(28.9/155.13) = 1.3080. Therefore, the correction factor is s = 1.2143/1.3080 = 0.9284.

NMR spectra of **4** (known compound)[84]**:**

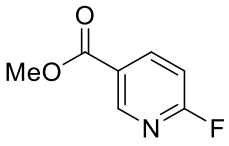

4

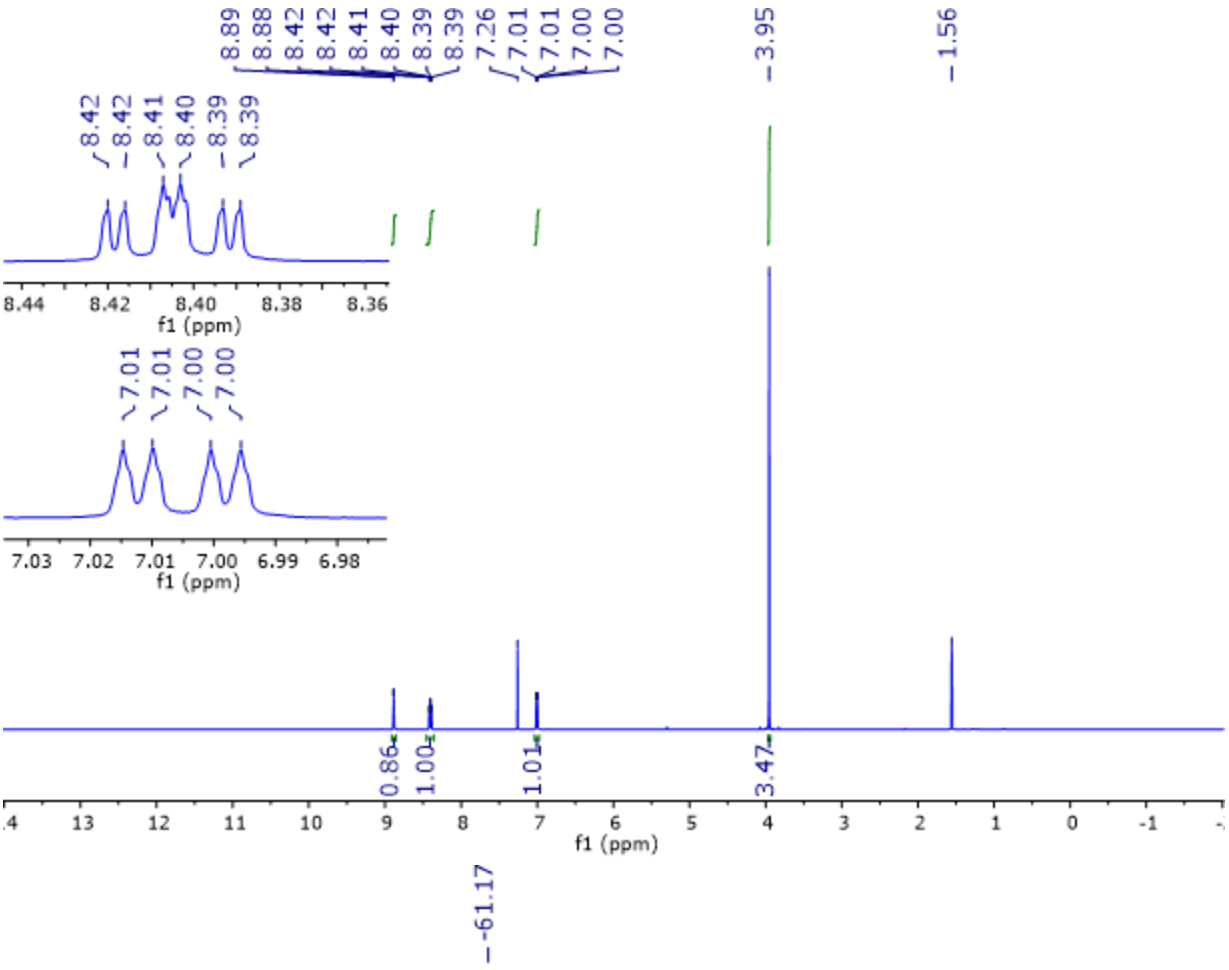
8.89
8.88
8.42
8.42
8.41
8.40
8.39
8.39
7.26
7.01
7.01
7.00
7.00
3.95
1.56
8.42
8.42
8.41
8.40
8.39
8.39
8.44 8.42 8.40 8.38 8.36
f1 (ppm)
7.01
7.01
7.00
7.00
7.03 7.02 7.01 7.00 6.99 6.98
f1 (ppm)
0.86
1.00
1.01
3.47
13 12 11 10 9 8 7 6 5 4 3 2 1 0 -1
f1 (ppm)

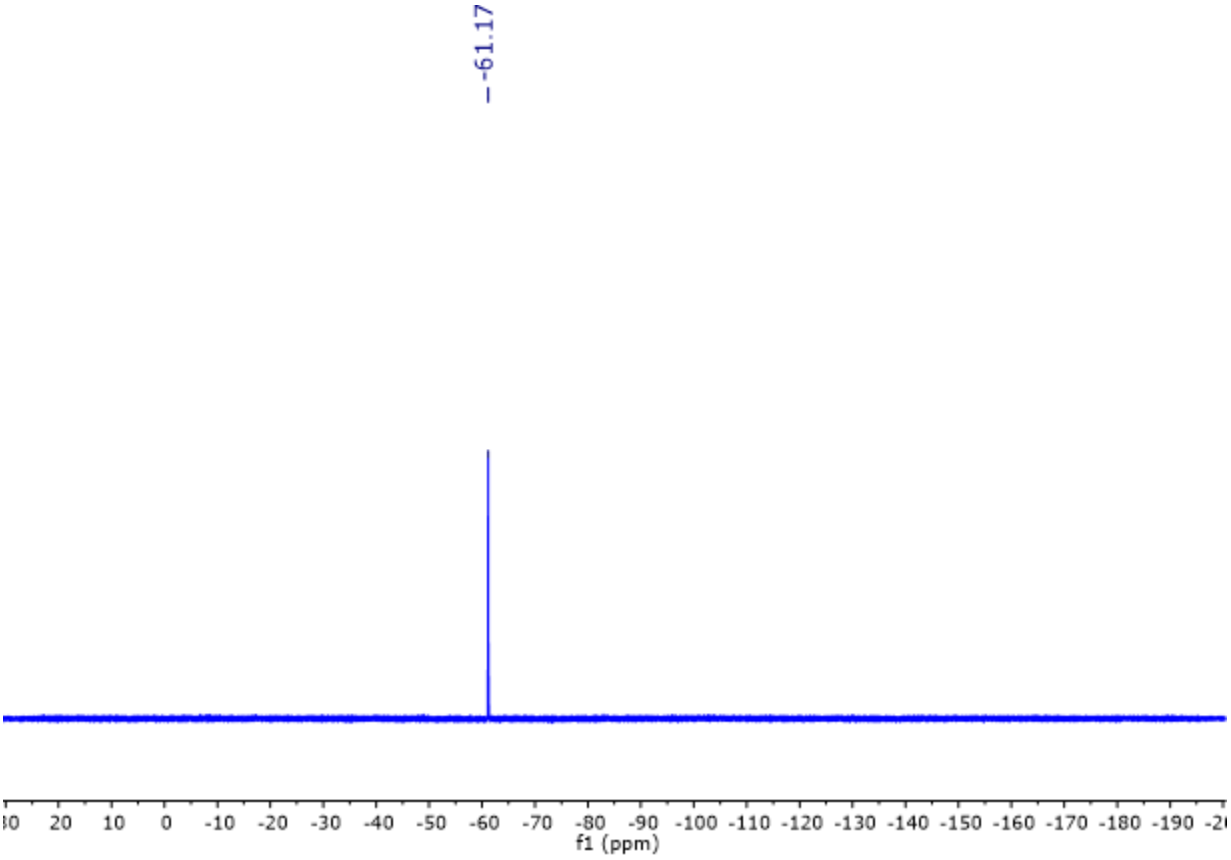
-61.17
20 10 0 -10 -20 -30 -40 -50 -60 -70 -80 -90 -100 -110 -120 -130 -140 -150 -160 -170 -180 -190
f1 (ppm)

NMR spectra of product-enriched mixture (100 mg of **3** + 80 mg of **4**):

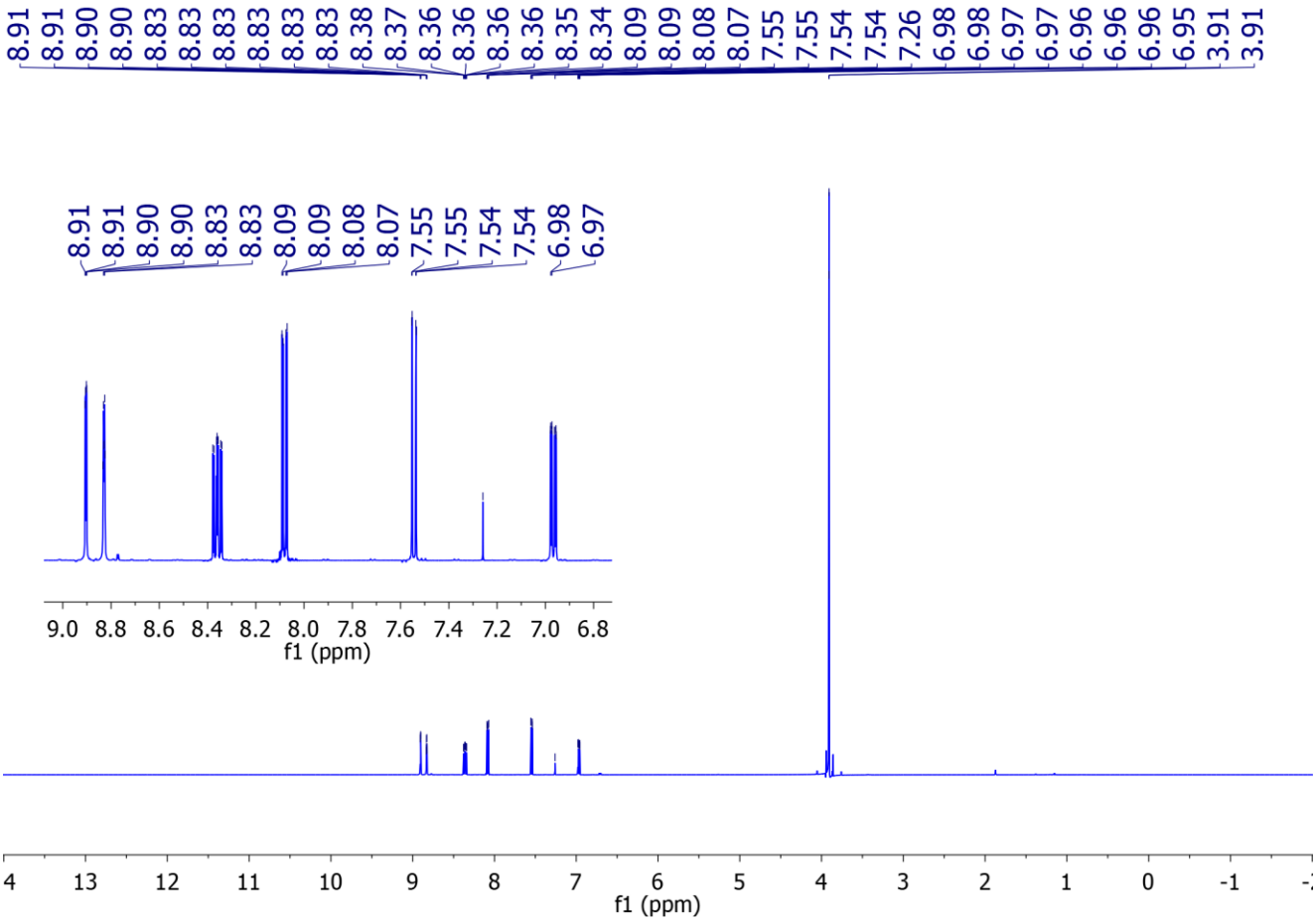

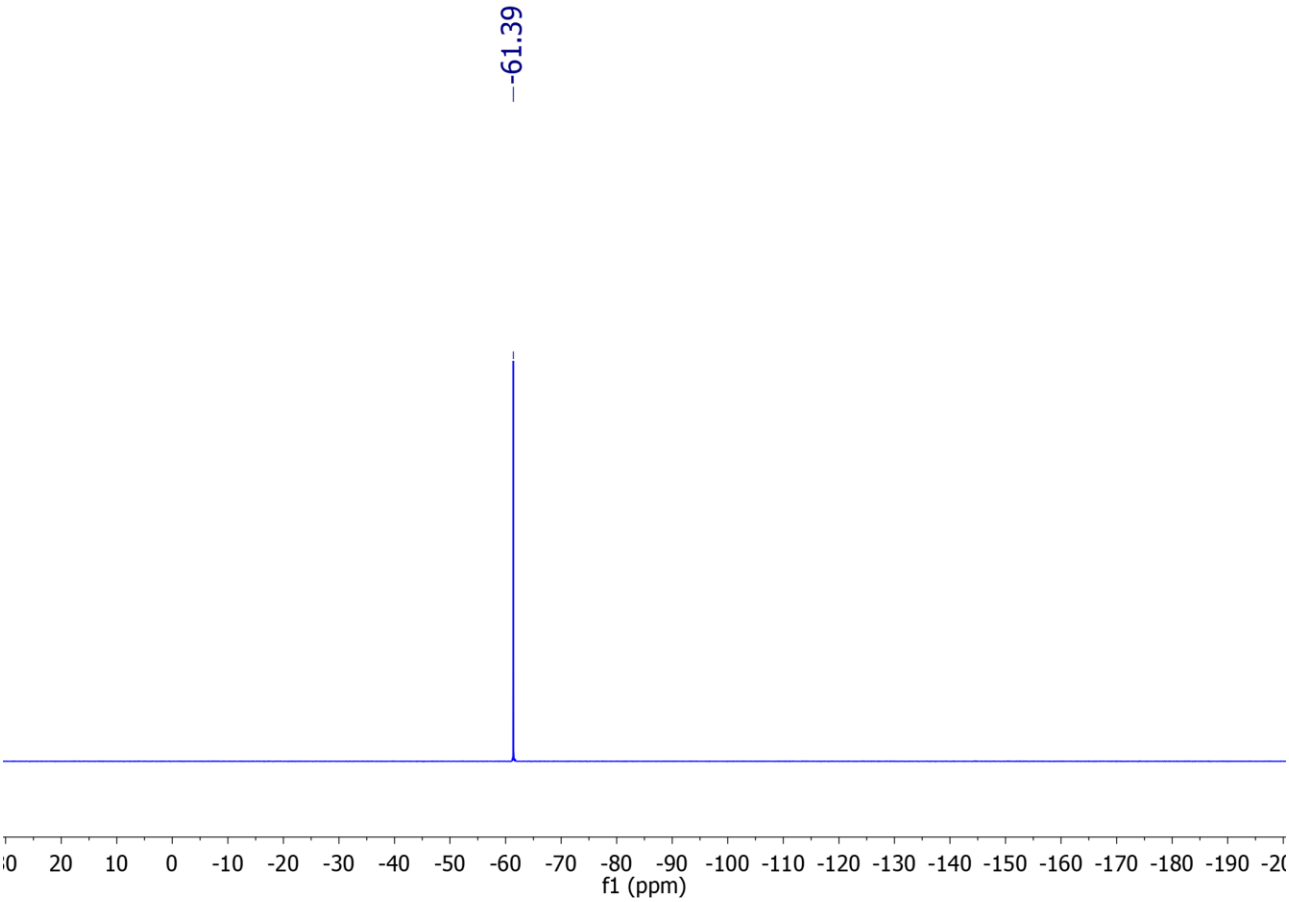

(d) Compound **1**[85] (reaction C)

Full conversion:

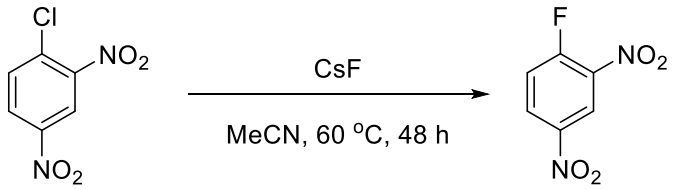

5 **1**

To a dry 50 mL flask was added CsF (1.215 g, 8 mmol, 4 equiv) and 2,4-dinitrochlorobenzene (405 mg, 2 mmol, 1 equiv) in MeCN (10 mL). The mixture was stirred at 60 °C for 48 hours. The solvent was removed under vacuum and the reaction mixture was purified by flash column chromatography (gradient elution: 0% to 20% EtOAc/hexanes) to afford **1** as a colorless oil (345.6 mg, 93%).

Partial conversion:

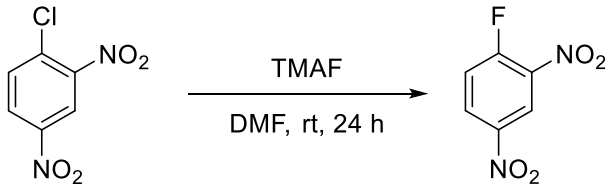

5 **1**

To a dry 50 mL flask was added 2,4-dinitrochlorobenzene (used as received, 1.013 g, 5 mmol, 1 equiv) and TMAF (118 mg). DMF (8 mL) was added and the mixture was stirred at room temperature for 24 hours. After reaction, a certain amount of *p*-difluorobenzene (28.9 mg) was added as internal standard and the conversion (11.5%) of starting material was determined by quantitative proton-decoupled ^{19}F spectra (delay = 30 sec with tof set to the midpoint between the fluorine peaks of the internal standard and the product; correction factor: s = 1.06, see below). The reaction mixture was diluted with 200 mL Et_2O and washed with water (3x200 mL), and brine (150 mL). The organic phase was dried over $MgSO_4$ and concentrated *in vacuo*. The resulting residue was purified by flash column chromatography (gradient elution: 0% to 25% hexanes/ethyl acetate) to afford the product as a colorless oil (92 mg, 10%).

Calibration of internal standard and **1** in quantitative ^{19}F NMR:

p-Difluorobenzene (15.6 mg) and **1** (22.6 mg) were dissolved in $CDCl_3$ (0.6 mL) and a quantitative ^{19}F NMR spectrum was obtained. The integral ratio of internal standard and **1** was 2.3972, compared with a theoretical value of [(15.6/114.09)*2]/(22.6/186.1) = 2.2519. Therefore, the correction factor is s = 2.3972/2.2519 = 1.0645.

NMR spectra of **1** (known compound)[85]:

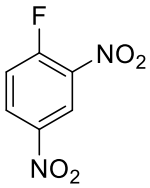

1

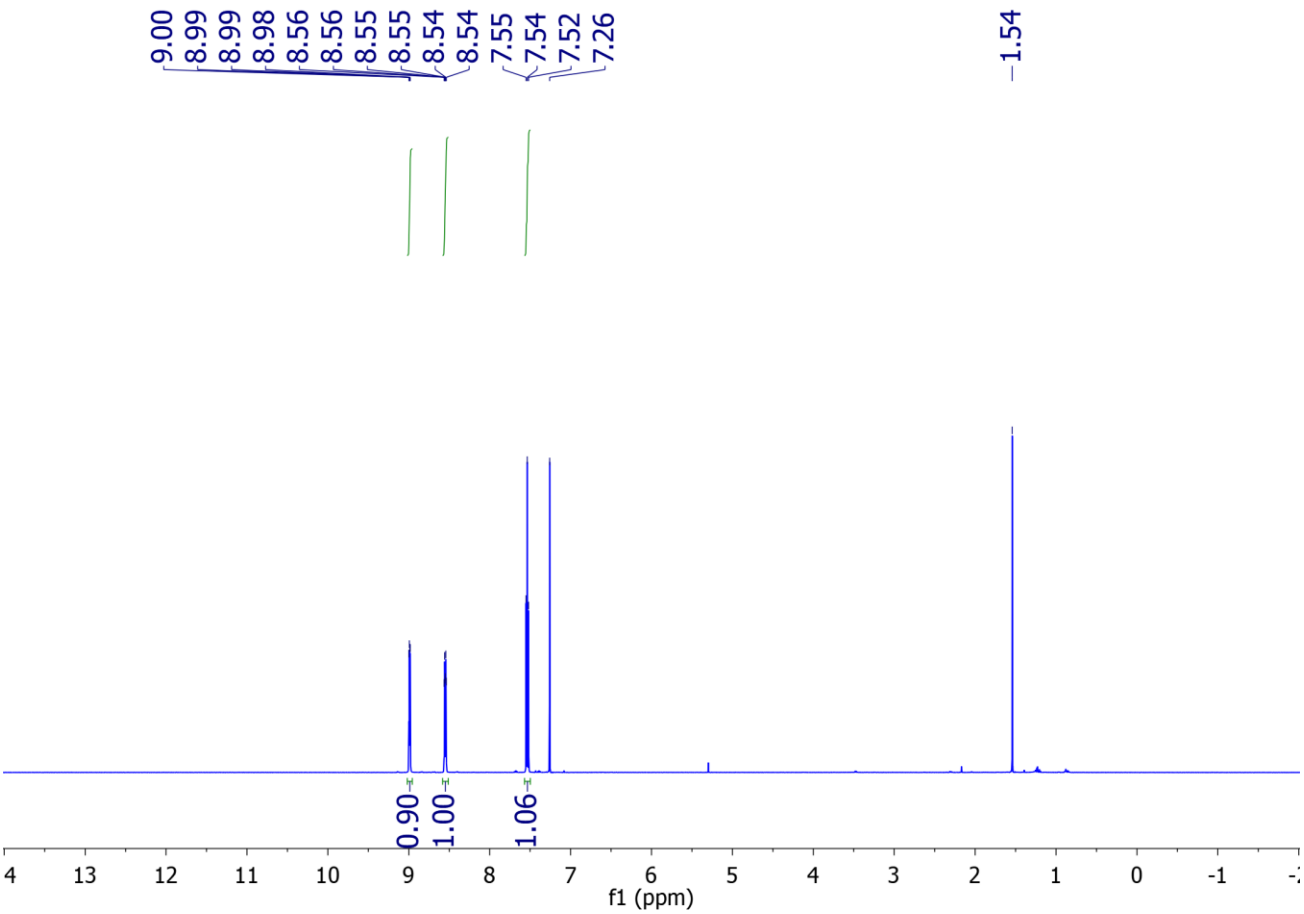
9.00
8.99
8.99
8.98
8.56
8.56
8.55
8.55
8.54
8.54
7.55
7.54
7.52
7.26
1.54
0.90
1.00
1.06
f1 (ppm)

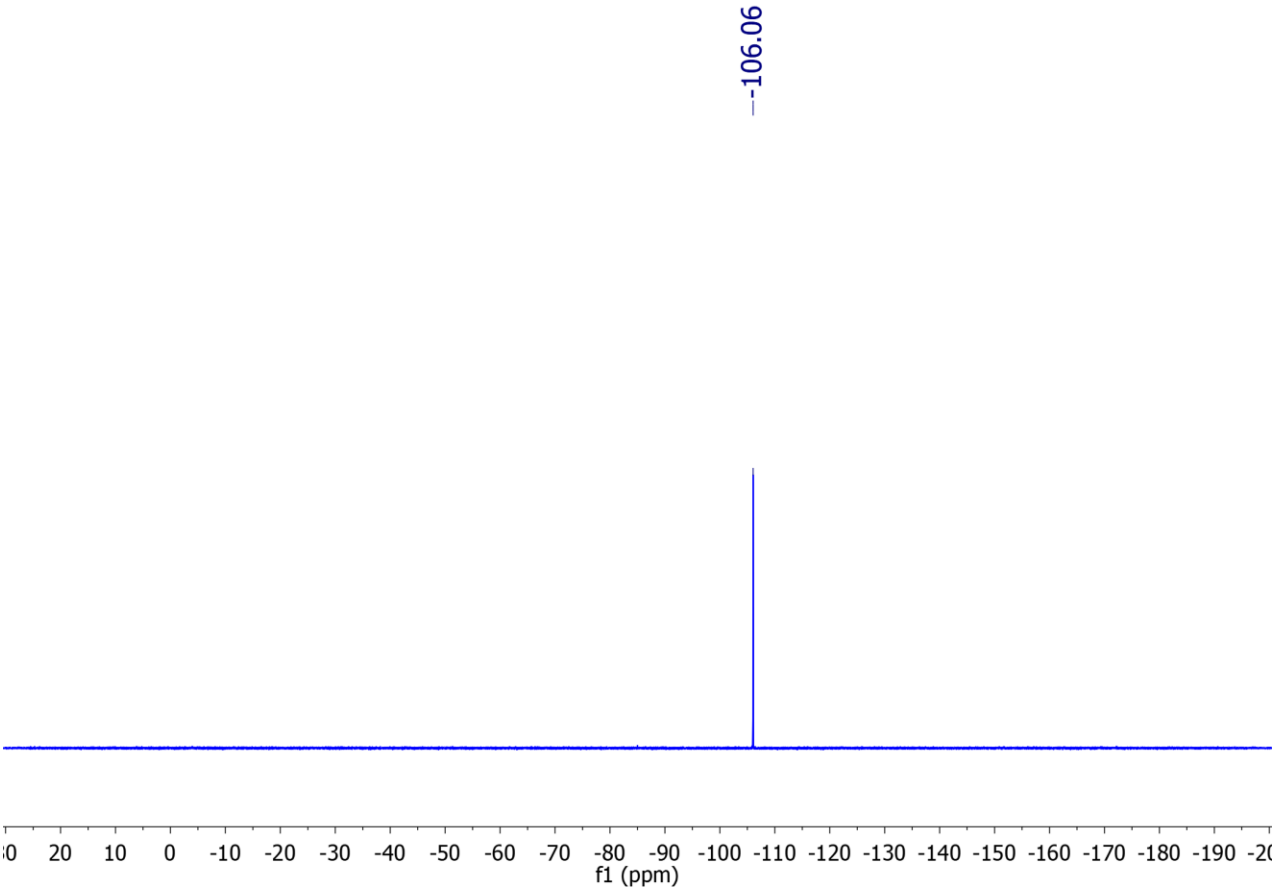
-106.06
f1 (ppm)

3. Kinetic Isotope Effects

a. MQF Pulse Sequence

The MQF pulse sequence was adjusted slightly based on whether the molecule being studied contained one or two fluorine atoms.

Procedure for **7** (sequence A):

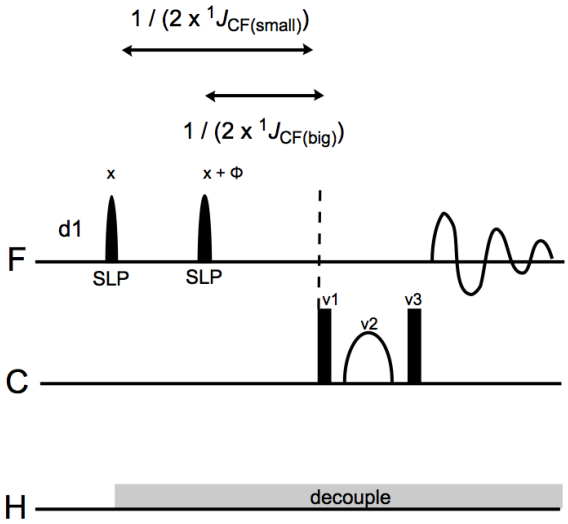

Because of the large ^{19}F chemical shift range, a standard 90 degree pulse is insufficient to excite both fluorine resonances. Additionally, the CF_3 and CF groups have significantly different coupling constants ($^1J_{CF}$). For maximum performance, the group with the smaller coupling constant (CF) was excited first with a low-power shifted laminar square pulse (SLP).[86] Subsequent excitation of the CF_3 group leads to generation of an anti-phase states on both groups with no relative phase shift and nearly identical excitation efficiency.

The transmitter offset was set to the midpoint of the two fluorine resonances. Square pulses using 86 steps and a total duration of 43 us were used at +/– 35285.6 Hz with a starting phase of 200 degrees (Φ) for the latter pulse. This phase shift is necessary to correct for the delay between the first and second SLPs. The rest of the sequence transfers the antiphase magnetization to multiple quantum coherence and back. Phase cycling was used to select for this coherence transfer pathway (see below). Extensive testing showed that refocusing of the anti-phase magnetization causes a sensitivity loss due to relaxation, and provides no benefit. Carbon decoupling is counterproductive, as the residual parent and satellite peaks becomes very close together. Additionally, gradients cause a loss of sensitivity, both due to the loss of one coherence transfer pathway and diffusion.

A hard pulse was utilized as the inversion pulse on the carbon channel. Although broadband inversion pulses (BIPs) were tested, these provided inferior. Standard WALTZ-16 inverse-gated decoupling on the proton channel with the decoupler modulation frequency was set to the reciprocal of the proton 90° pulse width at the decoupler power. The “dmfadj” macro was used to ensure an integer number of composite pulse decoupling cycles. Decoupling was performed at the maximum possible power (48 dB) and was calibrated very precisely to minimize decoupling sidebands. Decoupling was used on the proton channel during both pulses and acquisition (dm = ‘nny’). 262K complex points were collected in blocks of 32 scans. Longitudinal (T_1)

relaxation times were determined by inversion recovery (T_1 ~ 4s) and the repetition delay was set to greater than 5*T_1.

Procedure for all other compounds (sequence B):

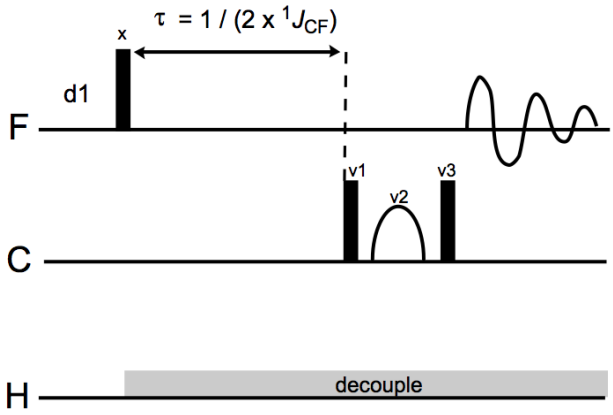

When only one fluorine group must be quantitated, the procedure was much simpler. Instead of utilizing two selective excitation pulses, a single hard fluorine pulse was utilized with the transmitter offset centered on the peak of interest. The rest of the procedure was common to both one- and two-fluorine molecules.

Phase Cycle:

A 32-step phase cycle was used (0=x, 1=y, 2=–x, 3=–y) to select for transfer to multiple quantum coherence and remove refocusing inefficiencies.

First carbon 90° (v1) = {0,2,0,2, 1,3,1,3, 0,2,0,2, 1,3,1,3, 0,2,0,2, 1,3,1,3, 0,2,0,2, 1,3,1,3}
Carbon 180° (v2) = {0,0,0,0, 0,0,0,0, 1,1,1,1, 1,1,1,1, 2,2,2,2, 2,2,2,2, 3,3,3,3, 3,3,3,3}
Second carbon 90° (v3) = {0,0,2,2, 1,1,3,3, 0,0,2,2, 1,1,3,3, 0,0,2,2, 1,1,3,3, 0,0,2,2, 1,1,3,3}
Receiver = {0,2,2,0, 0,2,2,0, 0,2,2,0, 0,2,2,0, 0,2,2,0, 0,2,2,0, 0,2,2,0, 0,2,2,0}

Sample MQF Spectra:

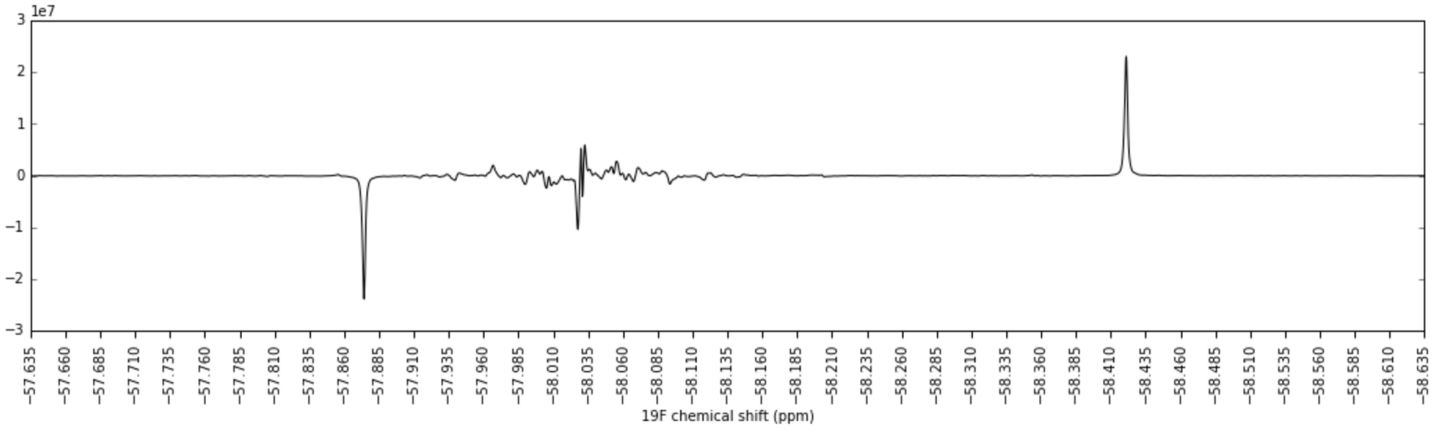

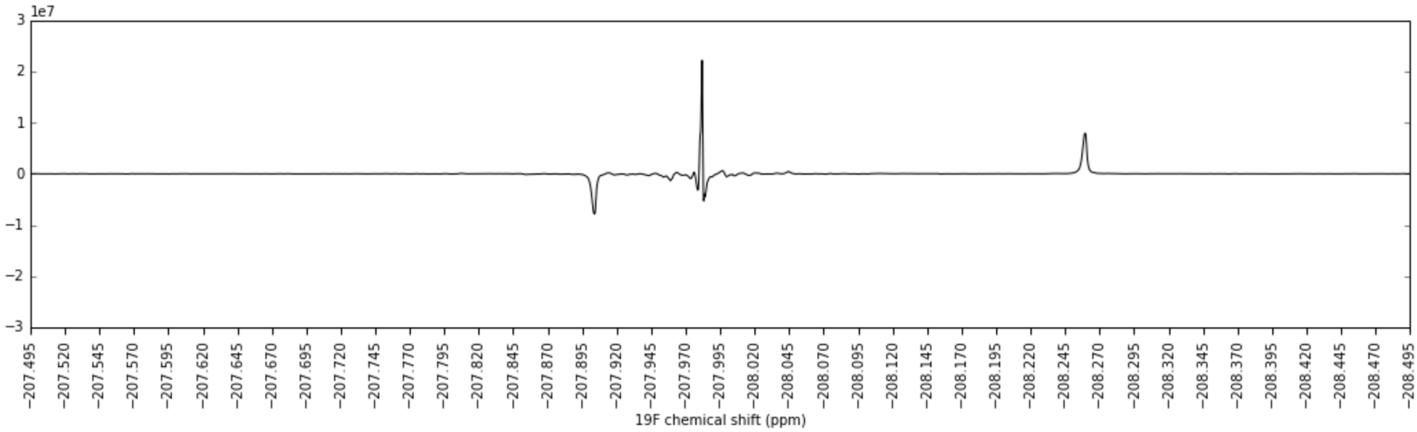

Top panel (32 scans, compound **7**): CF_3 group, bottom panel: CF group. The central peak (and noise) are what remains of the parent ^{12}C peak. All spectra are shown before baseline correction.

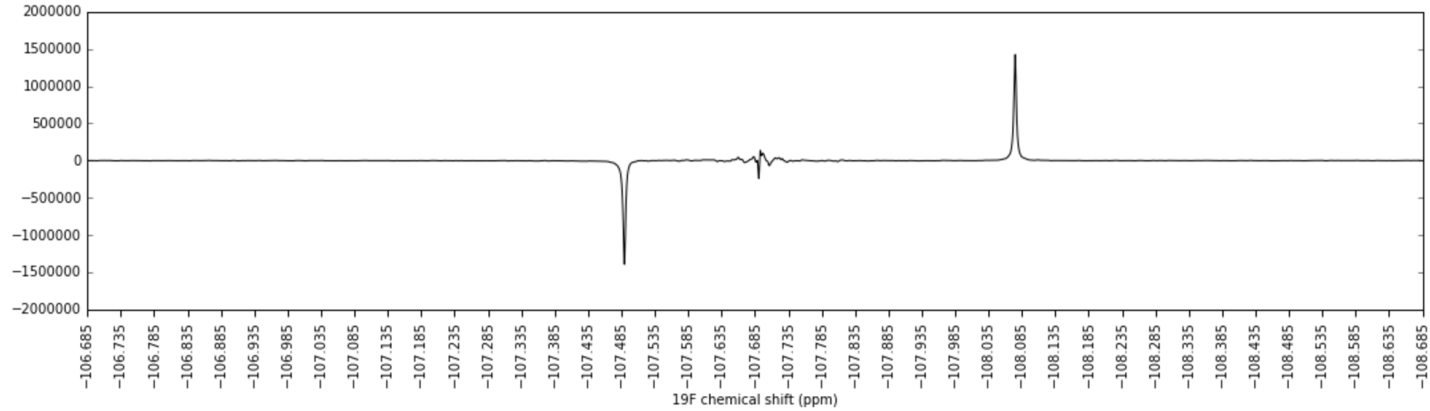

Compound **1** (32 scans).

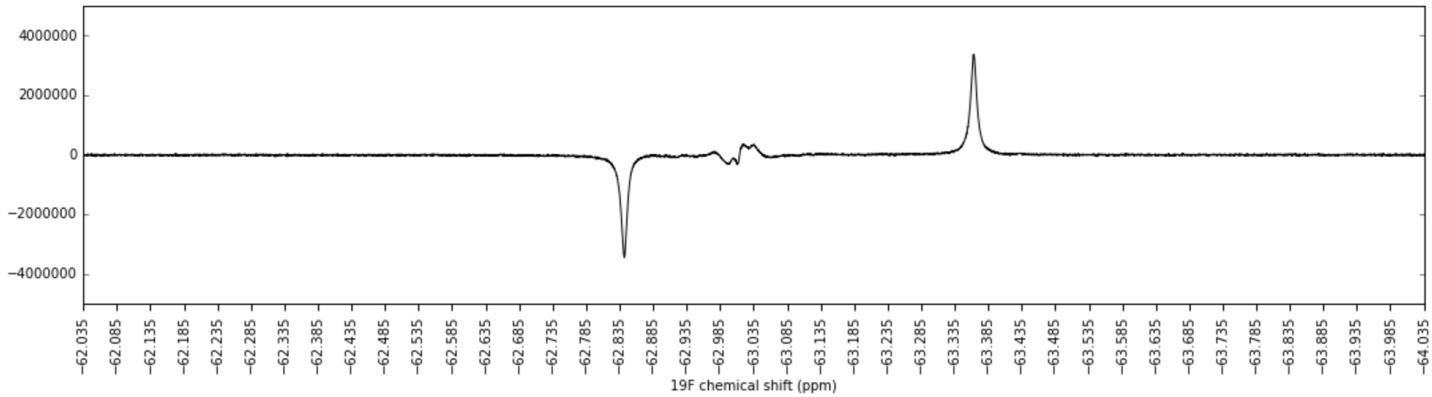

Compound **4** (32 scans). This reaction is more challenging because the starting material and product are inseparable. Thus, this is an MQF spectrum of a mixture of **3** and **4** (compound **3** is invisible because it does not contain fluorine). Additionally, the lines are more broad here (~10 Hz) due to quadrupolar broadening from the nitrogen.

b. Pulse Sequence Code

The following is Varian code for MQF sequence B. If sequence A is desired, the first pulse can be replaced with two pre-made SLPs and a delay.

```
/*
        MQF - Multiple Quantum Filtered 1D Fluorine Spectra
        This sequence gives antiphase peaks for the one-bond 13C satellites in 19F spectra.
        Notes:
        - Phase cycling removes the natural 12C peak.
        - Place the transmitter and decoupler offsets on resonance.
        - 1H decoupling should be used (WALTZ-16).
        - 13C decoupling should not be used.
        - nt should be a multiple of 2 and ideally a multiple of 32.
        Eugene Kwan and Harrison Besser, Harvard University, March 2018
    */

    #include <standard.h>
    #include <chempack.h>

    // phase table
    static int ph1[32] = {0,2,0,2, 1,3,1,3,  0,2,0,2, 1,3,1,3,  0,2,0,2, 1,3,1,3,  0,2,0,2, 1,3,1,3},
    // phase of first 19F 90
               ph2[32] = {0,0,0,0, 0,0,0,0,  1,1,1,1, 1,1,1,1,  2,2,2,2, 2,2,2,2,  3,3,3,3, 3,3,3,3},
    // phase of 13C 180
               ph3[32] = {0,0,2,2, 1,1,3,3,  0,0,2,2, 1,1,3,3,  0,0,2,2, 1,1,3,3,  0,0,2,2, 1,1,3,3},
    // phase of second 19F 90
               ph4[32] = {0,2,2,0, 2,0,0,2,  2,0,0,2, 0,2,2,0,  0,2,2,0, 2,0,0,2,  2,0,0,2, 0,2,2,0};
    // receiver phase

    pulsesequence()

    {
        double  j1cf = getval("j1cf"),                  // the size of the one-bond carbon-fluorine
    coupling constant in Hz
                tau = 1 / (2*j1cf),                     // the duration of the magnetization transfer
    delay in seconds
                pwx = getval("pwx"),                    // the duration of the 90 degree pulses on
    carbon in us
                pwxlvl = getval("pwxlvl"),              // the power level of the 90 degree pulses on
    carbon in dB
                invlvl = getval("invlvl"),              // the power level of the fluorine inversion
    pulse in dB
                invwidth = getval("invwidth");          // the length of the fluorine inversion pulse
    in us
        char    invshape[MAXSTR];                       // name of the inversion pulse shape
```

```
    getstr("invshape", invshape);

    // setup phase tables
    settable(t1, 32 , ph1);
    settable(t2, 32 , ph2);
    settable(t3, 32 , ph3);
    settable(t4, 32 , ph4);

    getelem(t1, ct, v1);
    getelem(t2, ct, v2);
    getelem(t3, ct, v3);
    getelem(t4, ct, oph);

    // delay period
    status(A);
    decpower(dpwr);
    delay(d1);

    // pulsing period
    status(B);
    obspower(tpwr);
    rgpulse(pw, zero, rof1, rof2);
    delay(tau);

    // transfer to MQC
    decpower(pwxlvl);
    decrgpulse(pwx, v1, rof1, rof2);

    // refocus dead time
    decpower(invlvl);
    decshaped_pulse(invshape, invwidth, v2, rof1, rof2);

    // transfer back to antiphase
    decpower(pwxlvl);
    decrgpulse(pwx, v3, rof1, rof2);
    decpower(dpwr);

    // acquire
    status(C);
}
```

c. Sample Preparation

For S_N2 reaction, three sets of four samples of **7** were prepared (300 mg of **7** in 350 µL of $CDCl_3$, 50 mg of **7** in 550 µL of $CDCl_3$, and 10 mg of **7** in 300 µL of $CDCl_3$). Two of the samples in each set were full conversion samples (F = 100%) with respect to the benzyl bromide starting material and two were partial conversion samples (F = 9%) with respect to the benzyl bromide starting material. The 300 mg and 50 mg samples were prepared in Wilmad 528-PP-9 NMR tubes and subsequently hermetically sealed under air at room temperature. The 10 mg samples were prepared in Shigemi tubes and sealed with parafilm to prevent solvent evaporation.

For S_NAr reaction A, four samples of **1** were prepared (50 mg of **1** in 550µL of $CDCl_3$). Two of the samples were starting material samples (F = 0%) and two were high conversion samples (F = 85.4% and 86.4%). Those samples were prepared in Wilmad 528-PP-9 NMR tubes and subsequently hermetically sealed under air at room temperature.

For S_NAr reaction B, four samples were prepared (80 mg of **4** and 100 mg of **3** in 550µL of $CDCl_3$). Two of the samples were full conversion samples (F = 100%) and two were low conversion samples (F = 21.0% and 25.8%). Those samples were prepared in Wilmad 528-PP-9 NMR tubes and subsequently hermetically sealed under air at room temperature.

For S_NAr reaction C, four samples of **1** were prepared (50 mg of **1** in 550µL of $CDCl_3$). Two of the samples were full conversion samples (F = 100%) and two were low conversion samples (F = 10.7% and 11.5%). Those samples were prepared in Wilmad 528-PP-9 NMR tubes and subsequently hermetically sealed under air at room temperature.

d. Data Acquisition

For the S_N2 reaction, the following parameters were used in data acquisition. The Singleton data were referenced to the 2 position of the phenyl ring (nt = 6 blocks of 32 scans, at = 2.779 s, d1 = 90 s). The MQF data refer to integrals from the right benzylic fluoride satellite. Those integrals were referenced to various varies depending on the method indicated. For the "^{13}C-^{19}F referenced" data, the reference peak was the right satellite of the trifluoromethyl group in the MQF spectrum. For the 50 mg test, the acquisition parameters were: nt = 8 blocks of 32 scans, at = 2.621 s, d1 = 30s. For the 10 mg test, the acquisition parameters were: nt = 16 blocks of 32 scans, at = 2.621 s, d1 = 30 s. For the "^{12}C-^{19}F referenced" data, the benzylic fluoride satellite peak in the ^{19}F spectrum was the reference peak. For the single pulse spectrum, the acquisition parameters were: nt = 8 blocks of 4 scans, at = 3.303 s, d1 = 30s. Typical experimental times were 17.5 mins for one block of MQF experiments, 55 mins for one block of Singleton experiments, and 2.5 mins for one block of ^{19}F experiments.

All KIEs for S_NAr reactions were measured using the "^{19}F referenced" MQF method. For reaction A, a randomized block design was used to acquire one set of standard ^{19}F spectra (8 blocks of 4 scans) and two sets of MQF spectra (8 blocks of 32 scans) using d1 = 15 s. For reaction B, a randomized block design was used to acquire three sets of standard ^{19}F spectra (8 blocks of 4 scans) and MQF spectra (15 blocks of 32 scans) using d1 = 15 s. For reaction C, a randomized block design was used to acquire one set of standard ^{19}F spectra (8 blocks of 4 scans) and two sets of MQF spectra (8 blocks of 32 scans) using d1 = 15 s.

All spectroscopic measurements were performed at 25 °C on a Varian Inova 500 MHz machine fitted with an indirect detection probe (HFC) and a gradient driver. Spinning was off for all experiments to minimize spinning sidebands. The XY shims were optimized using the ProShim feature in VNMRJ. The proton 90° pulse width was calibrated at both the transmitter and decoupler powers (63 dB and 48 dB, respectively) ensuring the transmitter was centered on the protons adjacent to the fluorine/carbon of interest. The carbon 90° pulse width was calibrated at the transmitter power (63 dB) with the transmitter placed in the middle of the spectra. This calibration required decoupling on both the proton (WALTZ-16 @ dpwr = 48 dB) and fluorine (CHIRP with pulse time ⅕ the largest J_{CF}) channels. The fluorine 90° pulse width was calibrated at both the transmitter and decoupler powers (63 dB and 48 dB, respectively) with the transmitter placed on resonance with the fluorine of interest for the former and in the middle of the spectrum for the latter.

e. Processing Procedure

NMR data were processed using Python and the nmrglue package (www.nmrglue.com). NMR data were collected in blocks of 32 scans in a single experiment using the array command (e.g., array('nt',6,32,0) would set up 6 blocks of 32 scans). (The Python program can be easily modified to deal with alternative input formats.) Each FID was zero-filled to four times the number of complex points, apodized with a line broadening of 0.25 Hz, and Fourier transformed. For each set of FIDs, one spectrum was manually referenced and phased. For the MQF spectra, regions of integration were defined with widths of 0.045 ppm for the CF_3 and 0.06 ppm for the CH_2F. For the ^{19}F spectra, the region of integration was defined with width 0.15 ppm. For the ^{1}H spectra, the region of integration was defined with a width of 0.08 ppm. The downfield member of the benzylic proton doublet was chosen as the reference peak. For the ^{13}C spectra, the regions of integration were defined with widths 0.12 ppm and 0.14 ppm. The regions were then centered individually on each peak. A first-order baseline correction was calculated by fitting a linear function to the non-signal regions and then subtracting it from the entire spectrum. In the case of the ^{19}F spectra, a second-order baseline correction was applied.

Signal to noise ratios were calculated for each peak by dividing the signal intensity at half height by the root-mean-square deviation of the signal in a noisy region. Integrals were simply calculated by summing the signal intensities over the peak regions. After the integrals were obtained, KIEs and their associated errors were calculated using an Excel document (in the provided archive file).

f. S/N Comparison

The performance of the MQF and traditional ^{13}C methods was compared using a typical sample of **7** (50 mg, 9% conversion). The data below shows the average S/N over repeated acquisitions of 32 scans (MQF: at = 2.621 s, d1 = 30 s, ^{13}C: at = 2.779 s, d1 = 90 s).

	MQF	MQF	^{13}C	^{13}C	^{13}C	^{13}C	^{13}C	^{13}C
Atom	^{13}C-F_3	^{13}C-H_2F	*i*-O$^{13}CF_3$	*i*-$^{13}CH_2F$	*o*-OCF_3	*o*-$^{13}CH_2F$	$^{13}CF_3$ quat	$^{13}CH_2F$
S/N	792	220	41	40	73	73	10	22

The theoretical increase in sensitivity is $½(\gamma_F/\gamma_C)^{5/2} \approx 13.6$. The factor of one half accounts for the fact that only one satellite is being integrated. A true comparison of the MQF and ^{13}C methods, however, is more

complicated. The theoretical number given above assumes that the probe being used is equally sensitive to both kinds of signals. However, these numbers correspond to a inverse-detection probe, which is approximately two times less sensitive to carbon signals. Nonetheless, it is a fair comparison, because such a setup is required for proton and fluorine decoupling. (To our knowledge, direct-detection H/F/C probes are not available.) The analysis above also assumes that the intrinsic sensitivity of each peak is the same. However, as can be seen in the carbon spectrum numbers above, the fluorine-bearing peaks have significantly lower sensitivity, perhaps due to transverse relaxation effects (these delays allow for complete longitudinal relaxation). The factor of 13.6 also assumes no transverse relaxation losses during either sequence. (In reality, the MQF sequence takes about 3 ms longer than the carbon sequence. This time has been minimized to maximize sensitivity.) Other considerations include the reduced relaxation time of fluorine over carbon and the ability to reduce noise by referencing to a large ^{12}C peak. Therefore, while a comparison of these values provides an indication of sensitivity, the agreement between the theoretical and experimental S/N advantages is to some extent fortuitous. However, it is clear from the data that the MQF method is a significant improvement, and the random error in the integrals so obtained is very much reduced.

g. Calculation of KIEs and Error Bars

For product-based KIE analyses, the KIE was calculated according to:

$$\frac{\log(1-F)}{\log\left(1-F\frac{R}{R_0}\right)}$$

where F is the fractional conversion, R is the $^{13}C/^{12}C$ ratio in the product, R_0 is the ratio in the starting material, and log refers to the natural logarithm. R_0 is experimentally determined by taking the reaction to 100% conversion and quantitating product because this minimizes errors caused by deviations in response factors. The propagated error in this formula was calculated in Mathematica (using https://github.com/FlashTek/mathematica-error-propagation):

```
TeXForm[FullSimplify[ErrorProgataionPrintFormula[
 Log[1 - F]/Log[1 - F*R/Subscript[R, 0]], {F, R, Subscript[R, 0]}]]]
```

$$\sqrt{\frac{(F-1)^2F^2R^2\log^2(1-F)\sigma_{R_0}^2+(F-1)^2F^2R_0^2\log^2(1-F)\sigma_R^2+R_0^2\sigma_F^2\left((F-1)R\log(1-F)+(R_0-FR)\log\left(1-\frac{FR}{R_0}\right)\right)^2}{(F-1)^2R_0^2(R_0-FR)^2\log^4\left(1-\frac{FR}{R_0}\right)}}$$

where σ is the error for F, R, and R_0. This formula is implemented in the Excel spreadsheet that is in the attached archive. Because different numbers of spectra were used to generate the ^{13}C and ^{12}C portions for each ratio, standard errors, rather than standard deviations, were propagated instead. The standard errors were based on the appropriate *t*-distribution.

For starting-material-based analyses, the corresponding formulas are:

$$\frac{\log(1-F)}{\log\left((1-F)\frac{R}{R_0}\right)}$$

```
TeXForm[FullSimplify[ErrorProgataionPrintFormula[
 Log[1 - F]/Log[(1 - F)*R/Subscript[R, 0]], {F, R, Subscript[R, 0]}]]]
```

$$\sqrt{\frac{R_0^2\left(R^2\sigma_F^2\left(\log(1-F)-\log\left(-\frac{(F-1)R}{R_0}\right)\right)^2+(F-1)^2\log^2(1-F)\sigma_R^2\right)+(F-1)^2R^2\log^2(1-F)\sigma_{R_0}^2}{(F-1)^2R^2R_0^2\log^4\left(-\frac{(F-1)R}{R_0}\right)}}$$

The attached Excel spreadsheet gives standard errors for individual measurements. Reported KIEs are averages of these individual measurements.

4. Computations

a. General Procedures

(i) DFT Calculations

DFT calculations were carried out using *Gaussian 16, Revision A.03*:

M. J. Frisch, G. W. Trucks, H. B. Schlegel, G. E. Scuseria, M. A. Robb, J. R. Cheeseman, G. Scalmani, V. Barone, G. A. Petersson, H. Nakatsuji, X. Li, M. Caricato, A. V. Marenich, J. Bloino, B. G. Janesko, R. Gomperts, B. Mennucci, H. P. Hratchian, J. V. Ortiz, A. F. Izmaylov, J. L. Sonnenberg, D. Williams-Young, F. Ding, F. Lipparini, F. Egidi, J. Goings, B. Peng, A. Petrone, T. Henderson, D. Ranasinghe, V. G. Zakrzewski, J. Gao, N. Rega, G. Zheng, W. Liang, M. Hada, M. Ehara, K. Toyota, R. Fukuda, J. Hasegawa, M. Ishida, T. Nakajima, Y. Honda, O. Kitao, H. Nakai, T. Vreven, K. Throssell, J. A. Montgomery, Jr., J. E. Peralta, F. Ogliaro, M. J. Bearpark, J. J. Heyd, E. N. Brothers, K. N. Kudin, V. N. Staroverov, T. A. Keith, R. Kobayashi, J. Normand, K. Raghavachari, A. P. Rendell, J. C. Burant, S. S. Iyengar, J. Tomasi, M. Cossi, J. M. Millam, M. Klene, C. Adamo, R. Cammi, J. W. Ochterski, R. L. Martin, K. Morokuma, O. Farkas, J. B. Foresman, and D. J. Fox, Gaussian, Inc., Wallingford CT, 2016.

All stationary points were verified to be true local minima or saddle points by frequency analysis. Where possible, transition states were verified by intrinsic reaction coordinate, growing string, or quasiclassical trajectory analysis.

KIEs were calculated using *PyQuiver*, which is freely available from the authors at:

www.github.com/ekwan/PyQuiver

(ii) Gaussrate/Polyrate Calculations

GAUSSRATE and POLYRATE were used to calculate multi-dimensional tunnelling corrections:

GAUSSRATE version 2016/P2016-G09 (August 4, 2016)

by Jingjing Zheng, Shuxia Zhang, Jose C. Corchado, Ruben Meana-Paneda, Yao-Yuan Chuang, Elena L. Coitino, Benjamin A. Ellingson, and Donald G. Truhlar

POLYRATE version 2016 (August 4, 2016)

Jingjing Zheng, Ruben Meana-Paneda, Shuxia Zhang, Benjamin J. Lynch, Jose C. Corchado, Yao-Yuan Chuang, Patton L. Fast, Wei-Ping Hu, Yi-Ping Liu, Gillian C. Lynch, Kiet A. Nguyen, Charles F. Jackels, Antonio Fernandez Ramos, Benjamin A. Ellingson, Vasilios S. Melissas, Jordi Villa, Ivan Rossi, Elena L. Coitino, Jingzhi Pu, and Titus V. Albu

(iii) Coupled Cluster Calculations

Coupled cluster calculations were carried out using ORCA 4.0.0. Specifically, DLPNO-CCSD(T)/aug-cc-pVTZ gas phase single points using TightPNO cutoffs were used. Geometries were generated in Gaussian at B3LYP-D3(BJ)/jun-cc-pVTZ/PCM. All ORCA single points followed this template:

```
! aug-cc-pVTZ aug-cc-pVTZ/C DLPNO-CCSD(T) TightSCF TightPNO MiniPrint
%pal nproc 4 end
%maxcore 4000
%mdci
     density none
end

* xyz -1 1
C      -0.68948400      1.40320100     -0.07834300
[ geometry continues ]
*
```

(iv) Quasiclassical Dynamics

Quasiclassical trajectories[61,87] were initialized using unscaled harmonic frequencies calculated at B3LYP-D3(BJ)/6-31+G*/PCM in Gaussian with the freq=hpmodes keyword. For each vibrational mode, excluding those with wavenumbers below 50 cm^{-1}, an energy level was randomly selected from a Boltzmann distribution, with the assumption that the vibration can be modeled as a simple quantum harmonic oscillator. A displacement was randomly made in each mode according to the displacement-space probability distribution of simple quantum harmonic oscillator eigenstate of the appropriate level. The molecule was initialized at 298.15 K with the classical amount of kinetic energy necessary in each mode on the basis of the displacements. The direction of the velocity in each mode was sign-randomized, with the exception of the transition vector, which was given velocity towards product. Rotation was imparted to the entire molecule using a classical initialization scheme. For each principal axis, an angular momentum was drawn from a Gaussian distribution, such that the average energy of rotation around each axis was equal to the classical equipartition energy of kT/2. The expected and actual potential energies were calculated for each proposed initialization geometry. Only geometries that were within 0.000075% (reaction B) and 0.0001% (reaction C) of the energy in hartree were accepted. Trajectories were propagated using the velocity Verlet integration scheme in increments of 1.0 fs from -500 fs to 500 fs inclusive. Trajectories that did not originate from starting material were rejected. A total of 200 trajectories were generated for each reaction.

b. S_N2 Calculations

(i) Effect of Transition Structure

The predicted harmonic KIEs at B3LYP/6-31G*/PCM(THF) at 298 K were nearly independent of structure. KIEs below are given in parts per thousand:

	no counterion	counterion on nucleophile side	counterion on electrophile side
fluoride	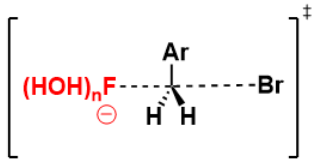 38, 43, 40, 37	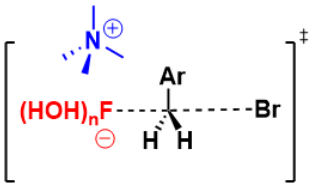 41, 39, 38, 34	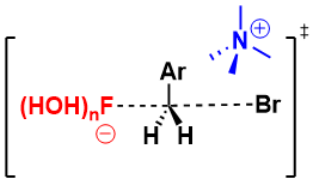 --, --, 41, 40
bifluoride	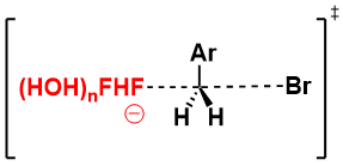 38, 36, 33, -- (n = 0, 1, 2, 3)	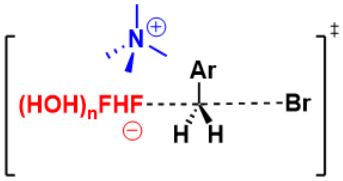 35, 35, 33, --	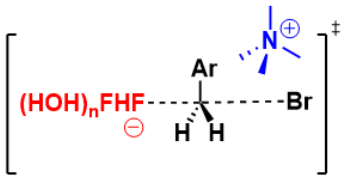 39, 38, 36, --

These perturbations likely had little effect because they only served to move the reaction back and forth along the reaction coordinate:

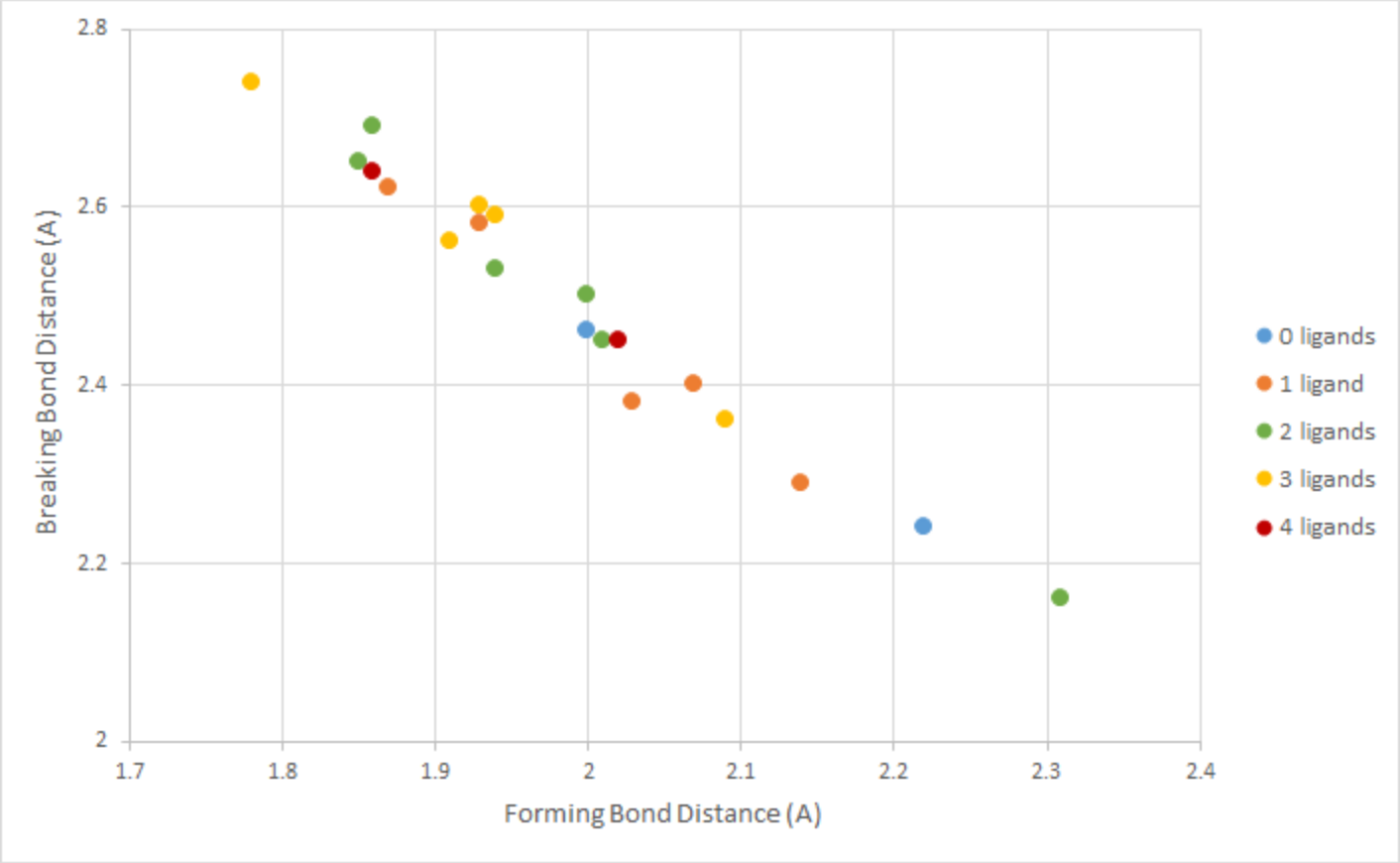

Primary carbon KIEs in S_N2 reactions are known to be relatively insensitive to geometry (reference 13).

(ii) Effect of DFT

The transition structure with two water ligands on fluoride and no counterion was calculated at cc-pVDZ/PCM using a variety of DFTs. The harmonic KIEs were nearly independent of DFT:

DFT	KIE	Bell correction
b1b95	1.0504	0.0104
b3lyp_d3bj	1.0454	0.0064
b3p86	1.0484	0.0085
b3pw91	1.0482	0.0084
b971	1.0476	0.0080
b972	1.0482	0.0084
b97d3_d3bj	1.0407	0.0030
b97d_d3bj	1.0407	0.0030
b98	1.0471	0.0079
bhandh	1.0556	0.0156
bhandhlyp	1.0502	0.0107
blyp_d3bj	1.0407	0.0029
bmk_d3bj	1.0528	0.0087
bp86_d3bj	1.0440	0.0044
cam_b3lyp_d3bj	1.0515	0.0115
hf	1.0495	0.0077
lcwpbe_d3bj	1.0601	0.0188
m05	1.0537	0.0117
m052x	1.0542	0.0171

m052x_d3	1.0526	0.0150
m05_d3	1.0533	0.0113
m06	1.0509	0.0100
m062x	1.0542	0.0171
m062x_d3	1.0543	0.0171
m06_hf	1.0538	0.0200
m06_hf_d3	1.0538	0.0200
m06l	1.0475	0.0062
m06l_d3	1.0475	0.0062
m11	1.0563	0.0199
mn12sx	1.0500	0.0100
mpw1lyp	1.0458	0.0073
mpw1pbe	1.0500	0.0098
mpw1pw91	1.0497	0.0096
mpw3pbe	1.0486	0.0087
n12sx	1.0508	0.0113
pbe0_d3bj	1.0503	0.0098
sogga11	1.0445	0.0050
tpsstpss_d3bj	1.0436	0.0041
vsxc	1.0429	0.0060
wb97xd	1.0535	0.0140

(iii) Effect of Basis Set

The basis set dependence was examined for a subset of the transition structures considered above using five common DFTs. The geometries and KIEs were well-converged at jun-cc-pVTZ.

IP KIE = infinite parabola KIE, corr = Bell correction, raw = harmonic KIE, forming = forming bond distance, breaking = breaking bond distance

fluoride, 2 waters, no counterion						
		IP KIE	**corr**	**raw**	**forming (A)**	**breaking (A)**
B3LYP-D3BJ	**6-31G***	1.048	0.008	1.040	2.01	2.45
	cc-pVDZ	1.045	0.006	1.039	2.03	2.48
	jul-cc-pVDZ	1.044	0.006	1.038	2.01	2.58
	cc-pVTZ	1.044	0.006	1.038	2.04	2.53
	jun-cc-pVTZ	1.043	0.006	1.037	2.02	2.59
B97D-D3BJ	**6-31G***	1.043	0.004	1.039	2.05	2.48
	cc-pVDZ	1.041	0.003	1.038	2.09	2.50
	jul-cc-pVDZ	1.037	0.002	1.035	2.06	2.63
	cc-pVTZ	1.038	0.002	1.035	2.10	2.56
	jun-cc-pVTZ	1.036	0.003	1.034	2.06	2.65
M06-2X	**6-31G***	1.055	0.018	1.038	1.95	2.39
	cc-pVDZ	1.054	0.017	1.037	1.97	2.42
	jul-cc-pVDZ	1.056	0.019	1.037	1.97	2.46
	cc-pVTZ	1.056	0.019	1.037	1.96	2.46
	jun-cc-pVTZ	1.056	0.019	1.037	1.95	2.48
PBE0-D3BJ	**6-31G***	1.052	0.011	1.041	1.96	2.41
	cc-pVDZ	1.050	0.010	1.041	1.98	2.44
	jul-cc-pVDZ	1.050	0.010	1.040	1.96	2.50
	cc-pVTZ	1.050	0.011	1.039	1.98	2.47
	jun-cc-pVTZ	1.050	0.011	1.039	1.96	2.50
wB97XD	**6-31G***	1.055	0.015	1.039	1.98	2.41
	cc-pVDZ	1.054	0.014	1.040	2.01	2.44
	jul-cc-pVDZ	1.053	0.013	1.039	2.01	2.50
	cc-pVTZ	1.053	0.013	1.039	2.01	2.49
	jun-cc-pVTZ	1.052	0.013	1.039	2.01	2.51

fluoride, 3 waters, counterion on Br side						
		IP KIE	**corr**	**raw**	**forming (A)**	**breaking (A)**
B3LYP-D3BJ	**6-31G***	1.048	0.009	1.040	2.02	2.45
	cc-pVDZ	1.046	0.007	1.040	2.04	2.47
	jul-cc-pVDZ	1.042	0.005	1.037	2.01	2.58
	cc-pVTZ	1.043	0.006	1.037	2.03	2.54
	jun-cc-pVTZ	1.043	0.006	1.038	2.05	2.53
B97D-D3BJ	**6-31G***	1.044	0.005	1.039	2.07	2.48
	cc-pVDZ	1.042	0.004	1.038	2.10	2.49
	jul-cc-pVDZ	1.035	0.002	1.033	2.04	2.65
	cc-pVTZ	1.036	0.002	1.034	2.09	2.58
	jun-cc-pVTZ	1.032	0.002	1.030	2.01	2.71
M06-2X	**6-31G***	1.056	0.019	1.037	1.96	2.39
	cc-pVDZ	1.056	0.019	1.037	1.97	2.42
	jul-cc-pVDZ	1.056	0.020	1.036	1.96	2.46
	cc-pVTZ	1.056	0.019	1.037	1.96	2.45
	jun-cc-pVTZ	1.056	0.019	1.036	1.95	2.47
PBE0-D3BJ	**6-31G***	1.052	0.012	1.040	1.97	2.40
	cc-pVDZ	1.051	0.010	1.041	1.99	2.43
	jul-cc-pVDZ	1.048	0.010	1.039	1.97	2.49
	cc-pVTZ	1.049	0.010	1.039	1.98	2.47
	jun-cc-pVTZ	1.048	0.010	1.038	1.97	2.49
wB97XD	**6-31G***	1.055	0.015	1.039	1.99	2.42
	cc-pVDZ	1.054	0.014	1.040	2.01	2.44
	jul-cc-pVDZ	1.052	0.013	1.039	2.01	2.51
	cc-pVTZ	1.052	0.013	1.039	2.01	2.49
	jun-cc-pVTZ	1.051	0.012	1.039	2.00	2.52

fluoride, 2 waters, counterion on F side						
		IP KIE	**corr**	**raw**	**forming (A)**	**breaking (A)**
B3LYP-D3BJ	**6-31G***	1.046	0.009	1.038	1.91	2.56
	cc-pVDZ	1.044	0.007	1.037	1.91	2.61
	jul-cc-pVDZ	did not converge				
	cc-pVTZ	1.042	0.006	1.035	1.95	2.62
	jun-cc-pVTZ	1.041	0.006	1.035	1.95	2.64
B97D-D3BJ	**6-31G***	1.040	0.004	1.035	1.90	2.64
	cc-pVDZ	1.036	0.003	1.033	1.90	2.72
	jul-cc-pVDZ	1.035	0.003	1.032	1.96	2.72
	cc-pVTZ	1.034	0.003	1.032	1.97	2.69
	jun-cc-pVTZ	1.031	0.002	1.029	1.92	2.79
M06-2X	**6-31G***	1.057	0.021	1.036	1.88	2.45
	cc-pVDZ	1.056	0.020	1.036	1.90	2.48
	jul-cc-pVDZ	1.056	0.021	1.035	1.92	2.50
	cc-pVTZ	1.056	0.021	1.035	1.90	2.50
	jun-cc-pVTZ	1.056	0.021	1.035	1.90	2.51
PBE0-D3BJ	**6-31G***	1.051	0.013	1.038	1.88	2.49
	cc-pVDZ	1.049	0.011	1.039	1.90	2.53
	jul-cc-pVDZ	1.048	0.011	1.038	1.92	2.54
	cc-pVTZ	1.048	0.011	1.037	1.92	2.53
	jun-cc-pVTZ	1.048	0.011	1.037	1.91	2.54
wB97XD	**6-31G***	did not converge				
	cc-pVDZ	1.052	0.013	1.040	1.94	2.51
	jul-cc-pVDZ	did not converge				
	cc-pVTZ	1.051	0.013	1.039	1.96	2.54
	jun-cc-pVTZ	did not converge				

(iv) Tunnelling Corrections

Multidimensional tunnelling corrections were explored at M06-2X/6-31G* on the 2 water, no counterion structure using the procedure described here:

Vetticatt, M. J. & Singleton, D. A. *Org. Lett.* **14**, 2370–2373 (2012)

At 298 K, the raw M06-2X/jun-cc-pVTZ KIE is 1.037 and the Bell-corrected KIE is 1.056. The SCT/CVT correction is 1.0164, which gives a KIE 1.054. This difference was assumed to be negligible and Bell corrections were used throughout.

(v) KIE Predictions

As shown above, the only significant difference between the various calculations is the amount of tunnelling, which in turn mostly depends on the imaginary frequency. The method that gave the best agreement with experiment was M11. There was a negligible dependence on solvation model:

method	raw KIE	corrected KIE
M11/jun-cc-pVTZ/gas	1.0372	1.0553
M11/jun-cc-pVTZ/PCM	1.0348	1.0560
M11/jun-cc-pVTZ/SMD	1.0342	1.0560

With PCM, the imaginary frequency was –554 cm^{-1} and its reduced mass was 12.02 amu, which indicates that the reaction coordinate involves essentially only heavy atom motion. The high degree of correspondence between the Bell and SCT/CVT corrections indicates that the only significant tunnelling is along the reaction coordinate. This tunnelling accounts for approximately one third of the observed isotope effect.

Each of these predictions was performed on a system with two explicit waters and no counterion.

c. Calculations for Reaction A

(i) Benchmark Calculations

B3LYP-D3(BJ)/jun-cc-pVTZ/PCM(MeOH) geometries were obtained on a grid of geometries in which the C–F and C–OMe distances were fixed (and all other geometric parameters were allowed to relax). DLPNO-CCSD(T)/aug-cc-pVTZ single point energies were calculated with TightPNO cutoffs in the gas phase on these geometries. This resulted in the following grid:

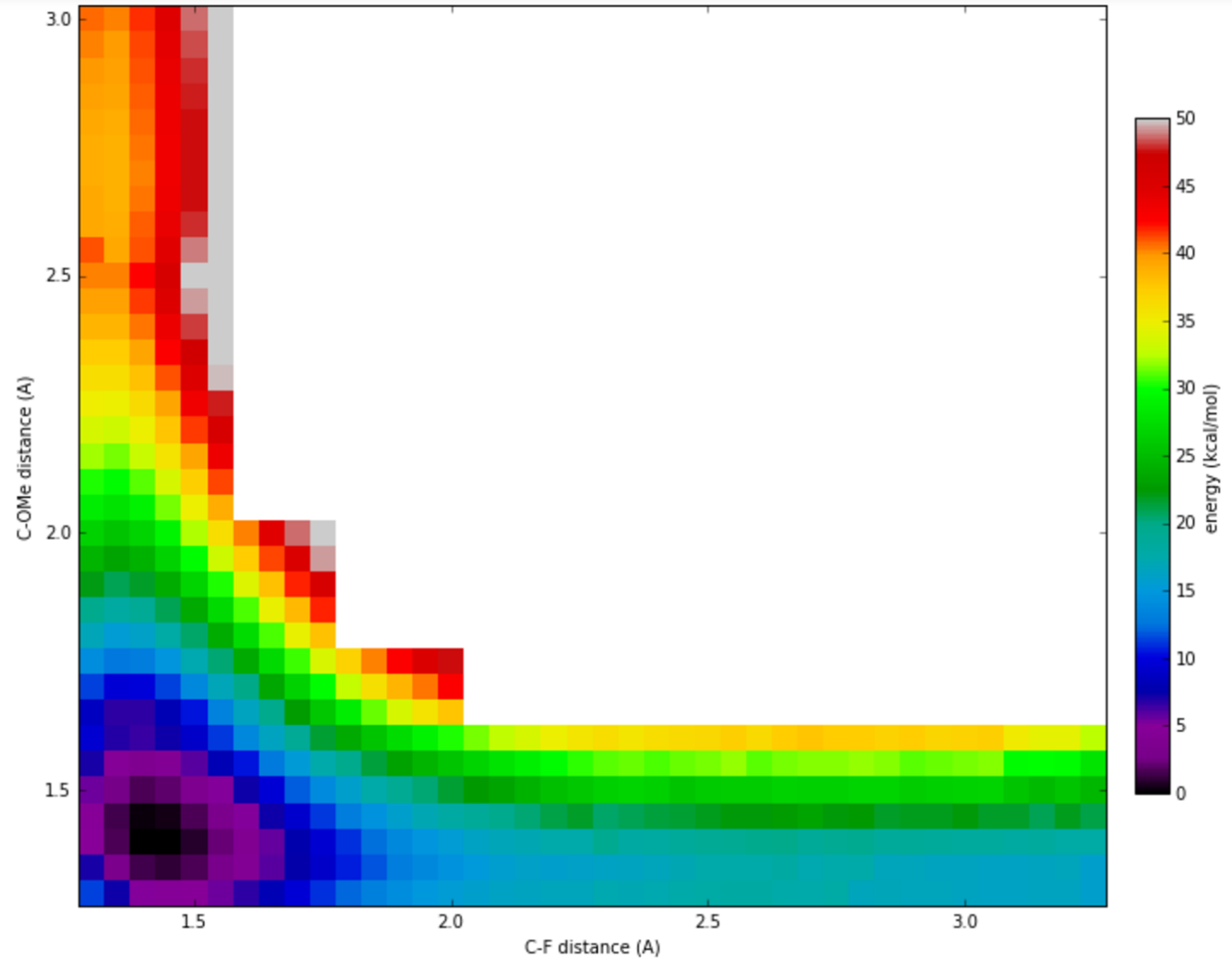

(ii) Effect of DFT

Single point energies were also calculated on the same energies as in the previous section using a variety of DFTs and the jun-cc-pVTZ basis set in the gas phase. The result for B3LYP-D3(BJ) is shown below:

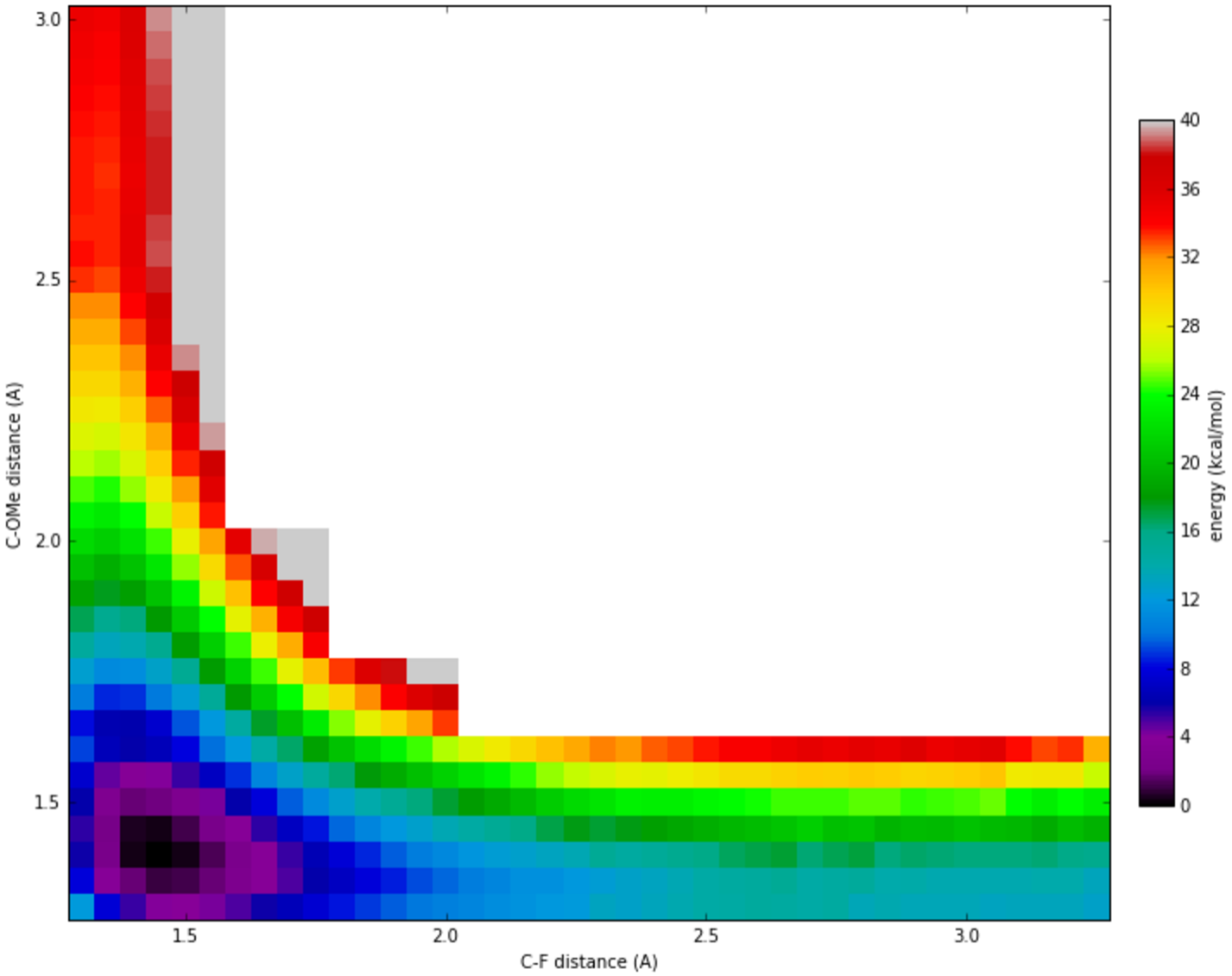

This was the optimal result for all tested functionals. In general, HF-rich methods such as BHandHLYP gave energies that were too high. These graphs are available in the attached Python notebook. Some additional results including solvation are also provided there.

The list of tested methods is: B97D-D3(BJ), PBE0-D3(BJ), BHandHLYP, BHandH, wB97xD, HF, BLYP-D3(BJ), M06-2X, M06-2X-D3, M11, M06-HF-D3.

(iii) Effect of Basis Set

Single point energies on the same geometries as above were calculated in the gas phase using the following basis sets: 6-31G*, 6-31+G*, 6-311+G*, cc-pVDZ, jul-cc-pVDZ, jun-cc-pVTZ. These graphs are available in the attached Python notebook.

The result for 6-31+G* is shown below (the jun-cc-pVTZ result is already shown above):

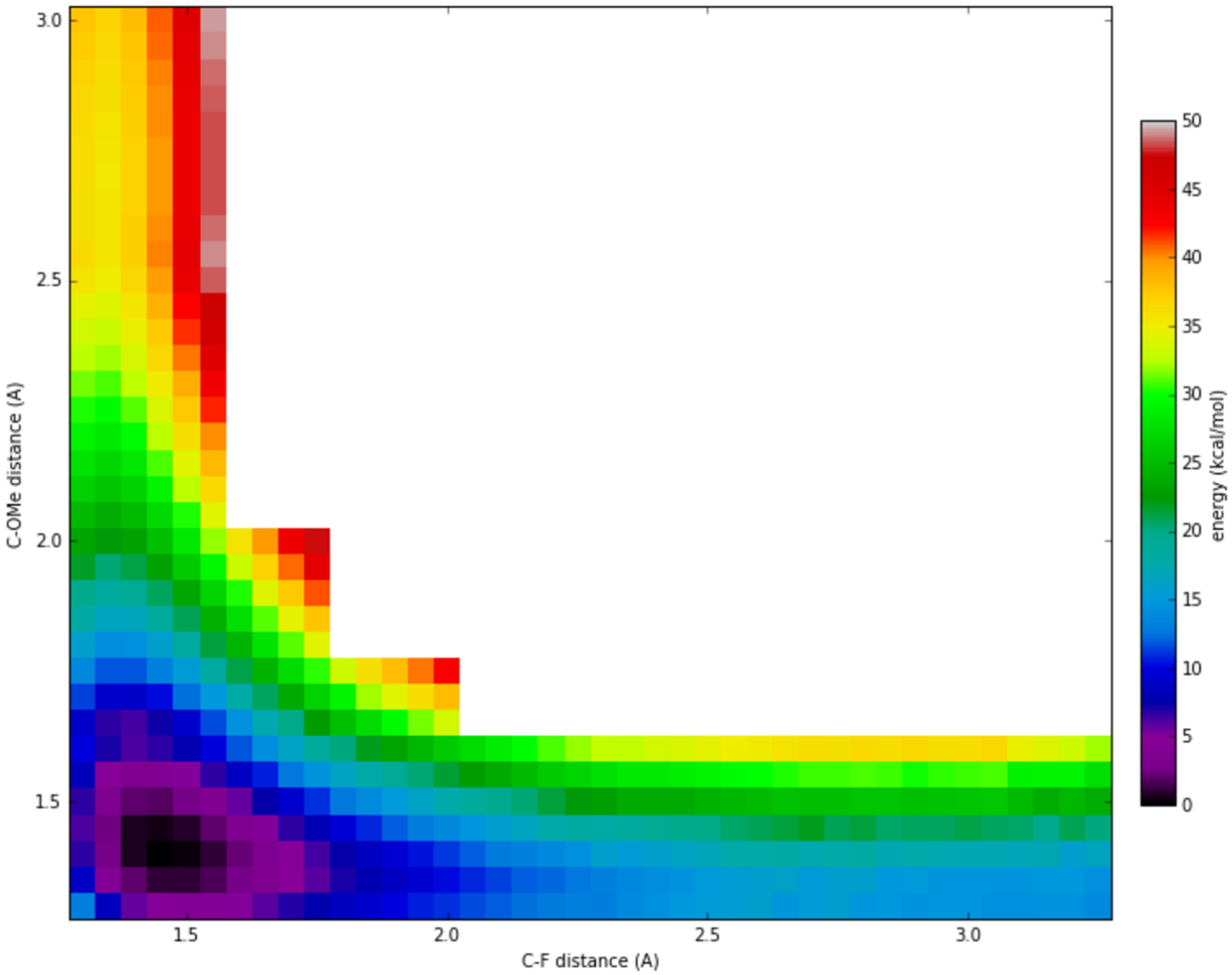

(iv) Effect of Transition Structure

Stationary points were located for the starting material, addition transition state (“step 1”), intermediate, and elimination transition state (“step 2”) using B3LYP-D3(BJ) and default PCM settings for a range of basis sets. At jul-cc-pVDZ, the exclusion (1.034) or inclusion (1.036) of an explicit methanol molecule had a negligible effect. Explicit methanol molecules were not included in the final prediction. Geometries, energies, and frequencies for all files considered are available in the attached archive.

(v) KIE Predictions

Predictions were made using B3LYP-D3(BJ) at 298 K and include a Bell tunnelling term:

Experimental: 1.035(3)

PCM (default settings, i.e., UFF radii scaled by 1.1):
jul-cc-pVDZ: 1.035
jun-cc-pVTZ: 1.037
may-cc-pVQZ: 1.037

PCM (UFF radii scaled by 1.2):
jul-cc-pVDZ: 1.029
jun-cc-pVTZ: 1.033
may-cc-PVQZ: 1.033

The bolded prediction is the value reported in the paper. The same settings were used to report the predicted KIEs for reactions B and C.

d. Calculations for Reaction B

(i) Benchmark Calculations

B3LYP-D3(BJ)/jun-cc-pVTZ/PCM(MeOH) geometries were obtained on a grid of geometries in which the C–F and C–Br distances were fixed (and all other geometric parameters were allowed to relax). DLPNO-CCSD(T)/aug-cc-pVTZ single point energies were calculated with TightPNO cutoffs in the gas phase on these geometries. This resulted in the following grid:

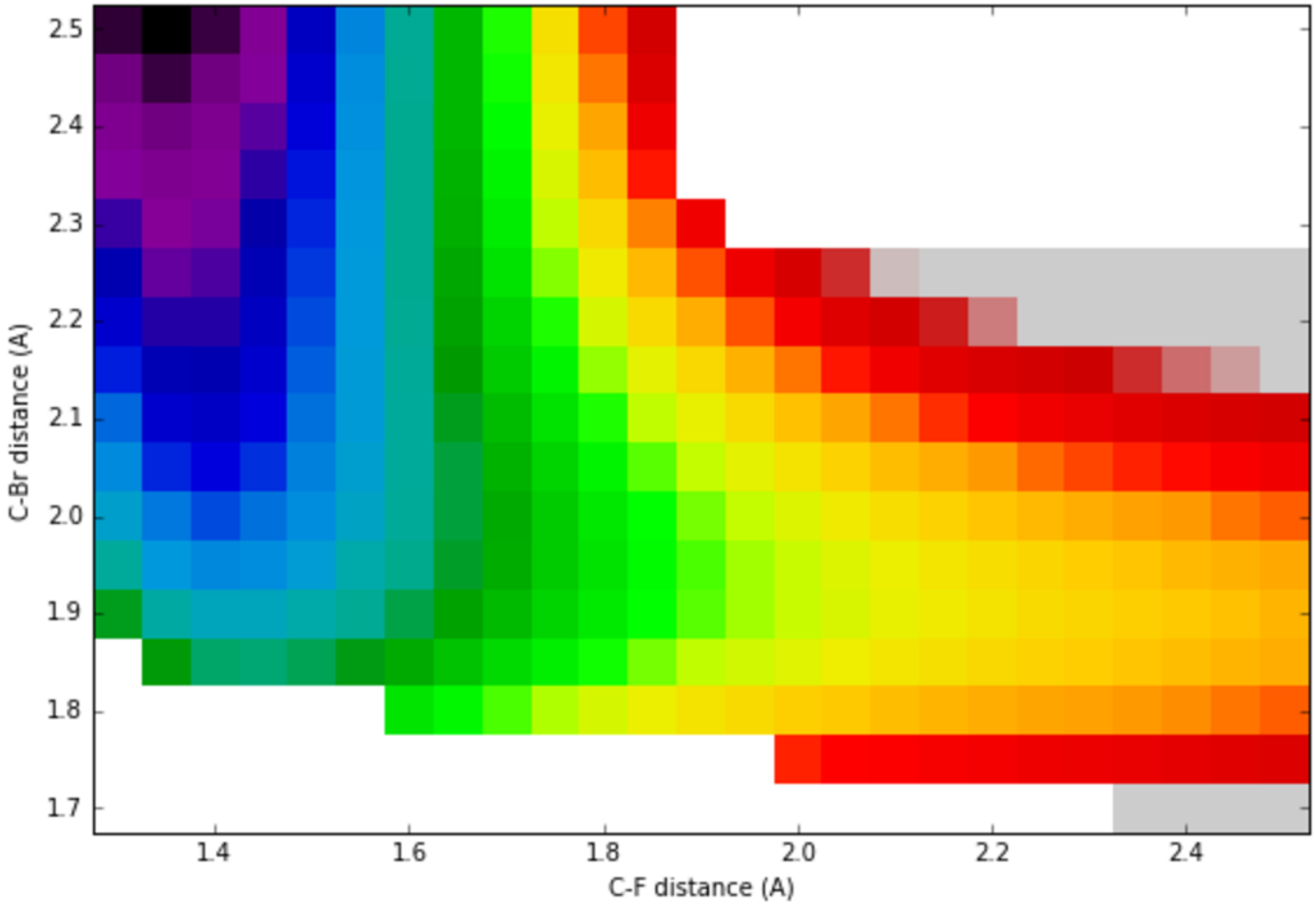

The transition state for addition is at the right edge of the graph. This transition state in the gas phase is very early because fluoride is extremely nucleophilic without solvation.

(ii) Effect of DFT

Single point energies were also calculated on the same energies as in the previous section using a variety of DFTs and the jun-cc-pVTZ basis set in the gas phase. The result for B3LYP-D3(BJ) is shown below:

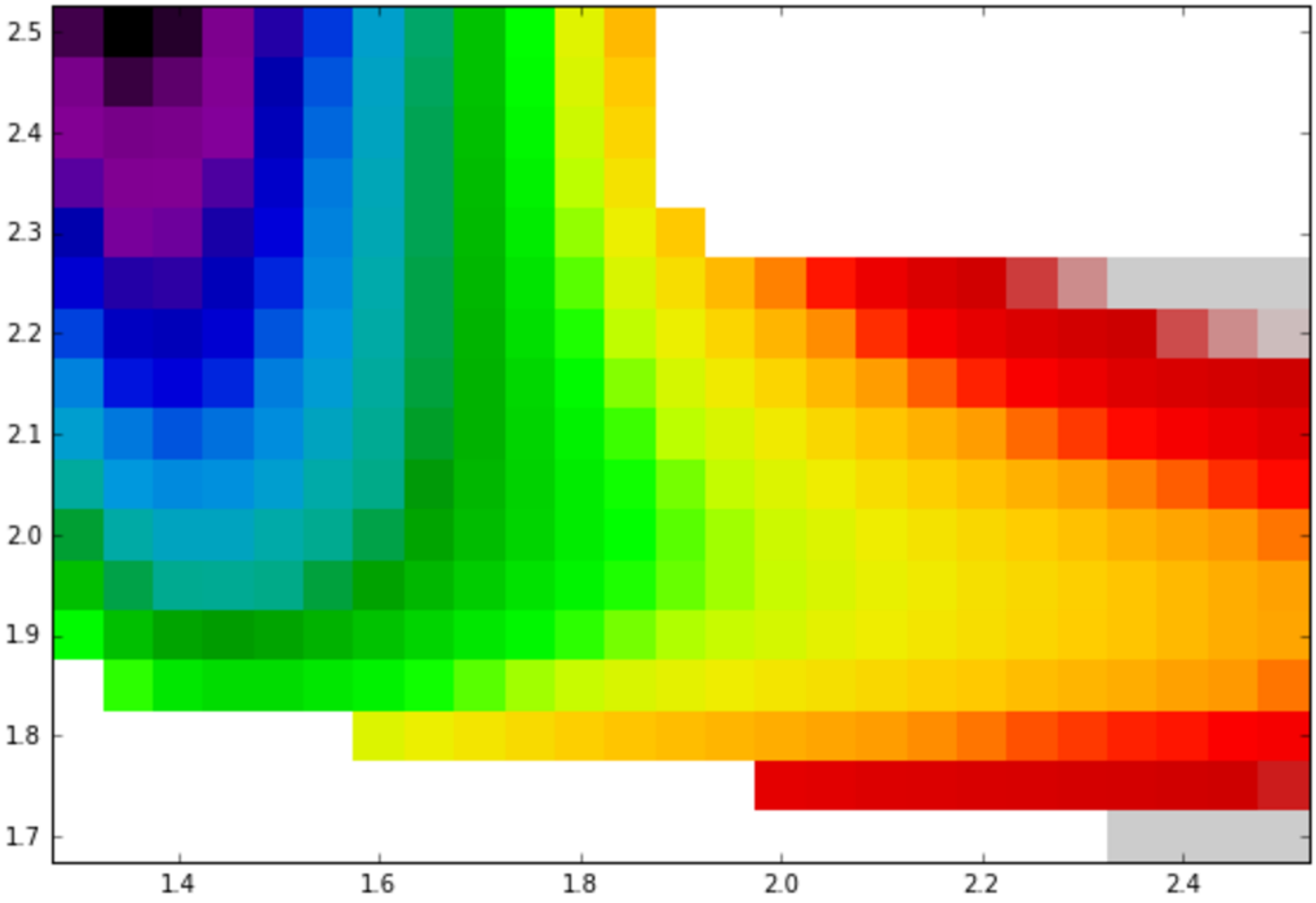

The same functionals were screened as in reaction A and the files are available in the archive. The same trends were observed.

(iii) Effect of Basis Set

Single point energies on the same geometries as above were calculated in the gas phase as above. These graphs are available in the attached Python notebook.

The result for 6-31+G* is shown below (the jun-cc-pVTZ result is already shown above):

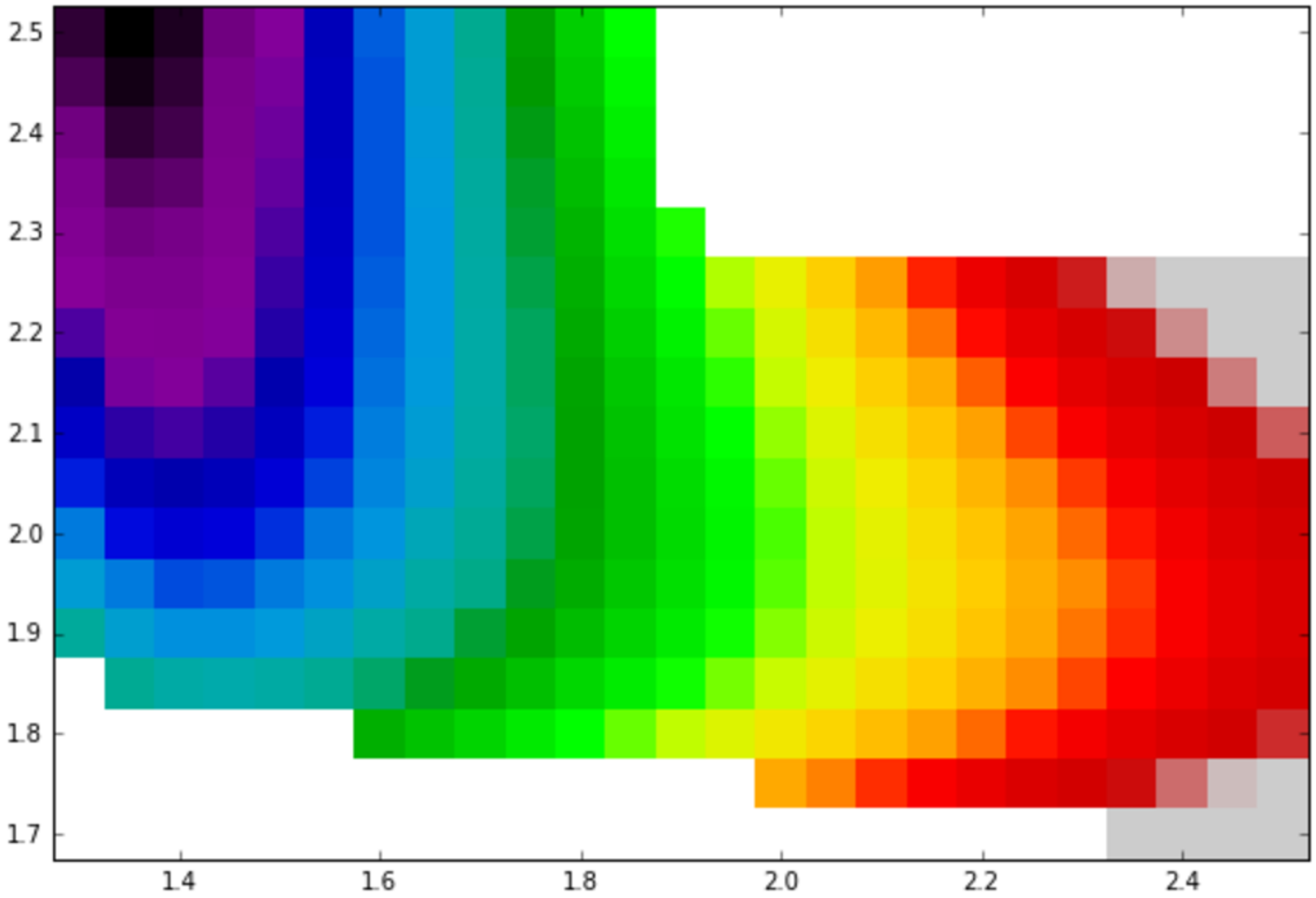

(iv) Effect of Transition Structure

Stationary points were located for the starting material and concerted transition state using B3LYP-D3(BJ) and default PCM settings for a range of basis sets. At jun-cc-pVTZ, the exclusion (1.0414) or inclusion (1.0410) of an explicit water molecule had a negligible effect. Explicit water molecules were not included in the final prediction. Geometries, energies, and frequencies for all files considered are available in the attached archive.

(v) KIE Predictions

Predictions were made using B3LYP-D3(BJ) at 298 K and include a Bell tunnelling term:

Experimental: 1.035(3)

PCM (default settings, i.e., UFF radii scaled by 1.1):
jul-cc-pVDZ: 1.040
jun-cc-pVTZ: 1.041
may-cc-pVQZ: 1.041

PCM (UFF radii scaled by 1.2):
jul-cc-pVDZ: 1.038
jun-cc-pVTZ: 1.039
may-cc-PVQZ: 1.039

The bolded prediction is the value reported in the paper. The same settings were used to report the predicted KIEs for reactions A and C.

(vi) Analysis of the Reaction Coordinate

An intrinsic reaction coordinate analysis was performed at B3LYP/6-31+G*/PCM on the transition state with a step size of 0.03 bohr, recalculating the Hessian every 30 steps. At each point, a Hirshfeld population analysis was performed. The charge on the ring atoms was summed to give the following:

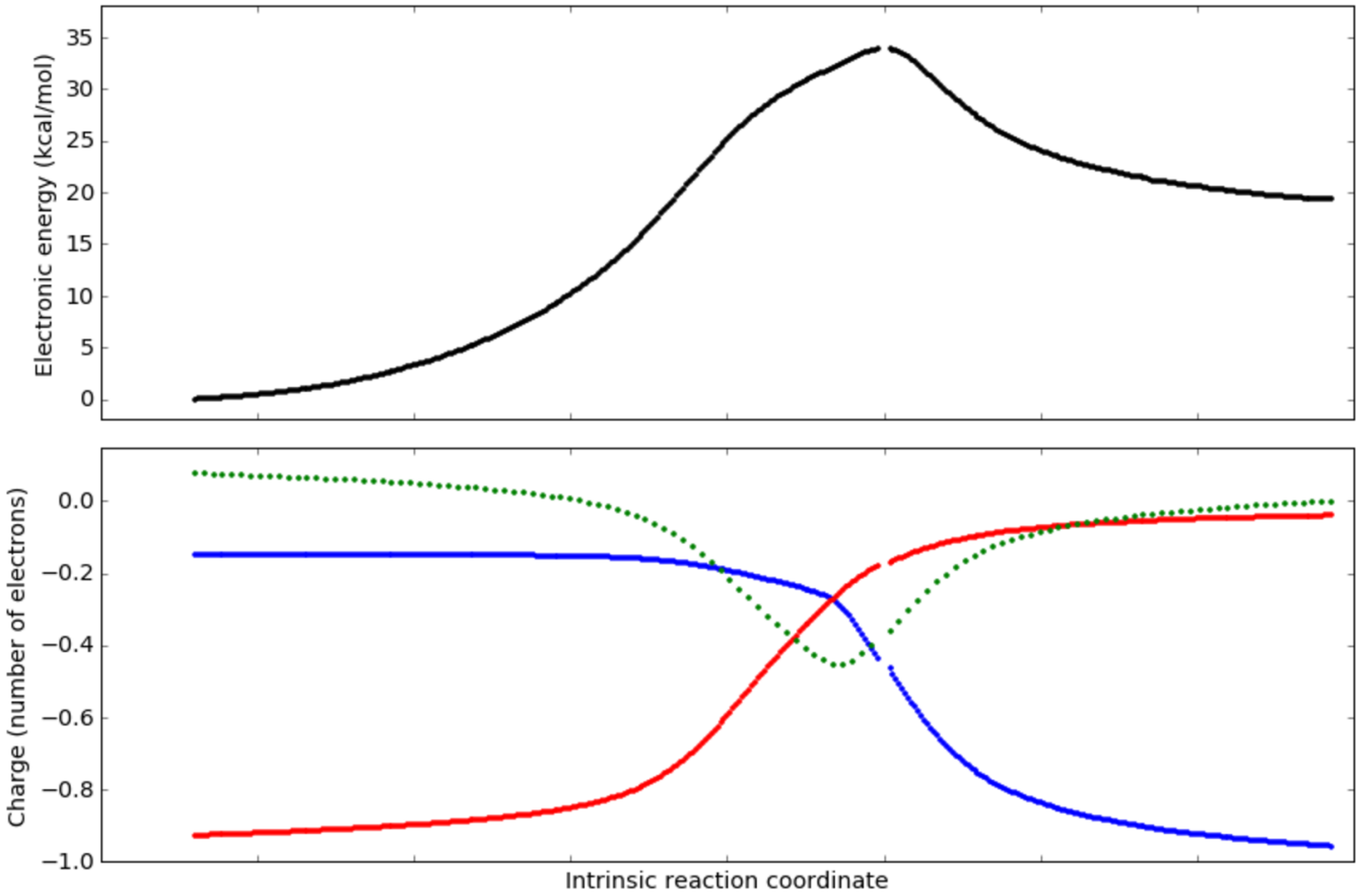

(These graphs are discussed in the main text.) The NICS(0) parameter was also calculated:

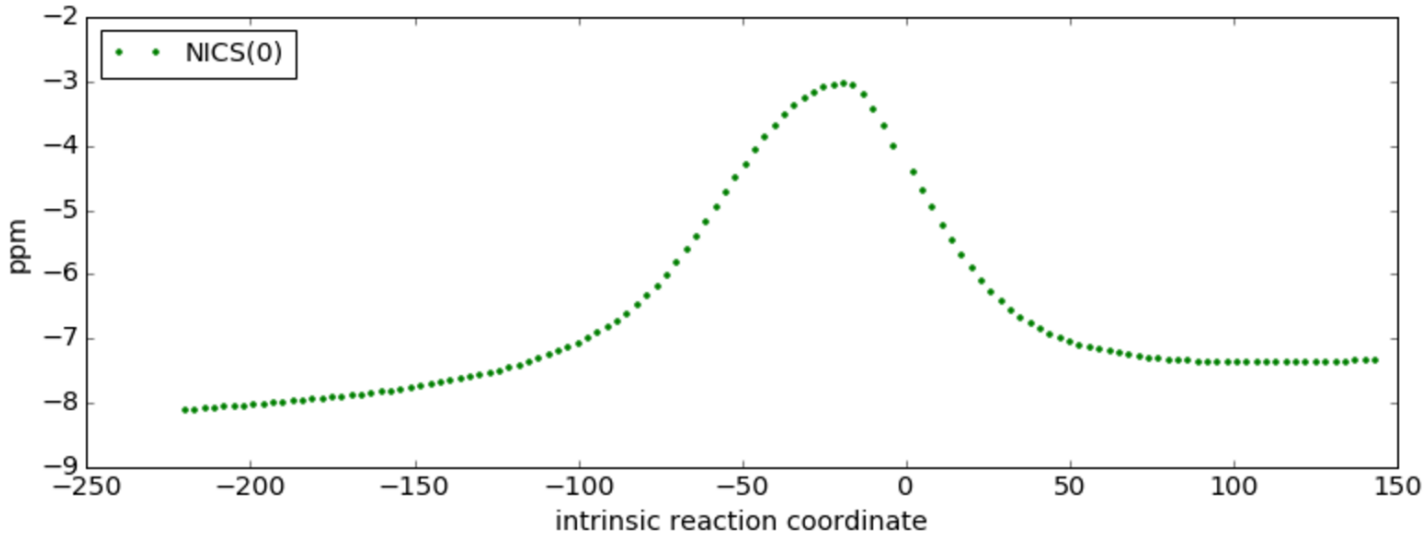

The peak near the transition state indicates a loss of aromaticity, suggesting that the Lewis structure of the transition state is like cyclohexadienyl anion. (The NICS(1) values above and below the ring gave similar trends.) To define the Lewis structure more precisely, NBO analysis was also performed at each point along the IRC. Using the `$CHOOSE` formalism, localized descriptions of the electron density were forced to conform to the starting material, Meisenheimer, and product Lewis structures:

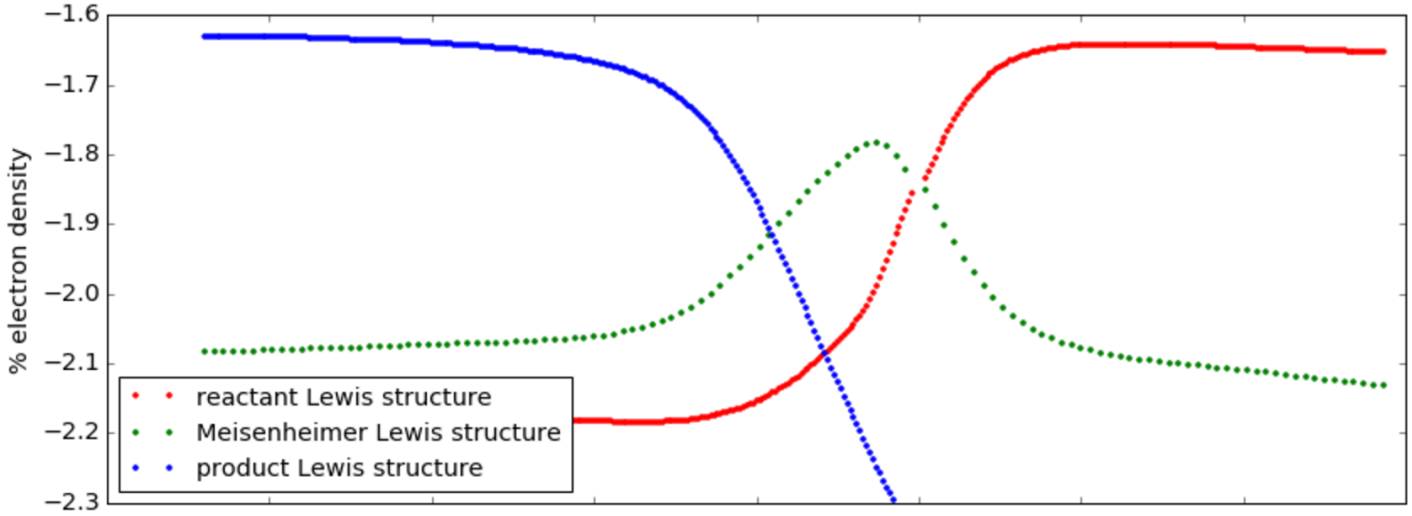

The y-axis shows how much of the electron density is not described by a particular Lewis structure. For example, a red point at –2.0% means that the reactant Lewis structure describe 98% of the electron density at that particular geometry. This analysis shows that the transition state has a high degree of Meisenheimer character.

The NBO output also permits an analysis of hyperconjugation. In the forward direction, the reaction can be described as occurring in two stages: donation of the lone pair on fluorine (n_F) into the π* of the C=N bond (starting material Lewis description), followed by donation of the lone pair on nitrogen (n_N) into the σ* of the C–Br bond (Meisenheimer Lewis description). The top plot shows that the former interaction (red) occurs before the latter interaction (blue), consistent with an asynchronous mechanism:

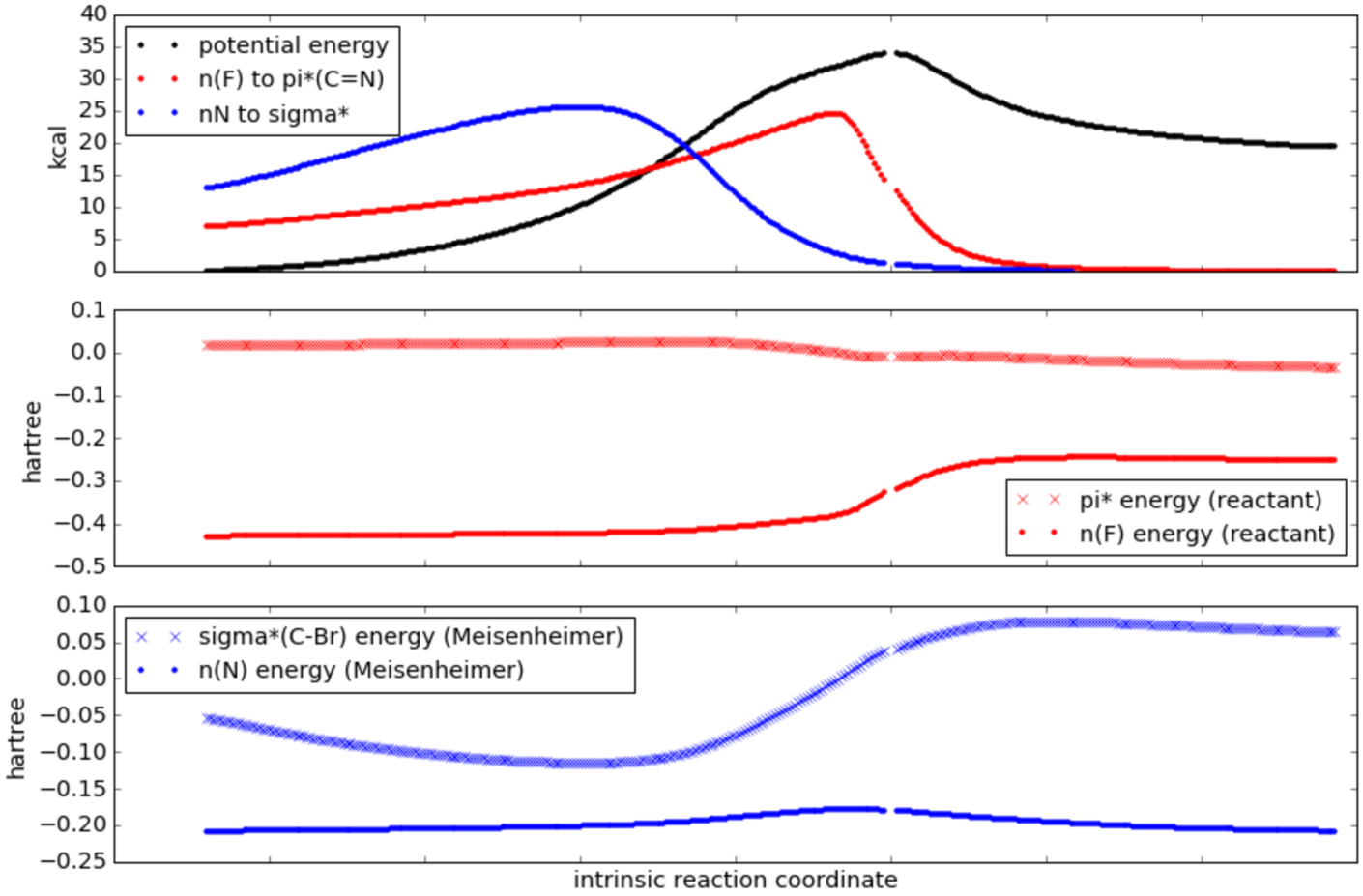

As the red interaction increases, the electrons of the fluoride lone pair become more tightly bound, resulting in a decrease in energy (middle plot). The blue interaction does not become feasible until the σ* energy is sufficiently lowered by the presence of an anion (bottom plot).

The asynchronous nature of the reaction can also be seen from this plot of bond distances along the reaction coordinate:

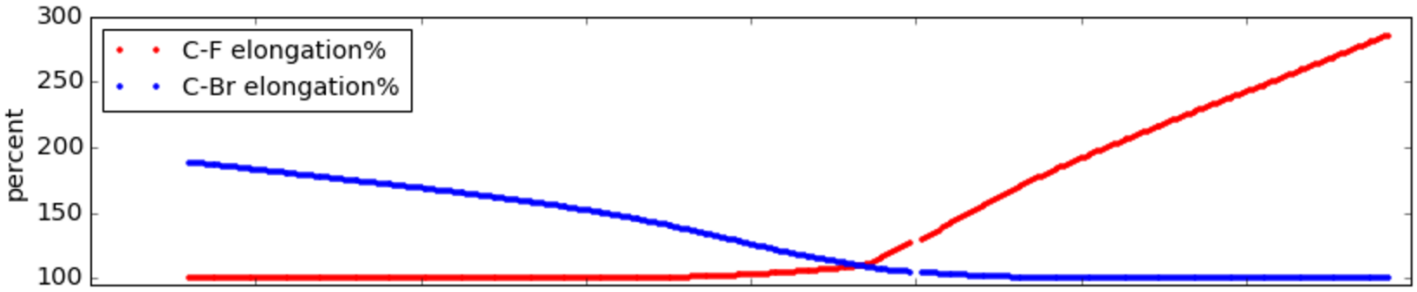

(The equilibrium bond lengths are scaled to 100%.)

The raw data for these analyses is available in the attached archive.

(vii) Quasiclassical Dynamics

200 trajectories were initialized from the B3LYP/6-31+G* transition state (default PCM, 298 K) and run forwards and backwards for a total time of 1 ps:

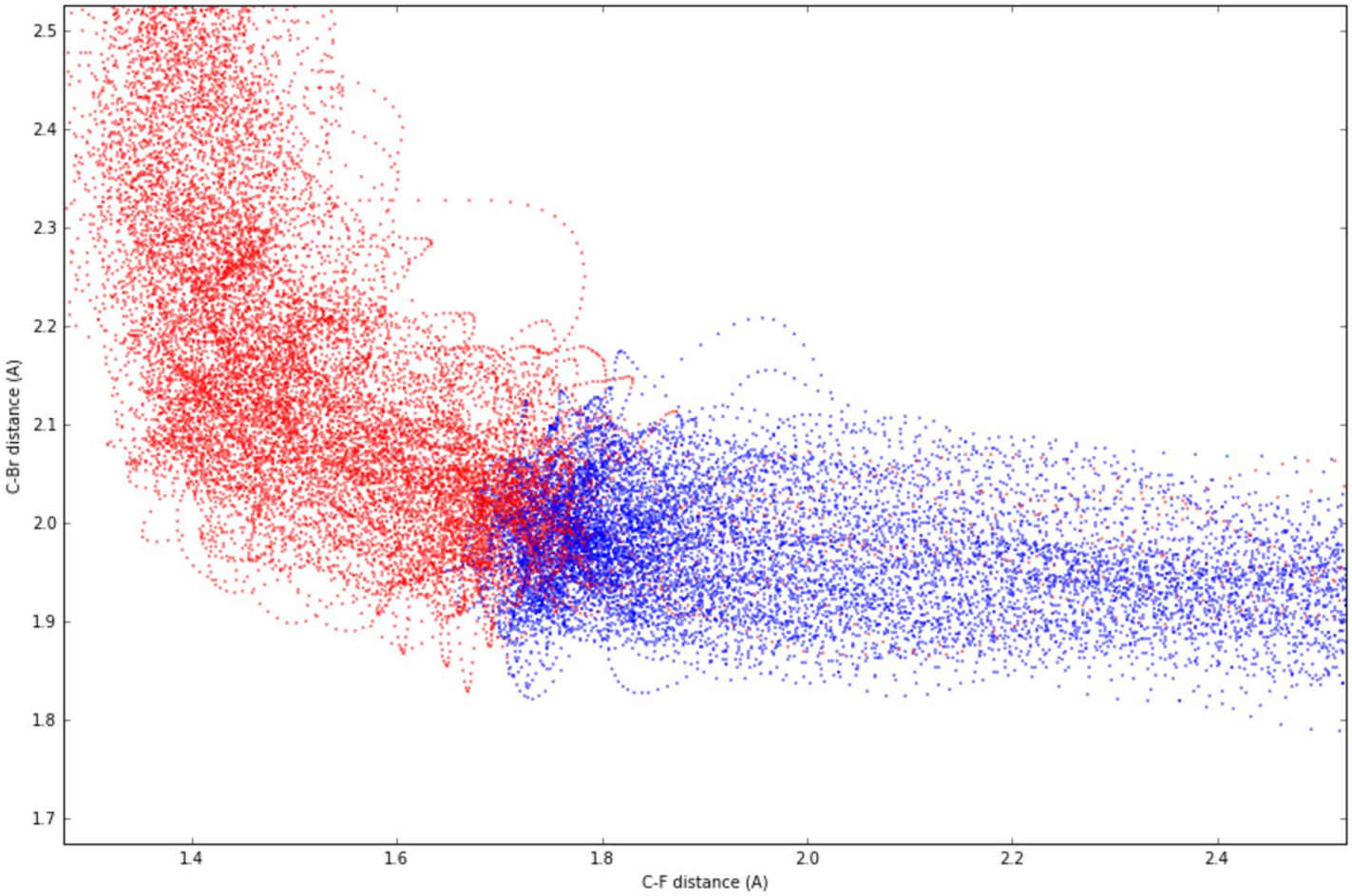

Blue and red points indicate backward and forward points, respectively. (Trajectories that did not originate from starting material were thrown out and replaced.) The variational transition state is visible as the region where the red and blue points intersect. Recrossing is rare and the trajectories spend no time in the intermediate region in the lower left of the graph. There is no evidence of a hidden intermediate.

e. Calculations for Reaction C

(i) Benchmark Calculations

B3LYP-D3(BJ)/jun-cc-pVTZ/PCM(DMF) geometries were obtained on a grid of geometries in which the C–F and C–Cl distances were fixed (and all other geometric parameters were allowed to relax). DLPNO-CCSD(T)/aug-cc-pVTZ single point energies were calculated with TightPNO cutoffs in the gas phase on these geometries. This resulted in the following grid:

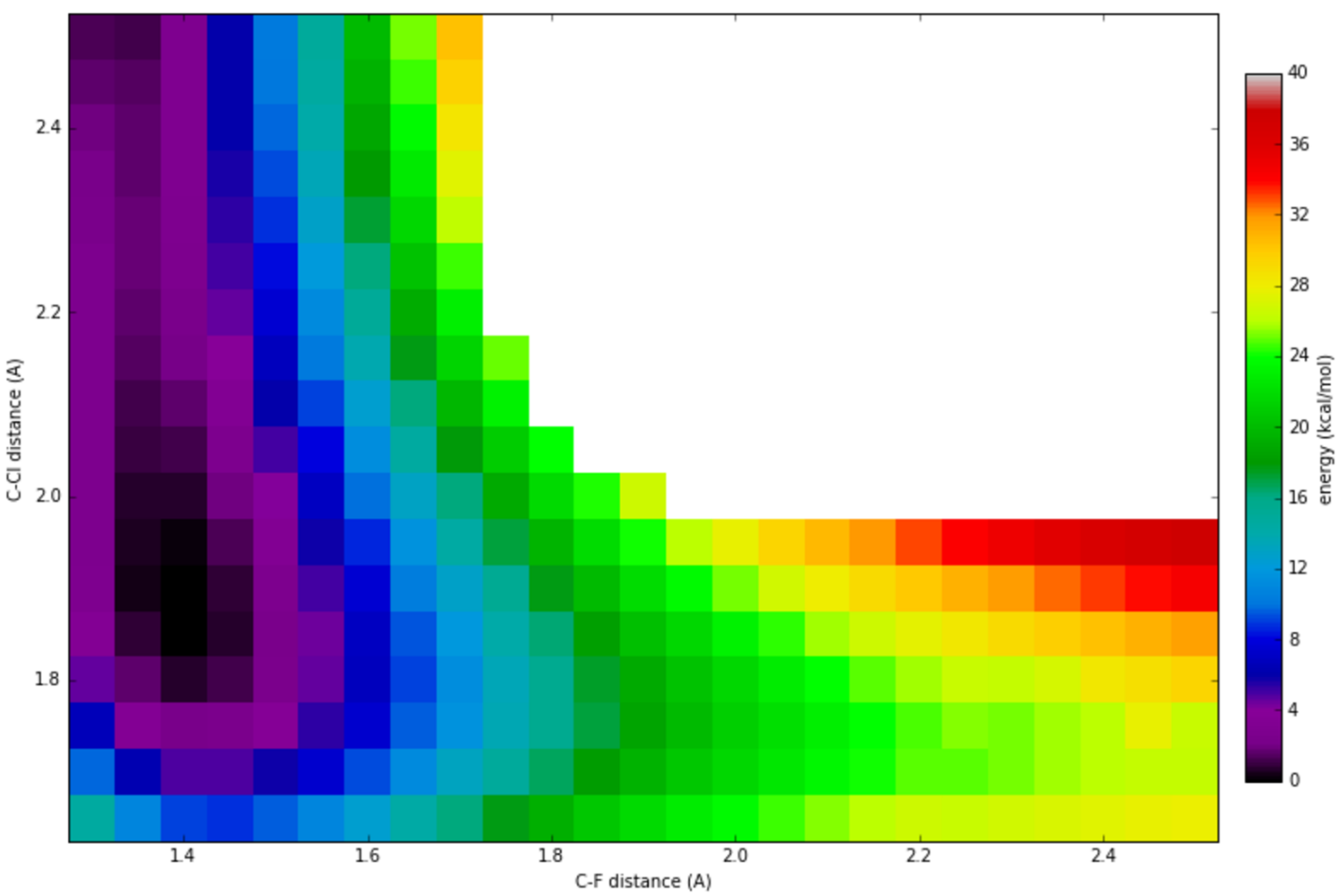

As the KIE predictions were ultimately made with the inclusion of an explicit water molecule, the above grid (which includes no explicit solvent) was also computed with the same model. The results are very similar and the files are provided in the attached archive.

(ii) Effect of DFT

Single point energies were also calculated on the same energies as in the previous section using a variety of DFTs and the jun-cc-pVTZ basis set in the gas phase. The result for B3LYP-D3(BJ) is shown below:

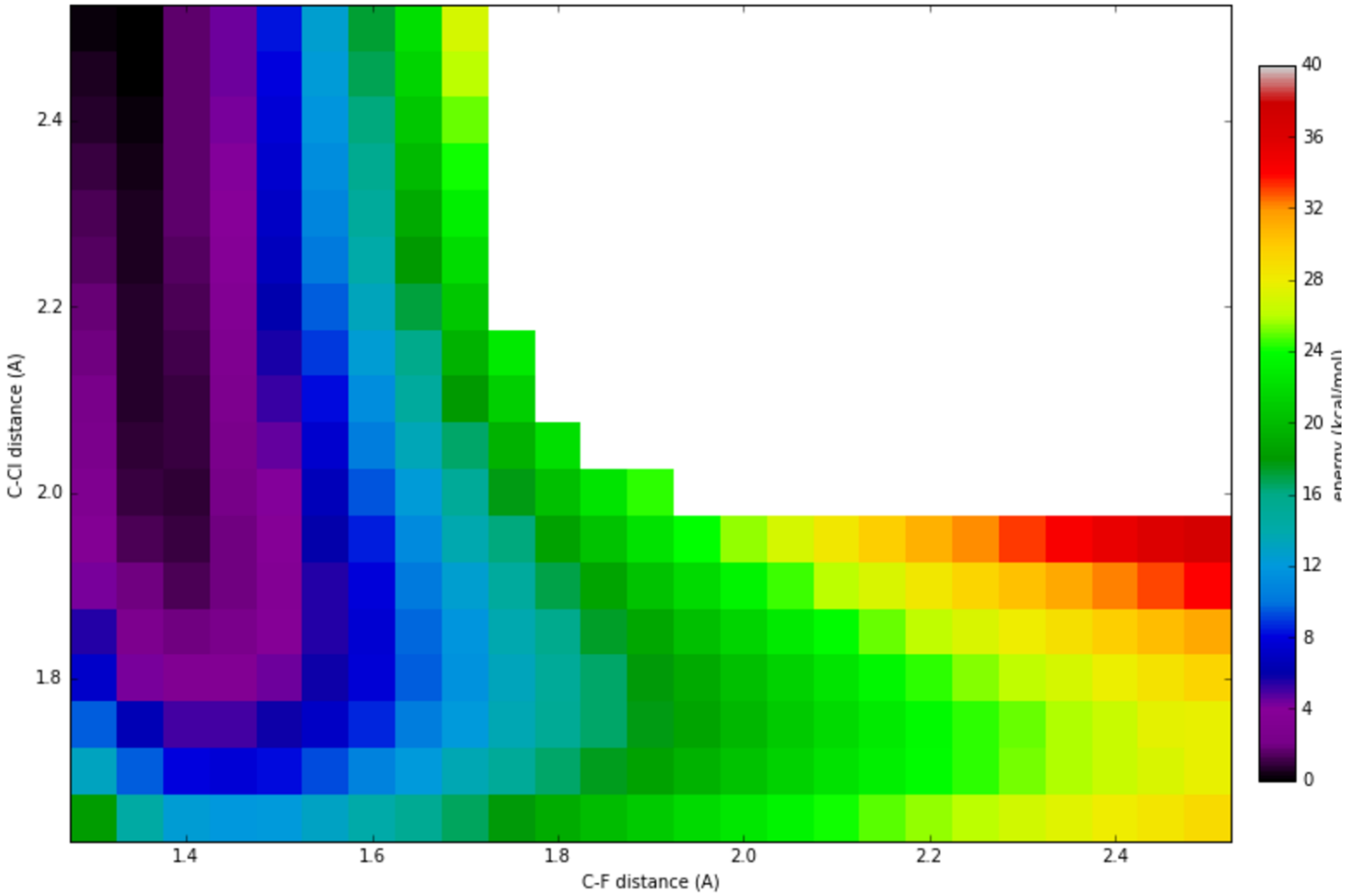

The same functionals were screened as in reaction A and the files are available in the archive. The same trends were observed.

(iii) Effect of Basis Set

Single point energies on the same geometries as above were calculated in the gas phase as above. These graphs are available in the attached Python notebook.

The result for 6-31+G* is shown below (the jun-cc-pVTZ result is already shown above):

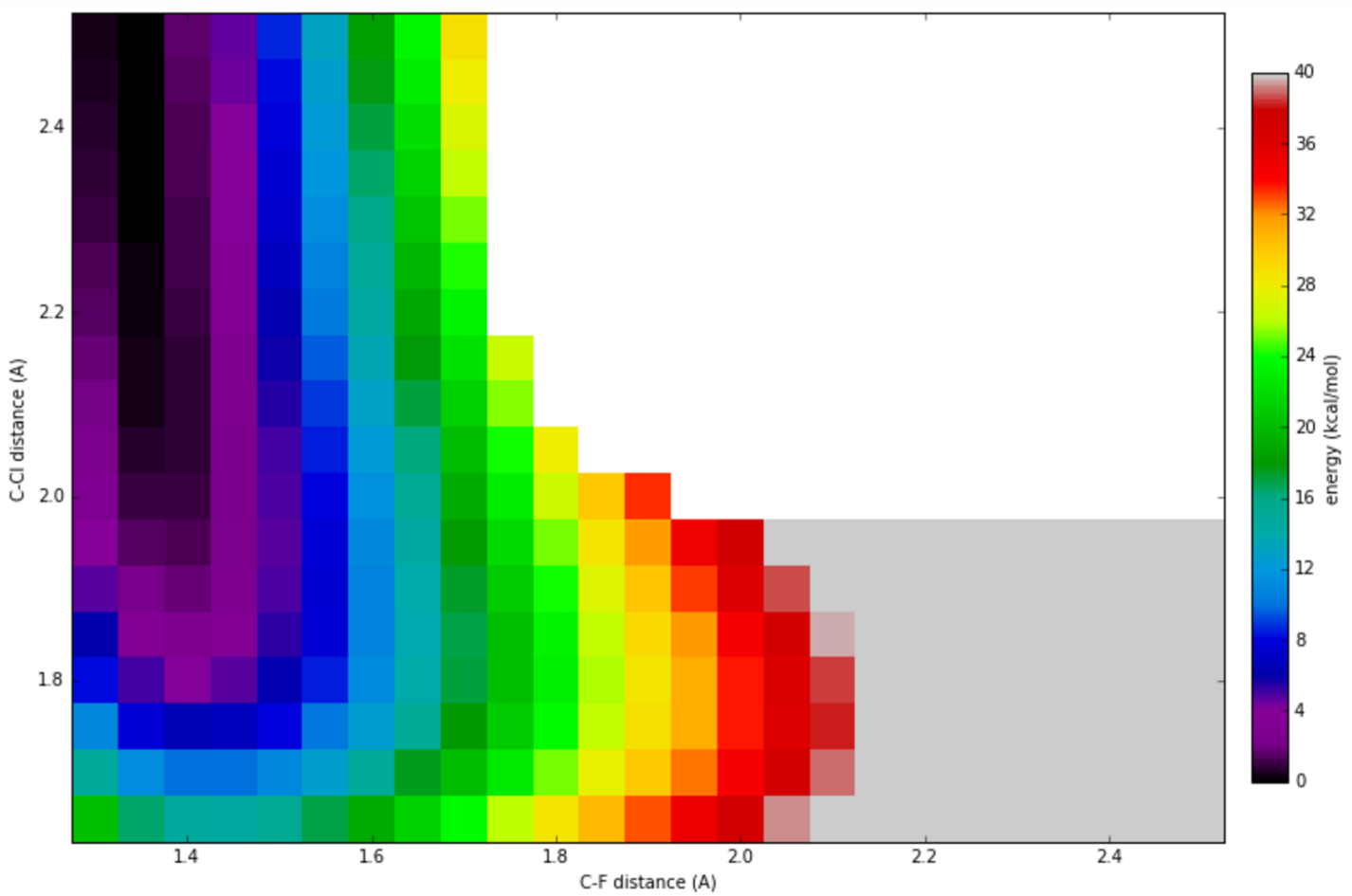

Although the structures in the starting material region are too high in energy, the overall shape of the surface and the energetics in the interesting post-transition-state region are reasonable. This justifies the use of this level of theory for the molecular dynamics simulations.

(iv) Effect of Transition Structure

Stationary points were located for the starting material and concerted transition state using B3LYP-D3(BJ) and default PCM settings at jul-cc-pVDZ. The influence of explicit water was considered:

```
dinitro_Cl_F-ts-b3lyp_d3bj-juldz-dmf_pcm              1.0303      (no waters)
dinitro_Cl_F-1H2O_5-ts-b3lyp_d3bj-juldz-dmf_pcm       1.0400      (one water, no cation)
dinitro_Cl_F-1H2O-Me4N_1-ts-b3lyp_d3bj-juldz-dmf_pcm  1.0400      (one water, Me4N+)
dinitro_Cl_F-1H2O-Me4N_2-ts-b3lyp_d3bj-juldz-dmf_pcm  1.0384      (other geometries)
dinitro_Cl_F-1H2O-Me4N_3-ts-b3lyp_d3bj-juldz-dmf_pcm  1.0397
dinitro_Cl_F-2H2O_1-ts-b3lyp_d3bj-juldz-dmf_pcm       1.0402      (two waters, no cation)
dinitro_Cl_F-2H2O_2-ts-b3lyp_d3bj-juldz-dmf_pcm       1.0396      (other geometries)
dinitro_Cl_F-2H2O_3-ts-b3lyp_d3bj-juldz-dmf_pcm       1.0400
dinitro_Cl_F-2H2O_4-ts-b3lyp_d3bj-juldz-dmf_pcm       1.0402
dinitro_Cl_F-2H2O_5-ts-b3lyp_d3bj-juldz-dmf_pcm       1.0393
```

Clearly, the inclusion of one water molecule is important, but the precise details of positioning and whether a cation is present are not important. Therefore, one explicit water molecule and no cation were included in the final prediction. Geometries, energies, and frequencies for all files considered are available in the attached archive.

(v) KIE Predictions

Predictions were made using B3LYP-D3(BJ) at 298 K and include a Bell tunnelling term:

Experimental: 1.045(3)

PCM (default settings, i.e., UFF radii scaled by 1.1):
jul-cc-pVDZ: 1.040
jun-cc-pVTZ: 1.041
may-cc-pVQZ: 1.041

PCM (UFF radii scaled by 1.2):
jul-cc-pVDZ: 1.039
jun-cc-pVTZ: 1.040
may-cc-PVQZ: 1.040

The bolded prediction is the value reported in the paper. The same settings were used to report the predicted KIEs for reactions A and B.

(vi) Quasiclassical Dynamics

200 trajectories were initialized from the B3LYP/6-31+G* transition state (default PCM, 298 K) and run forwards and backwards for a total time of 1 ps:

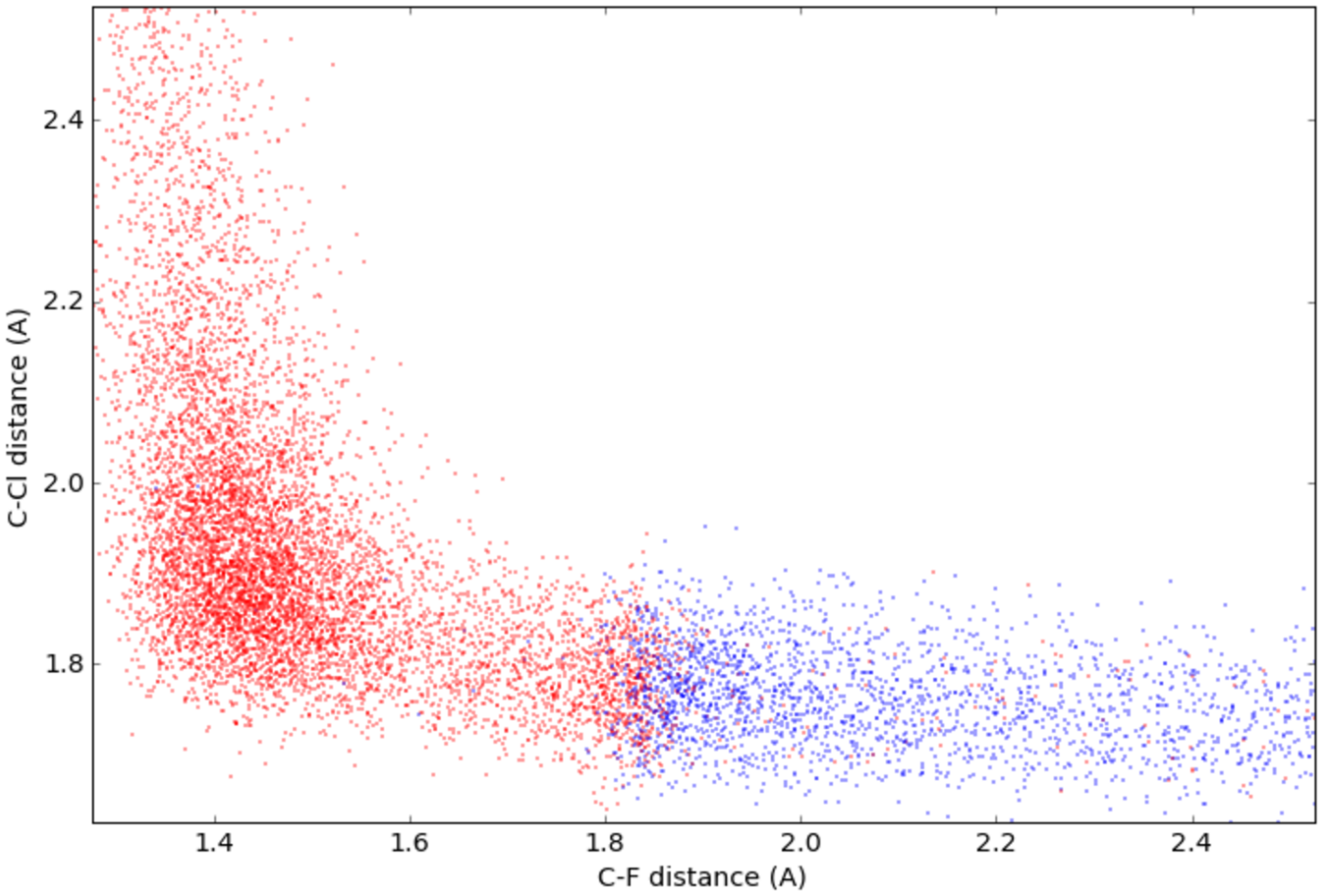

Blue and red points indicate backward and forward points, respectively. (Trajectories that did not originate from starting material were thrown out and replaced.) The variational transition state is visible as the region where the red and blue points intersect. Recrossing is rare. The clustering of red points in the bottom left represents the hidden intermediate.

f. Effect of Solvation Parameters on KIE Predictions for S_NAr Reactions

The potential energy surfaces of all the reactions change considerably on going from gas phase to solution. Qualitatively, gas phase nucleophiles are much more reactive, resulting in earlier transition states and substantially lower KIEs. As a result, it was crucial to assess the effect of different solvation models. In all cases, the default IEFPCM model was used. The effect of different sphere radii, radii scaling factors, and solvents was examined.

Radii (scaling factor was set to the default of 1.1 unless otherwise specified): SMD, UA0, UFF (this is the default choice; scaling factors were examined from 0.8–1.3), UAKS, Pauling, Bondi

Solvents: water, DMF, *n*-hexane, THF, acetone, argon, chloroform, gas phase

The full factorial grid of these parameters was calculated at 298 K using B3LYP-D3(BJ)/jul-cc-pVDZ. A few calculations could not be converged, but the majority of the combinations are available in the attached archive. Only the most pertinent trends will be discussed below.

Results for Reaction A

The experimental KIE is 1.035(3) and the reaction was carried out in MeOH. The following predictions refer to KIEs calculated for the second step (i.e., elimination). The inclusion of explicit methanol molecules had no effect.

The predicted KIE is higher in more polar solvents:

```
gas                     1.0037
pcm_uff_1.1_argon       1.0043
pcm_uff_1.1_hexane      1.0048
pcm_uff_1.1_chloroform  1.0240
pcm_uff_1.1_thf         1.0283
pcm_uff_1.1_acetone     1.0336
pcm_uff_1.1_meoh        1.0341
pcm_uff_1.1_dmf         1.0343
pcm_uff_1.1_water       1.0347
```

The choice of solvent radii had a modest effect:

```
pcm_ua0_meoh            1.0327
pcm_uff_1.1_meoh        1.0341
smd_meoh                1.0364
pcm_bondi_meoh          1.0373
pcm_uaks_meoh           1.0376
pcm_uahf_meoh           1.0377
pcm_pauling_meoh        1.0398
```

The choice of scaling factor had a large effect:

```
pcm_uff_1.3_meoh        1.0217
pcm_uff_1.2_meoh        1.0287
pcm_uff_1.1_meoh        1.0341
pcm_uff_1.0_meoh        1.0367
pcm_uff_0.9_meoh        1.0388
pcm_uff_0.8_meoh        1.0405
```

Regardless of the choice of solvent, radii, or scaling factor, the KIE remains below 1.04, which is inconsistent with the larger KIE expected for a concerted mechanism.

Results for Reaction B

The experimental KIE is 1.034(2) and the reaction was carried out in DMF. The inclusion of explicit water molecules had no effect.

Again, less polar solvents give lower KIEs:

```
gas                     1.0085
pcm_uff_1.1_argon       1.0063
pcm_uff_1.1_hexane      1.0102
```

```
pcm_uff_1.1_chloroform  1.0361
pcm_uff_1.1_thf         1.0384
pcm_uff_1.1_acetone     1.0401
pcm_uff_1.1_dmf         1.0403
pcm_uff_1.1_water       1.0404
```

The choice of solvent radii had a small effect:

```
pcm_ua0_dmf             1.0399
pcm_uff_1.1_dmf         1.0403
smd_dmf                 1.0406
pcm_uaks_dmf            1.0417
pcm_uahf_dmf            1.0418
pcm_bondi_dmf           1.0427
pcm_pauling_dmf         1.0434
```

The scaling factor had a pronounced effect:

```
pcm_uff_1.3_dmf         1.0344
pcm_uff_1.2_dmf         1.0378
pcm_uff_1.1_dmf         1.0403
pcm_uff_1.0_dmf         1.0418
pcm_uff_0.9_dmf         1.0448
pcm_uff_0.8_dmf         1.0468
```

The experimental KIE of 1.035(3) is consistent with the predictions for a concerted mechanism (1.034–1.047), but incompatible with a stepwise mechanism (about 1.01 from Figure 2d).

Results for Reaction C:

The experimental KIE is 1.045(3) and the reaction was carried out in DMF. The inclusion of at least one explicit water molecule in the transition state was important. Without explicit water, the prediction drops to ~1.03. The addition of more than one water molecule had a negligible effect.

Less polar solvents give lower KIEs:

```
gas                     1.0086
pcm_uff_1.1_hexane      1.0089
pcm_uff_1.1_chloroform  1.0367
pcm_uff_1.1_thf         1.0383
pcm_uff_1.1_acetone     1.0398
pcm_uff_1.1_meoh        1.0400
pcm_uff_1.1_dmf         1.0401
pcm_uff_1.1_water       1.0403
```

The choice of solvent radii had a small effect:

```
pcm_ua0_dmf             1.0396
pcm_uff_1.1_dmf         1.0401
smd_dmf                 1.0412
pcm_uahf_dmf            1.0417
```

```
pcm_uaks_dmf            1.0417
pcm_bondi_dmf           1.0423
pcm_pauling_dmf         1.0429
```

The scaling factor had a pronounced effect:

```
pcm_uff_1.3_dmf         1.0364
pcm_uff_1.2_dmf         1.0388
pcm_uff_1.1_dmf         1.0401
pcm_uff_1.0_dmf         1.0417
pcm_uff_0.9_dmf         1.0426
pcm_uff_0.8_dmf         1.0460
```

The experimental KIE of 1.045(3) is consistent with the predictions for a concerted mechanism (1.037–1.046) but inconsistent with that of a stepwise mechanism (~1.03).

g. Survey of S_NAr Reactions

For the eight substrate classes analyzed (135-NO_2 benzene, 13-NO_2 benzene, 3-NO_2 benzene, 3-COMe benzene, benzene, pyridine, pyrazine, and pyrimidine. The leaving groups screened were halogens (F, Cl, Br) and the nucleophiles assessed ranged in strength.

The potential energy surfaces of 120 nucleophilic aromatic substitution reactions were studied to determine what factors control concertedness. 8 types of rings of varying degrees of electronic stabilization were examined:

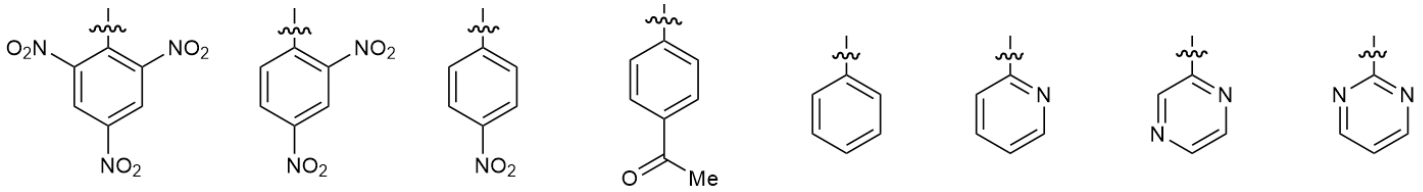

For each ring type, each combination of five nucleophiles ($^{-}$OCHO, N_3^{-}, F^{-}, MeO^{-}, Me_2N^{-}) spanning a range of strengths and three leaving groups (F^{-}, Cl^{-}, Br^{-}) of different abilities was studied:

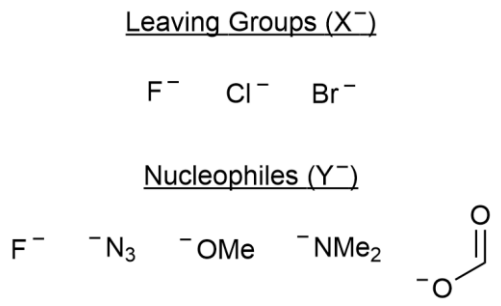

All calculations were performed with B3LYP-D3(BJ)/6-31+G*/PCM(DMSO). For each reaction, we attempted to locate an intermediate. For reactions where an intermediate was found, every effort was made to locate the transition states for both addition and elimination. For reactions where an intermediate was not found, every effort was made to locate the concerted transition state. In all but 3 cases, the appropriate transition states were located.

We also attempted to verify that each transition state connects the proper starting material and product. As a preliminary effort, we carried out intrinsic reaction coordinate searches for each transition state. Many of these calculations did not converge due to numerical problems. In the remaining cases, we constructed a chain-of-states using the growing string method (reference 44). In all but 13 cases, one of these procedures was successful.

The difficult cases mostly involved the addition of a very reactive nucleophile, dimethylamide. In such cases, the reaction is extremely exothermic and any transition state on the potential energy surface becomes very early, or vanishes entirely. This should not affect the conclusions the of the study because it was possible to locate both intermediates and transition states in some of these cases.

A peculiar feature of these reactions that is made clear by the IRC and growing string calculations is that the transition states are connected by pre- and post anion-π-complexes in which the nucleophile is bound to a hydrogen of the aryl or heteroaryl group. In some cases, there is a transition state both for moving the anion out of plane and for addition; in others, these transition states are merged. Thus, the imaginary mode for some structures involves a fair amount of lateral motion in addition to C–X bond formation, but nonetheless do represent true transition states. Supplementary files that describe this phenomenon are available on request.

Of the 120 reactions screened, 99 (83%) were found to be concerted and 21 (17%) were found to be stepwise. Most of the stepwise cases featured both strong electron-withdrawing groups and poor leaving groups. Detailed results can be found below:

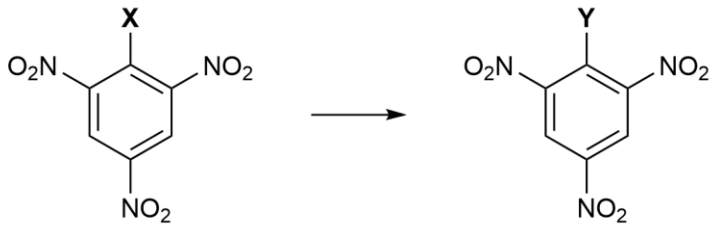

X	Y	Mechanism	Intermediate Located?	Transition State(s) Located?	Transition State(s) Confirmed? How?	Concerted		Addition		Elimination	
						C-X	C-Y	C-X	C-Y	C-X	C-Y
F	$^{--}$OCHO	Stepwise	Yes	Addition and Elimination	Both; growing string method	x	x	1.32	2.15	2.43	1.36
F	F^{--}	Stepwise	Yes	Addition/Elimination	Yes; growing string method	x	x	1.32	2.73	2.73	1.32
F	N_3^{--}	Stepwise	Yes	Addition and Elimination	Both; growing string method	x	x	1.33	2.22	2.26	1.38

F	$^{-}NMe_2$	Stepwise	Yes	Elimination only	Elimination only; growing string method	x	x	x	x	1.79	1.38
F	^{-}OMe	Stepwise	Yes	Addition and Elimination	Both; growing string method	x	x	1.32	2.60	2.22	1.33
Cl	$^{-}OCHO$	Concerted	x	Yes	Yes; growing string method	1.75	2.06	x	x	x	x
Cl	F^{-}	Concerted	x	Yes	Yes; growing string method	1.74	2.02	x	x	x	x
Cl	N_3^{-}	Concerted	x	Yes	No	1.74	2.27	x	x	x	x
Cl	$^{-}NMe_2$	Concerted	x	No	x	x	x	x	x	x	x
Cl	^{-}OMe	Concerted	x	Yes	No	1.72	2.54	x	x	x	x
Br	$^{-}OCHO$	Stepwise	Yes	Addition and Elimination	Addition only; growing string method	x	x	1.92	2.04	2.31	1.40
Br	F^{-}	Stepwise	Yes	Addition and Elimination	Both; growing string method	x	x	1.88	2.27	2.46	1.34
Br	N_3^{-}	Concerted	x	Yes	No	1.89	2.47	x	x	x	x
Br	$^{-}NMe_2$	Concerted	x	Yes	Yes; growing string method	1.88	2.83	x	x	x	x
Br	^{-}OMe	Concerted	x	Yes	Yes; growing string method	1.89	3.38	x	x	x	x

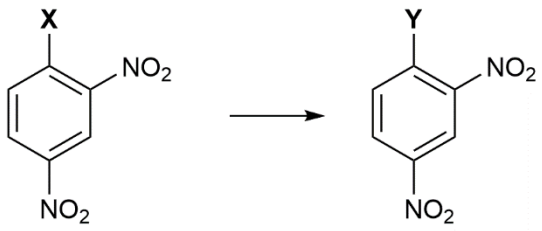

X	Y	Mechanism	Intermediate Located?	Transition State(s) Located?	Transition State(s) Confirmed? How?	Concerted		Addition		Elimination	
						C-X	C-Y	C-X	C-Y	C-X	C-Y
F	$^{-}$OCHO	Stepwise	Yes	Addition and Elimination	Both; growing string method	x	x	1.35	1.90	2.04	1.39
F	F^{-}	Stepwise	Yes	Addition/Elimination	Yes; growing string method	x	x	1.34	2.13	2.13	1.34
F	N_3^{-}	Stepwise	Yes	Addition and Elimination	Both; intrinsic reaction coordinate	x	x	1.36	1.98	1.92	1.41
F	$^{-}NMe_2$	Stepwise	Yes	Addition and Elimination	Both; growing string method	x	x	1.35	2.66	1.73	1.38
F	$^{-}$OMe	Stepwise	Yes	Addition and Elimination	Both; growing string method	x	x	1.33	3.13	2.43	1.33
Cl	$^{-}$OCHO	Concerted	x	Yes	Yes; growing string method	1.78	1.88	x	x	x	x
Cl	F^{-}	Concerted	x	Yes	Yes; growing string method	1.75	2.01	x	x	x	x
Cl	N_3^{-}	Concerted	x	Yes	Yes; intrinsic reaction coordinate	1.79	1.98	x	x	x	x
Cl	$^{-}NMe_2$	Concerted	x	Yes	Yes; growing string method	1.74	3.96	x	x	x	x
Cl	$^{-}$OMe	Concerted	x	Yes	Yes; growing string method	1.74	3.15	x	x	x	x
Br	$^{-}$OCHO	Concerted	x	Yes	Yes; growing string method	1.95	1.88	x	x	x	x

Br	F^{--}	Concerted	x	Yes	Yes; growing string method	1.91	1.96	x	x	x	x
Br	N_3^{--}	Concerted	x	Yes	Yes; intrinsic reaction coordinate	1.95	2.01	x	x	x	x
Br	$^{--}NMe_2$	Concerted	x	Yes	Yes; growing string method	1.89	3.59	x	x	x	x
Br	^{--}OMe	Concerted	x	Yes	Yes; growing string method	1.89	3.65	x	x	x	x

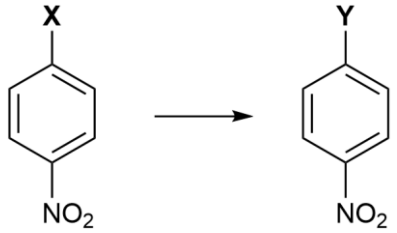

						Concerted		Addition		Elimination	
X	**Y**	**Mechanism**	**Intermediate Located?**	**Transition State(s) Located?**	**Transition State(s) Confirmed? How?**	**C-X**	**C-Y**	**C-X**	**C-Y**	**C-X**	**C-Y**
F	$^{--}OCHO$	Stepwise	Yes	Addition and Elimination	Both; growing string method	x	x	1.38	1.89	2.07	1.39
F	F^{--}	Stepwise	Yes	Addition/Elimination	Yes; intrinsic reaction coordinate	x	x	1.35	2.62	2.62	1.35
F	N_3^{--}	Stepwise	Yes	Addition and Elimination	Both; growing string method	x	x	1.39	1.91	2.32	1.41
F	$^{--}NMe_2$	Stepwise	Yes	Addition and Elimination	Both; growing string method	x	x	1.36	4.06	2.16	1.41
F	^{--}OMe	Stepwise	Yes	Addition and Elimination	Both; growing string method	x	x	1.37	3.06	2.11	1.36

Cl	$^{-}$OCHO	Concerted	x	Yes	Yes; intrinsic reaction coordinate	1.83	1.78	x	x	x	x
Cl	F^{-}	Concerted	x	Yes	Yes; intrinsic reaction coordinate	1.80	1.81	x	x	x	x
Cl	N_3^{-}	Concerted	x	Yes	Yes; intrinsic reaction coordinate	1.83	1.85	x	x	x	x
Cl	$^{-}NMe_2$	Concerted	x	Yes	Yes; growing string method	x	x	x	x	x	x
Cl	$^{-}$OMe	Concerted	x	Yes	Yes; growing string method	1.76	2.38	x	x	x	x
Br	$^{-}$OCHO	Concerted	x	Yes	Yes; intrinsic reaction coordinate	2.01	1.78	x	x	x	x
Br	F^{-}	Concerted	x	Yes	Yes; intrinsic reaction coordinate	1.95	1.78	x	x	x	x
Br	N_3^{-}	Concerted	x	Yes	Yes; growing string method	1.99	1.86	x	x	x	x
Br	$^{-}NMe_2$	Concerted	x	Yes	Yes; growing string method	1.90	3.55	x	x	x	x
Br	$^{-}$OMe	Concerted	X	Yes	Yes; growing string method	1.91	2.42	x	x	x	x

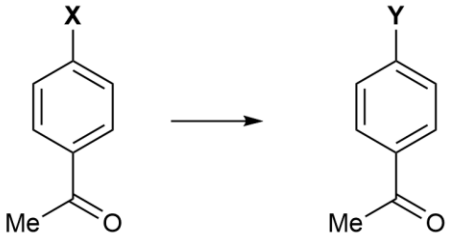

X	Y	Mechanism	Intermediate Located?	Transition State(s) Located?	Transition State(s) Confirmed? How?	Concerted		Addition		Elimination	
						C-X	C-Y	C-X	C-Y	C-X	C-Y
F	$^{--}$OCHO	Stepwise	Yes	Addition and Elimination	Both; intrinsic reaction coordinate	x	x	1.69	2.63	1.65	1.45
F	F^{--}	Stepwise	Yes	Addition/Elimination	Yes; intrinsic reaction coordinate	x	x	1.40	1.73	1.73	1.40
F	N_3^{--}	Stepwise	Yes	Addition and Elimination	Both; growing string method	x	x	1.42	1.75	1.65	1.49
F	$^{--}NMe_2$	Concerted	x	Yes	No	1.36	3.12	x	x	x	x
F	$^{--}$OMe	Stepwise	Yes	Addition and Elimination	Both; growing string method	x	x	1.37	2.23	1.66	1.42
Cl	$^{--}$OCHO	Concerted	x	Yes	Yes; intrinsic reaction coordinate	1.91	1.77	x	x	x	x
Cl	F^{--}	Concerted	x	Yes	Yes; intrinsic reaction coordinate	1.85	1.73	x	x	x	x
Cl	N_3^{--}	Concerted	x	Yes	Yes; intrinsic reaction coordinate	1.90	1.81	x	x	x	x
Cl	$^{--}NMe_2$	Concerted	x	Yes	No	1.76	3.09	x	x	x	x
Cl	$^{--}$OMe	Concerted	x	Yes	Yes; growing string method	1.79	2.13	x	x	x	x
Br	$^{--}$OCHO	Concerted	x	Yes	Yes; intrinsic reaction coordinate	2.08	1.79	x	x	x	x
Br	F^{--}	Concerted	x	Yes	Yes; intrinsic reaction coordinate	2.00	1.72	x	x	x	x

Br	N_3^-	Concerted	x	Yes	Yes; intrinsic reaction coordinate	2.07	1.82	x	x	x	x
Br	$^-NMe_2$	Concerted	x	Yes	Yes; growing string method	1.91	3.24	x	x	x	x
Br	^-OMe	Concerted	x	Yes	Yes; intrinsic reaction coordinate	1.95	2.12	x	x	x	x

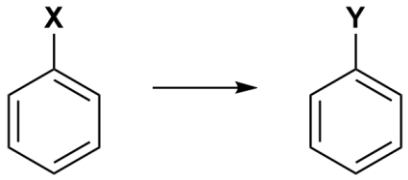

						Concerted		Addition		Elimination	
X	**Y**	**Mechanism**	**Intermediate Located?**	**Transition State(s) Located?**	**Transition State(s) Confirmed? How?**	**C-X**	**C-Y**	**C-X**	**C-Y**	**C-X**	**C-Y**
F	^-OCHO	Concerted	x	Yes	Yes; intrinsic reaction coordinate	1.52	1.63	x	x	x	x
F	F^-	Concerted	x	Yes	Yes; growing string method	1.52	1.52	x	x	x	x
F	N_3^-	Concerted	x	Yes	Yes; intrinsic reaction coordinate	1.52	1.66	x	x	x	x
F	$^-NMe_2$	Concerted	x	Yes	Yes; growing string method	1.39	2.34	x	x	x	x
F	^-OMe	Concerted	x	Yes	Yes; intrinsic reaction coordinate	1.42	1.90	x	x	x	x
Cl	^-OCHO	Concerted	x	Yes	Yes; intrinsic reaction coordinate	2.10	1.86	x	x	x	x
Cl	F^-	Concerted	x	Yes	Yes; intrinsic reaction coordinate	1.96	1.73	x	x	x	x
Cl	N_3^-	Concerted	x	Yes	Yes; intrinsic reaction coordinate	2.12	1.95	x	x	x	x

Cl	$^{-}NMe_2$	Concerted	x	Yes	No	1.80	2.37	x	x	x	x
Cl	^{-}OMe	Concerted	x	Yes	Yes; intrinsic reaction coordinate	1.87	1.94	x	x	x	x
Br	$^{-}OCHO$	Concerted	x	Yes	Yes; intrinsic reaction coordinate	2.24	1.87	x	x	x	x
Br	F^{-}	Concerted	x	Yes	Yes; intrinsic reaction coordinate	2.12	1.71	x	x	x	x
Br	N_3^{-}	Concerted	x	Yes	Yes; intrinsic reaction coordinate	2.26	1.94	x	x	x	x
Br	$^{-}NMe_2$	Concerted	x	Yes	No	1.95	2.43	x	x	x	x
Br	^{-}OMe	Concerted	x	Yes	Yes; intrinsic reaction coordinate	2.03	1.98	x	x	x	x

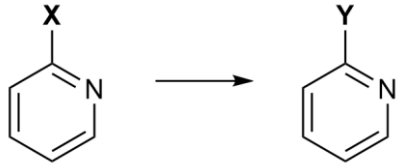

						Concerted		Addition		Elimination	
X	**Y**	**Mechanism**	**Intermediate Located?**	**Transition State(s) Located?**	**Transition State(s) Confirmed? How?**	**C-X**	**C-Y**	**C-X**	**C-Y**	**C-X**	**C-Y**
F	$^{-}OCHO$	Concerted	x	Yes	Yes; growing string method	1.48	1.61	x	x	x	x
F	F^{-}	Concerted	x	Yes	Yes; growing string method	1.49	1.49	x	x	x	x
F	N_3^{-}	Concerted	x	Yes	Yes; growing string method	1.47	1.66	x	x	x	x
F	$^{-}NMe_2$	Concerted	x	Yes	Yes; growing string method	1.37	2.58	x	x	x	x
F	^{-}OMe	Concerted	x	Yes	Yes; growing string method	1.36	2.44	x	x	x	x

Cl	$^{-}OCHO$	Concerted	x	Yes	Yes; growing string method	2.06	1.86	x	x	x	x
Cl	F^{-}	Concerted	x	Yes	Yes; intrinsic reaction coordinate	1.92	1.73	x	x	x	x
Cl	N_3^{-}	Concerted	x	Yes	Yes; intrinsic reaction coordinate	2.07	1.93	x	x	x	x
Cl	$^{-}NMe_2$	Concerted	x	Yes	No	1.78	2.62	x	x	x	x
Cl	^{-}OMe	Concerted	x	Yes	No	1.82	2.10	x	x	x	x
Br	$^{-}OCHO$	Concerted	x	Yes	Yes; intrinsic reaction coordinate	2.22	1.85	x	x	x	x
Br	F^{-}	Concerted	x	Yes	Yes; intrinsic reaction coordinate	2.09	1.72	x	x	x	x
Br	N_3^{-}	Concerted	x	Yes	Yes; intrinsic reaction coordinate	2.20	1.92	x	x	x	x
Br	$^{-}NMe_2$	Concerted	x	Yes	No	1.93	2.70	x	x	x	x
Br	^{-}OMe	Concerted	x	Yes	Yes; growing string method	1.92	2.62	x	x	x	x

						Concerted		Addition		Elimination	
X	**Y**	**Mechanism**	**Intermediate Located?**	**Transition State(s) Located?**	**Transition State(s) Confirmed? How?**	**C-X**	**C-Y**	**C-X**	**C-Y**	**C-X**	**C-Y**
F	$^{-}OCHO$	Concerted	x	Yes	Yes; growing string method	1.44	1.63	x	x	x	x
F	F^{-}	Concerted	x	Yes	Yes; growing string method	1.48	1.48	x	x	x	x
F	N_3^{-}	Concerted	x	Yes	Yes; intrinsic reaction coordinate	1.43	1.71	x	x	x	x

F	$^{-}NMe_2$	Concerted	x	Yes	Yes; growing string method	1.36	2.60	x	x	x	x
F	^{-}OMe	Concerted	x	Yes	Yes; growing string method	1.36	2.20	x	x	x	x
Cl	$^{-}OCHO$	Concerted	x	Yes	Yes; intrinsic reaction coordinate	1.96	1.78	x	x	x	x
Cl	F^{-}	Concerted	x	Yes	Yes; intrinsic reaction coordinate	1.87	1.69	x	x	x	x
Cl	N_3^{-}	Concerted	x	Yes	Yes; intrinsic reaction coordinate	1.96	1.82	x	x	x	x
Cl	$^{-}NMe_2$	Concerted	x	Yes	No	1.77	2.63	x	x	x	x
Cl	^{-}OMe	Concerted	x	Yes	Yes; growing string method	1.79	2.21	x	x	x	x
Br	$^{-}OCHO$	Concerted	x	Yes	Yes; intrinsic reaction coordinate	2.12	1.77	x	x	x	x
Br	F^{-}	Concerted	x	Yes	Yes; intrinsic reaction coordinate	2.04	1.68	x	x	x	x
Br	N_3^{-}	Concerted	x	Yes	Yes; intrinsic reaction coordinate	2.12	1.87	x	x	x	x
Br	$^{-}NMe_2$	Concerted	x	Yes	No	1.92	2.67	x	x	x	x
Br	^{-}OMe	Concerted	x	Yes	Yes; growing string method	1.93	2.26	x	x	x	x

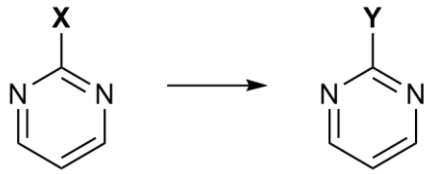

						Concerted		Addition		Elimination	
X	**Y**	**Mechanism**	**Intermediate Located?**	**Transition State(s) Located?**	**Transition State(s) Confirmed? How?**	**C-X**	**C-Y**	**C-X**	**C-Y**	**C-X**	**C-Y**

F	$^{-}$OCHO	Concerted	x	Yes	Yes; growing string method	1.45	1.55	x	x	x	x
F	F^{-}	Concerted	x	Yes	Yes; growing string method	1.46	1.46	x	x	x	x
F	N_3^{-}	Concerted	x	Yes	Yes; growing string method	1.43	1.65	x	x	x	x
F	$^{-}NMe_2$	Concerted	x	Yes	Yes; growing string method	1.35	3.23	x	x	x	x
F	$^{-}$OMe	Concerted	x	Yes	Yes; growing string method	1.35	2.43	x	x	x	x
Cl	$^{-}$OCHO	Concerted	x	Yes	Yes; intrinsic reaction coordinate	1.92	1.71	x	x	x	x
Cl	F^{-}	Concerted	x	Yes	Yes; intrinsic reaction coordinate	1.84	1.76	x	x	x	x
Cl	N_3^{-}	Concerted	x	Yes	Yes; intrinsic reaction coordinate	1.92	1.80	x	x	x	x
Cl	$^{-}NMe_2$	Concerted	x	No	x	x	x	x	x	x	x
Cl	$^{-}$OMe	Concerted	x	Yes	Yes; growing string method	1.78	2.32	x	x	x	x
Br	$^{-}$OCHO	Concerted	x	Yes	Yes; intrinsic reaction coordinate	2.08	1.74	x	x	x	x
Br	F^{-}	Concerted	x	Yes	Yes; intrinsic reaction coordinate	2.01	1.67	x	x	x	x
Br	N_3^{-}	Concerted	x	Yes	Yes; intrinsic reaction coordinate	2.07	1.84	x	x	x	x
Br	$^{-}NMe_2$	Concerted	x	Yes	No	1.91	3.33	x	x	x	x
Br	$^{-}$OMe	Concerted	x	Yes	Yes; growing string method	1.92	2.43	x	x	x	x

5. Summary of Archived Files

Selected raw data are available in an attached ZIP archive.

a. NMR Files

Sample FIDs for an MQF spectrum are provided along with a Python notebook for processing them. nmrglue and standard Python libraries are required (numpy, matplotlib). An Excel notebook of the raw integrals, KIEs, and error analysis for all data acquires is also provided. These files can easily be modified to study other reactions. We will happily assist you with this on request.

b. Computational Files

Due to space constraints, raw output files are not provided. Instead, key structures, energies, and frequencies are stored as .snip files in directories with self-explanatory names. Here is an example (truncated for clarity):

```
Electronic energy:  -3724.25163230
Zero-point correction= 0.347826 (Hartree/Particle)
 Thermal correction to Energy= 0.373661
 Thermal correction to Enthalpy= 0.374605
 Thermal correction to Gibbs Free Energy= 0.290532
 Sum of electronic and zero-point Energies= -3723.903807
 Sum of electronic and thermal Energies= -3723.877971
 Sum of electronic and thermal Enthalpies= -3723.877027
 Sum of electronic and thermal Free Energies= -3723.961100

Standard orientation
1  6 0     -0.06661600     -2.00300800     -1.09743900
2  6 0      1.03587200     -1.16717500     -1.23439600
…

Rotational constants (GHZ)
NAtoms= 43
SCF Done Field3 Field4  -3724.25163230
 (Enter /n/sw/g09_D.01/g09/l9999.exe) 1\1\GINC-DAE14\Freq\RwB97XD\CC-
pVDZ\C12H22Br1F4N1O3\ROOT\28-Feb-2017\0 \\#P Geom=AllCheck Guess=TCheck SCRF=Check GenChk
RwB97XD/CC-pVDZ Freq \\title\\0,1\C,-0.026284383,-1.9943994495,-
1.1100861683\C,1.0565542905
…
,0.00000094,-0 .00000273,-0.00000062,0.00000127,0.00000417,0.00000046,0.00000160,0.00
000392,-0.00000034,0.00000040,0.00000764,0.00000228,0.00000106,0.00000 770,-
0.00000211,0.00000176,0.00000800\\\@
```

Thus, .snip files mimic Gaussian output file format, but are much more compact. The bottom section (usually rather large) is a copy of the Gaussian archive and contains the frequencies.

These files are compatible with PyQuiver. Where applicable, shell scripts are provided for generating the predicted KIEs reported above.

6. References

82. Ariza-Castolo, A., Guerrero-Alvarez, J. A. & Peralta-Cruz, J. Full multinuclear magnetic resonance analysis of 2,4-dinitrofluorobenzene. *Magn. Reson. Chem*. **41**, 49–52 (2003).
83. Aridoss, G. & Laali, K. K. Ethylammonium nitrate (EAN)/Tf2O and EAN/TFAA: ionic liquid based systems for aromatic nitration. *J. Org. Chem*. **76**, 8088–8094 (2011).
84. Puy, V. D. M. Direct fluorination of substituted pyridines. *Tetrahedron Lett*. **28**, 255-258 (1987).
85. Ung, G. & Bertrand, G. C–F bond activation with an apparently benign ethynyl dithiocarbamate, and subsequent fluoride transfer reactions*. Chem. – Eur. J*. **18**, 12955–12957 (2012).
86. Patt, S. L. Single and multiple-frequency-shifted laminar pulses. *J. Magn. Reson*. **96**, 94–102 (1992).
87. Kwan, E.E. & Liu, R.Y. Enhancing NMR predictions for organic compounds using molecular dynamics. *J. Chem. Theor. Comput*. **11**, 5083–5089 (2015).